

January 2015

Effect of Dosage of Non-Chloride Accelerator versus Chloride Accelerator on the Cracking Potential of Concrete Repair Slabs

Thomas F. Meagher

University of South Florida, tmeagher@mail.usf.edu

Follow this and additional works at: <http://scholarcommons.usf.edu/etd>

 Part of the [Civil Engineering Commons](#)

Scholar Commons Citation

Meagher, Thomas F., "Effect of Dosage of Non-Chloride Accelerator versus Chloride Accelerator on the Cracking Potential of Concrete Repair Slabs" (2015). *Graduate Theses and Dissertations*.

<http://scholarcommons.usf.edu/etd/5743>

This Thesis is brought to you for free and open access by the Graduate School at Scholar Commons. It has been accepted for inclusion in Graduate Theses and Dissertations by an authorized administrator of Scholar Commons. For more information, please contact scholarcommons@usf.edu.

Effect of Dosage of Non-Chloride Accelerator versus Chloride
Accelerator on the Cracking Potential of Concrete Repair Slabs

by

Thomas F. Meagher IV

A thesis submitted in partial fulfillment
of the requirements for the degree of
Master of Science in Civil Engineering
Department of Civil and Environmental Engineering
College of Engineering
University of South Florida

Major Professor: Abla Zayed, Ph.D.
Kyle Riding, Ph.D.
Rajan Sen, Ph.D.

Date of Approval:
July 3, 2015

Keywords: Calcium Nitrate, Semi-adiabatic Calorimetry, Free Shrinkage,
Rigid Cracking Frame, HIPERPAV

Copyright © 2015, Thomas F. Meagher IV

DEDICATION

This thesis is dedicated to my parents. Their never ending love and support has taught me to never give up. I would be nothing without them, and can never thank them enough for the foundation that they have provided for me.

ACKNOWLEDGMENTS

I would like to thank everyone who has helped me throughout this research study. I would first and foremost like to thank my advisor, Dr. Zayed, for all of her time, wisdom, and patience during my time as her student and for funding my research. I would also like to thank Dr. Riding for sharing his vast knowledge and significant contributions in this project. I would like to thank Dr. Sen for passing along his knowledge and personal experiences which I will take with me.

Thank you Natalya Shanahan for everything. You were always patient with me and very helpful during my research. It was a pleasure working with you and always having someone to talk to, and I wish you the best as you finish your research. Thank you Dan Buidens for your help; you are one of the hardest working people I know. Thank you Andre Bien-Aime for your valuable input especially with semi-adiabatic calorimetry. Thank you Victor Tran for your never ending help in the lab and for keeping me laughing throughout this whole experience. Good luck with your research! Thank you Tony, Andrew, and Etienne for your help in the lab, our research depended on your assistance, and it was pleasing watching y'all learn everything so quickly. Thank you Kevin Johnson for helping with numerous calibrations and for all of your help in the structures lab; you were always available without hesitation or expecting anything in return. Thank you Danny Winters and the USF machine shop for your assistance in constructing the rigid cracking frame.

Lastly, I would like to thank Dr. DeFord for the valuable discussions and acknowledge the Florida Department of Transportation (FDOT) for the partial funding of this research.

TABLE OF CONTENTS

LIST OF TABLES	iii
LIST OF FIGURES	iv
ABSTRACT	vii
CHAPTER 1: INTRODUCTION	1
1.1 Background.....	1
1.2 Research Objectives.....	3
1.3 Outline of Thesis.....	3
CHAPTER 2: LITERATURE REVIEW	5
2.1 Accelerators.....	5
2.2 Causes of Early-Age Cracking in Concrete	6
2.2.1 Shrinkage Due to Moisture Gradient	6
2.2.2 Shrinkage Due to Temperature Gradient	7
2.3 Non-Standard Testing of Concrete	8
2.3.1 Semi-Adiabatic Calorimetry	8
2.3.2 Free Shrinkage.....	10
2.3.3 Rigid Cracking Frame.....	11
2.4 Modeling.....	12
2.4.1 HIPERPAV	12
2.4.2 ConcreteWorks.....	22
CHAPTER 3: MATERIALS AND METHODS.....	23
3.1 Materials	23
3.1.1 Cement Properties.....	23
3.1.2 Chemical Admixtures	25
3.1.3 Aggregates.....	27
3.1.4 Concrete Mixture Designs.....	29
3.2 Experimental Testing	30
3.2.1 Mixing Procedure	30
3.2.2 Fresh Concrete Properties	30
3.2.3 Maturity.....	31
3.2.4 Isothermal Calorimetry	31
3.2.5 Semi-adiabatic Calorimetry	32
3.2.6 Time of Set	43
3.2.7 Concrete Mechanical Properties.....	43

3.2.8 Free Shrinkage.....	44
3.2.9 Rigid Cracking Frame.....	45
3.3 Modeling.....	47
3.3.1 ConcreteWorks Inputs	47
3.3.2 HIPERPAV Inputs.....	47
CHAPTER 4: RESULTS AND DISCUSSION.....	50
4.1 Concrete Mechanical Properties	50
4.2 Maturity Studies.....	52
4.2.1 Mortar Cube Compressive Strengths.....	52
4.2.2 Strength-Based Apparent Activation Energy	54
4.3 Calorimetry.....	55
4.3.1 Isothermal.....	55
4.3.2 Semi-Adiabatic	58
4.4 Setting Time.....	64
4.5 Free Shrinkage	65
4.6 Rigid Cracking Frame	70
4.7 HIPERPAV Analysis	75
4.7.1 Effect of Dosage of Nitrate-Based Accelerator.....	77
4.7.2 Effect of Placement Time	79
4.7.3 Effect of Initial Concrete Placement Temperature.....	84
CHAPTER 5: CONCLUSIONS	85
REFERENCES	87
APPENDIX A: SUPPLEMENTARY MATERIALS.....	93
APPENDIX B: PERMISSIONS.....	96

LIST OF TABLES

Table 1	Oxide Chemical Composition of As-Received Cement	24
Table 2	Bogue-calculated Potential Compound Content for As – Received Cement	24
Table 3	Cement Mineralogical Composition Using Rietveld Analysis and Fineness	25
Table 4	Chemical Admixture Compositions	26
Table 5	Mixture Design per Cubic Yard	29
Table 6	Compressive Strength of Cylinders at 23°C	51
Table 7	Tensile Splitting Strength of Cylinders at 23°C.....	51
Table 8	Modulus of Elasticity.....	52
Table 9	Heat of Hydration-Based Activation Energy	58
Table 10	Calibration Factors	59
Table 11	Hydration Parameters and Adiabatic Temperature Rise.....	59
Table 12	ConcreteWorks General Inputs	65
Table 13	ConcreteWorks Environmental Inputs	66
Table 14	HIPERPAV Mixture Inputs	75
Table 15	HIPERPAV Inputs - PCC Properties.....	76

LIST OF FIGURES

Figure 1 RCF During Construction.....	12
Figure 2 HIPERPAV III Modeling Flowchart.....	13
Figure 3 HIPERPAV III Sample Analysis Output	22
Figure 4 Coarse Aggregate Gradation.....	28
Figure 5 Fine Aggregate Gradation	28
Figure 6 Semi-Adiabatic Calorimeter Detail.....	32
Figure 7 Middle Thermocouple Placed and Plugged In.....	33
Figure 8 Measured Semi-Adiabatic Temperature C	36
Figure 9 Influence of αu on Hydration.....	38
Figure 10 Influence of β on Hydration.....	38
Figure 11 Influence of τ on Hydration	39
Figure 12 True vs False Adiabatic Temperature of C.....	43
Figure 13 Free Shrinkage Frame.....	44
Figure 14 Rigid Cracking Frame	46
Figure 15 Mortar Cube Strengths at 23°C.....	53
Figure 16 Mortar Cube Strengths at 38°C.....	53
Figure 17 Mortar Cube Strengths at 53°C.....	54
Figure 18 Strength-Based Activation Energy.....	55
Figure 19 Heat Flow Rate by Isothermal Calorimetry 23°C	56

Figure 20 Heat Flow Rate by Isothermal Calorimetry 38°C	57
Figure 21 Heat Flow Rate by Isothermal Calorimetry 48°C	57
Figure 22 Semi-Adiabatic Calorimeter Water Calibration.....	58
Figure 23 Effect of Accelerators on α u and β	60
Figure 24 Effect of Accelerator Dose on the τ	60
Figure 25 Measured vs. Modeled Semi-adiabatic Temperature C	61
Figure 26 Measured vs. Modeled Semi-adiabatic Temperature CNA.....	61
Figure 27 Measured vs. Modeled Semi-adiabatic Temperature CA.....	62
Figure 28 Measured vs. Modeled Semi-adiabatic Temperature CHAD	62
Figure 29 Measured vs. Modeled Semi-adiabatic Temperature CAD.....	63
Figure 30 Measured vs. Modeled Semi-adiabatic Temperature CDAD	63
Figure 31 Time of Initial Set	64
Figure 32 Time of Final Set.....	65
Figure 33 Free Shrinkage Realistic Temperature Profiles	67
Figure 34 Realistic Free Shrinkage Analysis at 23°C	67
Figure 35 Realistic Free Shrinkage Analysis at 38°C.....	68
Figure 36 Realistic 23°C Mixtures Compared after 20 Hours.....	69
Figure 37 Realistic 38°C Mixtures Compared after 20 Hours.....	70
Figure 38 Insulated RCF Temperature.....	71
Figure 39 Insulated RCF Stress	71
Figure 40 RCF 23°C Realistic Temperature Profiles.....	72
Figure 41 RCF 23°C Realistic Stress Profiles	73
Figure 42 RCF 38°C Realistic Temperature Profiles.....	73

Figure 43 RCF 38°C Realistic Stress Profiles	74
Figure 44 Tensile Strength – Maturity Relationship Input in HIPERPAV III	76
Figure 45 Environmental Inputs	77
Figure 46 Tensile Stress and Strength of Each Mixture Placed at 9am	78
Figure 47 Tensile Stress and Strength of Each Mixture Placed at 11pm	79
Figure 48 HIPERPAV- Max Tensile Stress at Different Construction Times	80
Figure 49 HIPERPAV Ambient Temperature for 11PM Construction Time	81
Figure 50 HIPERPAV Analysis at Bottom of Slab Using 11PM Construction Time	81
Figure 51 HIPERPAV Analysis at Top of Slab Using 11PM Construction Time	82
Figure 52 HIPERPAV Ambient Temperature for 9AM Construction Time	82
Figure 53 HIPERPAV Analysis at Bottom of Slab Using 9AM Construction Time	83
Figure 54 HIPERPAV Analysis at Top of Slab Using 9AM Construction Time	83
Figure 55 Effect of Initial Temperature on CAD at 11PM	84
Figure A-1 Cylinder Testing - Compressive Strength	93
Figure A-2 Cylinder Testing - Modulus of Elasticity	93
Figure A-3 Tensile Splitting Testing.....	94
Figure A-4 Rigid Cracking Frame Calibration Data.....	94
Figure A-5 RCF During Testing	95
Figure A-6 Copper Piping Throughout RCF Formwork.....	95

ABSTRACT

Due to strict placement time and strength constraints during the construction of concrete pavement repair slabs, accelerators must be incorporated into the mixture design. Since the most common accelerator, calcium chloride, promotes corrosion of concrete reinforcement, a calcium nitrate-based accelerator was studied as an alternative. To replicate mixtures used in the field, commercial accelerators commonly used in concrete pavement repair slabs were used in the current study. Crack risk of different mixtures was assessed using modeling and cracking frame testing. HIPERPAV modeling was conducted using several measured mixture properties; namely, concrete mechanical properties, strength-based and heat of hydration-based activation energies, hydration parameters using calorimetric studies, and adiabatic temperature rise profiles. Autogenous shrinkage was also measured to assess the effect of moisture consumption on concrete volume contraction. The findings of the current study indicate that the cracking risk associated with calcium nitrate-based accelerator matches the performance of a calcium-chloride based accelerator when placement is conducted during nighttime hours.

CHAPTER 1: INTRODUCTION

1.1 Background

An approved concrete repair slab mixture had a reported history of cracking of up to 40% in a south Florida repair project. Studies were performed to determine if the cause of cracking could be due to an overdose of the calcium chloride-based accelerator used during placement. During this study, a calcium nitrate-based accelerator was also examined as to study its effect on cracking while evaluating its accelerating properties to determine if it would make a good alternative as an accelerator.

Early-age cracking in concrete repair slabs is a recurring problem which limits the repair serviceability and increases maintenance costs. Change in volume due to shrinkage and thermal contraction could contribute significantly to early age cracking in repair slabs. As the subbase and adjacent slabs restrain the concrete, the decrease in volume due to shrinkage and thermal effects would ultimately induce tensile stresses. When these stresses surpass the tensile strength of concrete, which is relatively low at early ages, cracking occurs.

Repair construction typically requires concrete repair materials to retain workability during placement, harden quickly, and maintain ultimate strength capacity. In order to meet these requirements, combinations of admixtures are often used in concrete mixture. To reach high compressive strength, a low water-to-cement (w/c) ratio is typically used since it lowers capillary porosity [1]; however, a low w/c ratio decreases concrete workability. Often times, water reducing

and retarding admixtures are used to maintain workability of concrete mixtures that are batched with low w/c ratios or at high temperatures. However, retarders delay the setting time, so accelerators are added to speed up the hydration process. The effects of using a combination of accelerators with water reducers/retarders on cracking probability were studied here to represent realistic repair mixtures.

Accelerators decrease the setting time and increase the rate of strength gain at early age once concrete begins to harden [2]. This encourages the concrete to meet high early-strength requirements, and reduces time to opening-to-traffic thus avoiding potential delays to the traveling public. However, higher hydration rates increase the temperature rise during hardening which can potentially increase autogenous deformation [3]. The consequent increased rate of volume change can lead to higher stresses and increased cracking probability.

Different types of accelerators have been studied to determine their effectiveness as a setting or hardening accelerator. The most commonly used accelerator today is calcium chloride. However, calcium chloride promotes the corrosion of reinforcement by breaking down the passive oxide layer of steel [4], [5]. Due to this, chloride-free accelerators have been developed. Some common chloride-free accelerators include soluble inorganic salts – such as nitrates, nitrites, thiocyanates [6].

To ensure both setting and hardening properties are attained, accelerator blends comprised of multiple chemicals have been manufactured. Researchers have performed many tests on different accelerator blends and studied their effect on hydration, setting, and strength development [4], [7]–[10]. However, little research has been done on how these accelerators in combination with typical water-reducing and retarding and air entraining admixtures affect the overall cracking

potential of concrete mixtures. Experimental tests using a free shrinkage frame and rigid cracking frame were conducted and compared to cracking prediction software to study the effects of different chemical admixture combinations on the early age cracking potential of high early-strength concrete pavement repair slabs.

1.2 Research Objectives

The main objective of this research is to determine if a calcium nitrate-based accelerator can be used as an alternative to a calcium chloride-based accelerator on pavement repair jobs. The primary metrics focus was to determine the effectiveness of each accelerator on early age strength (tensile splitting and compressive) and modulus, setting time, hydration kinetics, adiabatic temperature rise, autogenous shrinkage and overall cracking potential for concrete pavement mixtures. This research also looks into the effects of varying the accelerator dosage on concrete mechanical properties, heat generation, and overall cracking potential.

1.3 Outline of Thesis

Chapter 2 presents a thorough review of the current literature on trends observed when using calcium nitrate or calcium chloride in concrete mixtures. It also presents experimental methods reported in the literature to assess the cracking potential of concrete mixtures. Chapter 3 outlines the methodology used throughout this study. The materials and mixtures design are presented along with a description of the different experimental testing procedures used. Chapter 4 presents and discusses the results from the experimental work which were then used as inputs to model the temperature profiles and cracking tendency of each mixture. Chapter 5 presents the final conclusions from this study and identifies areas of future work. This research was conducted as part of contract No. BDV25-977-01 issued by the Florida Department of Transportation (FDOT);

as such, major sections of this research are shared with the contract final report [11]. Additionally, this research has been submitted for publication in an international journal and is currently under review. Approval from the FDOT and the journal are presented in Appendix B.

CHAPTER 2: LITERATURE REVIEW¹

2.1 Accelerators

Calcium chloride is one of the most commonly used accelerators today due to its effectiveness and low cost. Ample research has been performed on the effects of calcium chloride on the properties of concrete including heat of hydration, sulfate resistance, strength, and setting time [11]. However, due to chloride induced corrosion, more recent research has been performed on chloride-free accelerators, namely, calcium nitrate since it is harmless and more cost effective compared to other inhibitors such as nitrites [9].

Calcium nitrate has been shown to be a very good set accelerator while not providing much early strength [12]–[14]. Research has been performed on the effects of calcium nitrate by itself and combined with other chemicals such as sodium thiocyanate, triethanolamine, or lignosulfonate on setting time [7], [8], heat of hydration [15]–[17], shrinkage [18] and strength [7], [10], [19].

Little research has been performed on the cracking potential of realistic concrete mixtures containing commercial accelerators with water reducer and air entrainer. This study will look into the effect of varying dosages of a calcium nitrate based accelerator on the cracking potential of concrete mixtures.

¹ Portions of this chapter were previously published in [48]. Permission is included in Appendix A.

2.2 Causes of Early-Age Cracking in Concrete

2.2.1 Shrinkage Due to Moisture Gradient

Shrinkage induced tensile stresses can be the result of several types of moisture-related shrinkage. Drying shrinkage and plastic shrinkage are two types of shrinkage which are caused by water loss typically at the surface of the slab, although suction of water from the concrete by the subbase or formwork material may also cause some shrinkage [1]. The term drying shrinkage usually applies to hardened concrete, while plastic shrinkage occurs while concrete is still in the “plastic” stage. When water is lost from concrete while in the plastic state, tensile forces develop in concrete causing tearing of the surface, similar to what occurs in mud flats. In hardened concrete, as moisture is lost, vapor-water interfaces develop in pores, causing surface tension and capillary underpressure which causes pores to tend to contract and subsequent tensile stresses to develop. Since a slab exposed surface can be subjected to environmental conditions such as wind, relative humidity, and ambient temperature, significant moisture loss can occur. In pavements, this difference in water loss causes a drying shrinkage moisture gradient which results in a higher reduction of volume in the concrete near the surface of the slab than near the bottom. This causes an upward curvature in the slab, referred to as warping. As restraint, gravity, and traffic loads pull down on the uplifted edges of the slab, tensile stresses develop.

Autogenous shrinkage is internal self-desiccation caused by a reduction in the relative humidity of the concrete due to the partial emptying of water from capillary pores [20]. Once the water content inside the pores drops so that a water-vapor interface is formed, the same mechanism that causes drying shrinkage occurs causing a net shrinkage. The volume occupied by the hydration products is less than that of the unreacted cement and water [21]. This becomes a concern

in concrete mixtures having a water-cementitious materials ratio (w/cm) typically below 0.45 [22] since the consumption of water will be greater, leaving anhydrous cement to react with water in the pores. Autogenous shrinkage has become more of a problem as an increase in demand for high performance concrete and rapid repair materials has led to more concrete mixtures with lower w/cm ratios. Clemmens et al. studied the chemical shrinkage of paste specimens containing both calcium chloride and calcium nitrate and concluded that calcium nitrate mixtures experience higher chemical shrinkage. Clemmens attributed this possibly to a change in gel morphology or gel composition.

2.2.2 Shrinkage Due to Temperature Gradient

The temperature development in concrete pavement is affected by cement mineralogy, fineness, water-cement ratio (w/c), and chemical admixtures along with many other factors. This study examines the effects of concrete heat of hydration, placement temperature, chemical admixtures, and environmental factors on the temperature development and cracking potential of concrete. The reaction between water and cement is exothermic [23], which means it releases heat. As the temperature within the concrete increases from the heat of hydration, the rate of hydration increases, further increasing the temperature. This early increase in heat causes expansion in concrete. After the initial temperature rise, the concrete starts to cool until its temperature matches the ambient temperature. This change in temperature causes a temperature gradient throughout the cross section of the concrete as the outside cools much quicker than the inside. This temperature gradient causes stress concentrations as the outside contracts while the inside is still in an expanded state. The change in temperature also causes thermal contraction in the hardened concrete. This bulk thermal deformation which is restrained by the concrete surroundings causes tensile stresses which may lead to cracking.

Change in ambient temperature causes a temperature gradient throughout the concrete pavement. As the ambient temperature decreases at night, the surface of the slab contracts greater than the warmer, bottom section of the slab. This causes the slab to encounter curling, where the edges of the slab are curved upward due to this temperature gradient. During the day, the temperature gradient of the slab will switch, and the slab will tend to curve downward as the surface of the slab expands due to the warmer air above it. When restrained or when traffic loads are applied, curling can cause tensile stresses which may lead to cracking.

Accelerators are known to increase heat generation of concrete mixtures. As the dosage level of an accelerator is increased or as accelerators are added to high cement content mixtures, an increased risk of thermal and shrinkage cracking is present due to rapid stiffening and increased heat evolution [5]. Poole et al. observed calcium nitrate specifically to increase heat of hydration while showing it to also decrease activation energy when combined with a lignosulfonate plasticizer [24].

Although some of the published literature may show increased shrinkage or thermal gradients with the addition of calcium chloride or calcium nitrate, the tensile strength of these mixtures must also be accounted for to determine the overall cracking probability of each mixture.

2.3 Non-Standard Testing of Concrete

2.3.1 Semi-Adiabatic Calorimetry

As mentioned previously, the hydration of cementitious materials is an exothermic process that encompasses chemical and physical reactions between cement and water [25]–[27]. These reactions are accelerated by higher temperatures, which cause an increase in the rate at which heat

is produced, further increasing the temperature of the concrete [28]. The heat generated by the cementitious materials influences several aspects of concrete such as thermal stresses and strength gain, especially during the early ages. Furthermore, the type and amount of cementitious materials and environmental conditions are among the driving forces that control the mixture's behavior and performance. Research efforts have been focused on assessing the hydration characteristics of concrete mixtures by determining the temperature rise of the mixture in order to minimize concrete cracking potential.

Adiabatic and semi-adiabatic calorimetry systems have been developed to assess the heat generated in concrete mixtures. The latter is a more economical and practical alternative in measuring the adiabatic temperature development of concrete mixtures. Adiabatic calorimetry requires an adiabatic process in which no heat loss or gain from a system's surroundings can occur. The adiabatic temperature rise provides the basis for simulating temperature development in a concrete member during hardening. RILEM, the International Union of Laboratories and Experts in Construction Materials, Systems and Structures, defines an adiabatic calorimeter as a "calorimeter in which the temperature loss of the sample is not greater than 0.02 K/h"[29], while a semi-adiabatic calorimeter is defined as one where "heat losses are less than 100 J/(h·K)"[29]. Because of the difficulty and expensive equipment needed to eliminate heat gain or loss in an adiabatic calorimetry test, semi-adiabatic testing was developed to estimate the adiabatic heat generated by a mixture. Due to the inherent hydration characteristics of the constituents of the concrete mixture, other physical and chemical properties of the mixture are used to estimate the adiabatic temperature rise from the measured heat rise and heat loss from the semi-adiabatic tests.

Semi-adiabatic calorimetry is used to measure the heat loss of a concrete specimen which has been minimized with the use of insulation rather than ensuring that no heat is lost from the concrete specimen such as with adiabatic calorimetry [30]. This measured heat loss and the concrete measured temperature can be used to calculate the adiabatic temperature of the specimen. However, in an adiabatic system, the heat lost from the semi-adiabatic test would have contributed to a higher temperature and therefore, a higher rate of hydration. As a result, a model is used to predict the semi-adiabatic temperature curve from an assumed adiabatic temperature rise and the measured heat loss. The true adiabatic temperature is then estimated by changing the assumed adiabatic temperature rise until the calculated semi-adiabatic temperature matches the measured semi-adiabatic temperature development. Currently, there is no standard testing methodology established for semi-adiabatic testing. As a result, this study follows the guidelines outlined in prominent literature [29], [31]. Since no standard of testing is currently available, the steps outlined in the “Hydration Study of Cementitious Materials using Semi-Adiabatic Calorimetry” by Poole et al. were followed closely to determine the adiabatic temperature rise. The procedure is outlined in section 3.2.5.

2.3.2 Free Shrinkage

One testing device used to measure autogenous shrinkage is the free shrinkage frame [32]. This test method measures the uniaxial strain of a concrete specimen that is not under restraint. The specimen is fully sealed by plastic sheets to prevent drying shrinkage, and is able to freely move as lubricant is used between the layers of plastic. Movable plates are used until the concrete reaches final set, at which time they are “backed off” to allow the free movement from expansion or contraction.

2.3.3 Rigid Cracking Frame

The effect of admixtures on the early-age concrete tensile stress development due to restraint is of great concern. The rigid cracking frame was developed by Springenschmid at the Technical University of Munich to compare the cracking resistance of different mixtures under restraint [33]. In the rigid cracking frame, a concrete specimen with a center cross section of 4x4 inch is restrained on both sides by dovetail-like crossheads as shown in Figure 1. Copper pipes run along the inside of the sides and top and bottom of the copper sheeting to allow for controlled temperature testing. The two metal crossheads are also hollow allowing a temperature controlled fluid to pass through them. Two 4 inch diameter invar bars are bolted to the crossheads on both sides. Strain gages are attached to the invar bars and used to measure the strain of each bar to then determine the load on the frame using calibration factors which are discussed later. This restraint reduces the contraction or expansion, due to shrinkage or thermal deformations, and transforms volume changes into restraint stresses which are measured through the invar bars. The degree of restraint can be calculated using the modulus of elasticity of the concrete, E_c , as shown in Equation 1 [30]:

$$\delta = \frac{100}{1 + \frac{E_c A_c}{E_s A_s}} \quad \text{Equation 1}$$

where δ = concrete degree of restraint; E_c , E_s = modulus of elasticity of concrete and invar, respectively (psi); A_c and A_s = cross-sectional areas of the concrete and invar bar, respectively (in²)

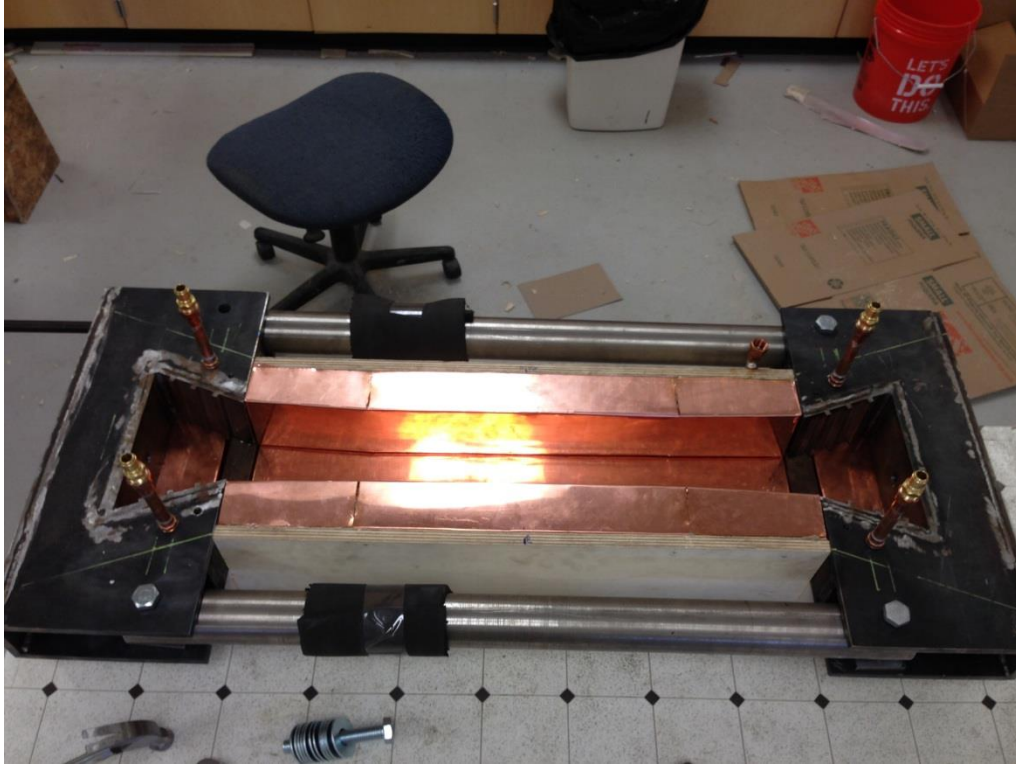


Figure 1: RCF During Construction

Rigid cracking frame tests measure the concrete stress under uniaxial compression and tension conditions and do not include the effects of warping and curling or drying shrinkage. Nevertheless, they provide a relative comparison of early-age concrete behavior.

2.4 Modeling

2.4.1 HIPERPAV

To simulate early age induced tensile stress development, any model used should take into account the changing thermal and moisture gradients in the pavement, the changing concrete elastic modulus as the concrete ages, restraint by the subbase, and the high levels of stress relaxation at early ages. Several software packages have been developed to assess the cracking risk associated with changing specific parameters that affect the first 72 hours of concrete

performance. In this research, the Federal Highway Administration (FHWA) sponsored software package HIPERPAV was used to predict the cracking risks associated with different mixtures.

In 1996, The Transtec Group, Inc., supported by FHWA, developed a concrete pavement software package, HIgh PERformance PAVing (HIPERPAV), to model the effects of different combinations of design, construction, and environmental factors on the early-age behavior (first 72 hours) of concrete pavements [34]. A more recent version of the HIPERPAV software, with modeling enhancements and strategy comparisons (HIPERPAV III) was used to predict the stress-strength relationship during the early age of six concrete mixtures used for pavement slabs.

The HIPERPAV III software is comprised of multiple individual modules, which are used together to predict the evolution of several properties such as temperature, modulus, restraint, stress, and strength of concrete mixtures. The parameters modeled, interdependence of these models, and how they are used to calculate the early-age cracking risk of the concrete pavement slab are shown in Figure 2 [35]–[37].

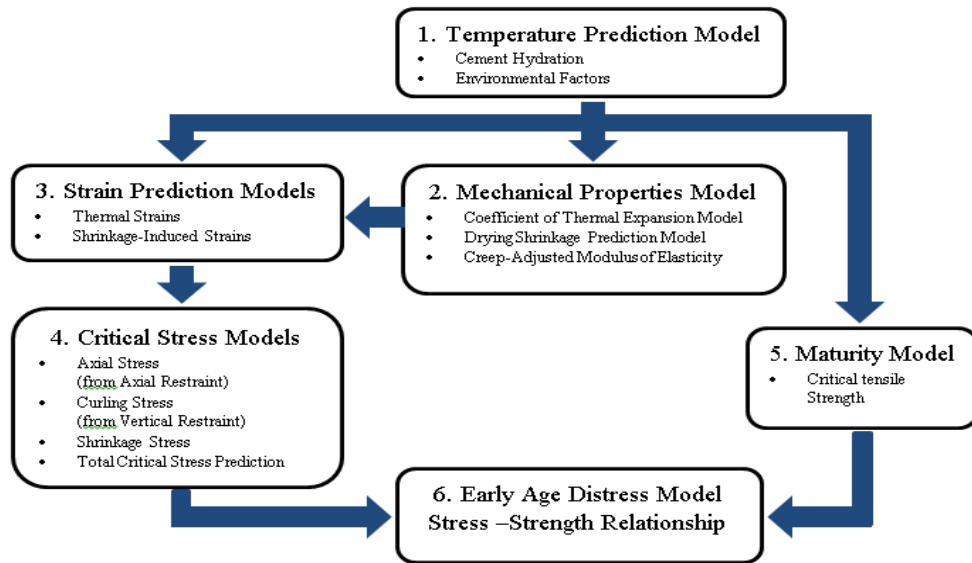


Figure 2: HIPERPAV III Modeling Flowchart

The steps outlined in the flow chart which are used to predict the stress-strength relationship are described, in more detail, as follows [5]-[8]:

1. HIPERPAV III first uses the experimentally determined hydration data and the environmental factors of each location to predict the concrete temperature model for each mixture. The equation used to determine the total heat of hydration of cement, H_u , is shown in Equation 2 [36]:

$$H_u = p_{C_3S}H_{C_3S} + p_{C_2S}H_{C_2S} + p_{C_3A}H_{C_3A} + p_{C_4AF}H_{C_4AF} + p_C H_C + p_{MgO}H_{MgO} \quad \text{Equation 2}$$

where H_i =heat of hydration of each compound(J/g); p_i =fraction by mass of each compound; H_u = ultimate heat of hydration (J/g)

The boundary conditions affecting heat transfer associated with the concrete pavement slab are different for the top and bottom of the slab. The top of the slab is subjected to the daily environmental conditions; therefore, convection, irradiation, and solar absorption must be taken into account. The bottom surface of the slab is affected by conduction from the temperature of the subbase. The temperature at the top of the surface is represented by Equation 3; while the temperature on the bottom surface does not include convection or radiation [36]:

$$-k\nabla T \cdot \tilde{n} + q_c + q_r - q_s = 0 \quad \text{Equation 3}$$

where k =thermal conductivity (W/m·°C); ∇T =temperature gradient (°C/mm); q_c =heat flux due to convection (W/m³); q_r =heat flux due to irradiation (W/m³); q_s =solar radiation absorption (W/m³); \tilde{n} =direction of heat flow by vector notation

After taking into account the heat of hydration and environmental factors, the concrete temperature can be calculated using the general model of heat transfer in two dimensions as shown in Equation 4 [38]:

$$k_x \cdot \frac{d^2T}{dx^2} + k_y \cdot \frac{d^2T}{dy^2} + Q_h(t, T) = \rho \cdot C_p \cdot \frac{dT}{dt} \quad \text{Equation 4}$$

where k_x, k_y = thermal Conductivity of concrete (W/m·°C); ρ = concrete density(kg/m³); C_p = specific heat (J/kg°C); Q_h = Heat generated from Heat of Hydration and External Sources (W/m³); T = concrete temperature at specified location (°C); t = time (s)

2. HIPERPAV III uses the predicted temperature model to predict the mechanical properties of the concrete such as tensile strength, age dependent coefficient of thermal expansion (CTE), modulus of elasticity, and drying shrinkage.

The maturity method outlined in ASTM 1074 is used to calculate the equivalent age of each mixture to determine the tensile strength of the concrete as it evolves with age. The equivalent age of the concrete and degree of hydration equations are presented in Equation 5 and Equation 6. The compressive or tensile strength can be calculated using the degree of hydration parameters. For HIPERPAV III, the tensile strength was used since it is to be compared to the induced tensile stresses. The tensile strength equation is shown in Equation 7 [36]:

$$t_e(T_r) = \sum_{t=0}^t \exp \left[\left(\frac{-E_a}{R} \right) \cdot \left(\frac{1}{273 + T_c} - \frac{1}{273 + T_r} \right) \Delta t \right] \quad \text{Equation 5}$$

$$\alpha(t_e) = \alpha_u \exp \left[- \left(\frac{\tau}{t_e} \right)^\beta \right] \quad \text{Equation 6}$$

$$S_{tensile} = S_{28,tensile} \left(\frac{\alpha_t - \alpha_{crit}}{\alpha_{28} - \alpha_{crit}} \right) \quad \text{Equation 7}$$

where E_a = activation energy from isothermal calorimetry (J/mol); R = universal gas constant, 8.314 J/(mol·K); $t_e(T_r)$ = equivalent age at the reference temperature (hours); T_r = reference temperature (°C); T_c =Concrete temperature at time interval (°C); Δt = time interval (hours); $\alpha(t_e)$ = degree of hydration at equivalent age, t_e ; α_u =ultimate degree of hydration; τ, β = time and shape parameters, respectively; α_t =degree of hydration at specific time; α_{crit} =degree of hydration at final set; α_{28} =degree of hydration 28 days $S_{tensile}$ = tensile strength of concrete at age t (lbf/in²); $S_{28, tensile}$ = 28-day tensile strength of concrete from laboratory testing

3. The CTE is essential in simulating the thermally-induced deformations of the concrete slab. The CTE of the concrete mixture is calculated using the CTE of both the paste, which drastically decreases with age, and the aggregate as expressed in Equation 8 [36]:

$$\psi_{conc} = C_m \left[\sum_{i=1}^{\# \text{ of agg}} \left(\psi_{agg,i} \frac{V_{agg,i}}{V_{conc}} \right) + \left(\psi_{paste} \frac{V_{paste}}{V_{conc}} \right) \right] \quad \text{Equation 8}$$

where ψ_{conc} = age-dependent CTE of concrete mixture ($\mu\epsilon/^\circ\text{C}$); C_m = moisture correction factor; $\psi_{agg,i}$ = age-dependent CTE of i^{th} aggregate ($\mu\epsilon/^\circ\text{C}$); ψ_{paste} = age-dependent CTE of paste; $V_{agg,i}$ = volume of i^{th} aggregate in mixture (m³); V_{paste} = volume of paste in mixture (m³); V_{conc} =total volume of concrete mixture (m³)

Concrete is a visco-elastic material with an elastic modulus that increases as the concrete hardens [1]. Because of this, the modulus of elasticity must be calculated at each age of the concrete after hardening. Through laboratory testing, the modulus of elasticity can be determined at specific test ages. To calculate the elastic modulus at the ages between the

tests, the maturity method outlined in ASTM 1074 combined with an empirically derived modulus-cement degree of hydration fit function, which is usually used to determine strength values, was modified for modulus and used. Following the Arrhenius relationship, Equation 9, which relates temperature with the rate of reaction, the equivalent age was calculated to determine the degree of hydration at each age in Equation 6. The degree of hydration can then be used to calculate the modulus of elasticity as presented in Equation 10 and Equation 11 which is very similar to the tensile strength equation used previously (Equation 7) [7, 9, 10]:

$$k = A \times \exp\left(\frac{-E_a}{RT}\right) \quad \text{Equation 9}$$

$$E_t = E_{28} \left(\frac{\alpha_t - \alpha_{crit}}{\alpha_{28} - \alpha_{crit}}\right)^{2/3} \quad \text{Equation 10}$$

$$\alpha_{crit} = 0.43 \times w/cm \quad \text{Equation 11}$$

where k= rate of heat evolution (W); T= temperature at which reaction occurs (K); A= proportionality constant (W)

To determine the ultimate drying shrinkage, the strength and elastic modulus at 28 days must be known from laboratory testing. The equation for ultimate drying shrinkage ($\epsilon_{sh\infty}$) is shown in Equation 12 [41]:

$$\epsilon_{sh\infty} = \epsilon_{s\infty} \frac{E(607)}{E(t_0 + \tau_{sh})} \quad \text{Equation 12}$$

$$E(t) = E(28) \left(\frac{t}{4 + 0.85t}\right)^{1/2} \quad \text{Equation 13}$$

$$\varepsilon_{s\infty} = C_1 C_2 [26w^{2.1}(f'c)^{-0.28} + 270] \quad \text{Equation 14}$$

$$\tau_{sh} = 190.8 t_0^{-0.08} f'c^{-0.25} (k_s D)^2 \quad \text{Equation 15}$$

where $E(t)$ = Elastic Modulus (lbf/in²) of the concrete at age t (days); t_0 = age of concrete when drying starts(days); $C_1=0.85$ for Type II cement; $C_2=1.2$ for specimens sealed during curing; w = water content of concrete (lb/ft³); $f'c$ = 28 day strength of concrete (lbf/in²); k_s =cross section shape factor, approx. 1 for slabs; D = thickness of slab (in); τ_{sh} = shrinkage half-time (days)

4. The outputs from the temperature development, modulus, and drying shrinkage models are used to predict the thermal and shrinkage-induced strains. The strains are calculated as “free strains” as if the concrete slab was unrestrained (the restraint is accounted for later in the software). The thermal strain is determined by Equation 16 [36]:

$$\nabla \varepsilon_T = \nabla T \cdot \psi_{conc} \quad \text{Equation 16}$$

where $\nabla \varepsilon_T$ =Thermal Strain Gradient ($\mu\varepsilon/\text{mm}$); ∇T =Temperature Gradient ($^{\circ}\text{C}/\text{mm}$); ψ_{conc} =CTE of concrete mixture ($\mu\varepsilon/^{\circ}\text{C}$)

The thermal strain can be resolved by two models, the curling strain model and the axial thermal strain model. The curling model adopted from Westergaard and enhanced by Bradbury is presented in Equation 17 [42]:

$$\varepsilon_{curl} = \frac{C\psi\Delta T}{2} \quad \text{Equation 17}$$

where ε_{curl} = curling strain; C = coefficient dependent on slab length and relative stiffness; ψ = coefficient of thermal expansion of concrete; ΔT = temperature differential ($^{\circ}\text{F}$)

Equation 19 shows the axial thermal strain model [36]:

$$\Delta T_z = \frac{\sum_{z=0}^h [(T_{z,current} - T_{z,final set}) \Delta z]}{h} \quad \text{Equation 18}$$

$$\varepsilon_z = \Delta T_z \psi \quad \text{Equation 19}$$

where ΔT_z = temperature differential used by axial strain model (°C); h = total slab thickness (mm); T_z = slab temperature at depth z (°C); Δz = change in depth (mm); ε_z =unrestrained axial strain

The total strain due to shrinkage(ε_{cs}) is also resolved into drying shrinkage strain (ε_{csd}) and autogenous shrinkage (ε_{cs0}). Autogenous shrinkage is calculated for concrete mixtures with w/cm ratio below 0.45 by using Equation 20 [37]:

$$\varepsilon_{cs0}(t) = \varepsilon_{s0\infty} \beta_{s0}(t) \quad \text{Equation 20}$$

$$\beta_{s0}(t) = \exp \left[- \left(\frac{t_{s0}}{t - t_{start}} \right)^{0.3} \right] \quad \text{Equation 21}$$

$$\varepsilon_{s0\infty} = \left(-0.65 + \frac{1.3w}{B} \right) \cdot 10^{-3} \quad \text{Equation 22}$$

where $\beta_{s0}(t)$ = time distribution of autogenous shrinkage; $\varepsilon_{s0\infty}$ = final value of autogenous shrinkage; t_{s0} = 5 days; t_{start} = 1 day; w = water content (kg/m^3); B = cement content + silica fume content(kg/m^3)

To predict the strain due to drying shrinkage the Equation 23 through Equation 26 are used [37]:

$$\varepsilon_{csd}(t) = \alpha_{sd} \varepsilon_{sd,tot} \beta_{sd}(t) \beta_{sd,RH} \quad \text{Equation 23}$$

$$\alpha_{sd} = \frac{u \cdot l_{sd}}{A_c} \leq 1 \quad \text{Equation 24}$$

$$l_{sd} = \frac{l_{sd,ref}}{0.5 - \frac{w}{B}} \quad \text{Equation 25}$$

$$\beta_{sd}(t) = \left(\frac{t - t_s}{t_{sd} + t - t_s} \right)^{0.5} \quad \text{Equation 26}$$

where $\varepsilon_{csd}(t)$ = additional strain due to drying/wetting of concrete; α_{sd} = cross section affected by surface drying; $\varepsilon_{sd,tot}$ = final drying shrinkage; $\beta_{sd,RH}$ =coefficient of drying shrinkage; $\beta_{sd}(t)$ = time development of drying shrinkage; u = perimeter of cross section subject to environmental humidity; A_c = cross section perpendicular to water flow; l_{sd} =length of surface for water exchange; $l_{sd,ref}$ =0.0045 m; $t-t_s$ = time after start of drying and wetting (days); t_s = age of concrete at start of drying and wetting (>1 day); t_{sd} = 200 days, typical rate of humidity exchange

Stress relaxation occurs in concrete at especially high rates at early ages. This results in early-age concrete stresses significantly different than what calculated elastic stresses would indicate. In HIPERPAV, these effects are calculated using a creep-adjusted modulus [36]. The stresses are calculated using the base restraint, strain, and creep adjusted modulus. Equation 27 through Equation 29 are used in HIPERPAV to determine the modulus after this stress relaxation is accounted for [36]:

$$E_{eff} = \frac{E_0}{|1 + J_t E_0|} \quad \text{Equation 27}$$

$$J_t = J'_t \delta_t \xi_t \Phi_t \quad \text{Equation 28}$$

$$J'_t = [28.74(1 - e^{-0.801t}) + 8.13(1 - e^{-45.38t}) + 4.468t] \quad \text{Equation 29}$$

$$\times 10^{-6}$$

where E_0 = Elastic modulus at time of load application(final set); J_t = adjusted creep factor (mm^2/N); J'_t = creep factor (mm^2/N); δ_t =stress correction factor; $\delta_t = 0.017\sigma + .701$;

ξ_t =loading time correction factor; $\xi_t=-1.107\ln(\tau)+1.538$; Φ_t =temperature correction factor; $\Phi_t=0.0257T+0.487$; T=age of concrete(days); σ = average concrete stress(N/mm²)
 τ = time from start of loading (days); T= average concrete temperature(°C)

5. The critical stress models include the previously calculated axial restraint and axial stresses, vertical restraint and curling stresses, and shrinkage stresses. The maximum tensile stress resulting from these strains is then used to determine the critical stress for the early age concrete pavement slab as shown in Equation 30 [36]:

$$\sigma_{critical} = MAX_{TENSILE} \left\{ \begin{array}{l} (\varepsilon_{axial,top} + \varepsilon_{cs}) \times R_F \times E_{eff} + \sigma_{curl,top} \\ \varepsilon_{axial,mid} \times R_F \times E_{eff} \\ \varepsilon_{axial,bottom} \times R_F \times E_{eff} + \sigma_{curl,bottom} \\ 0 \end{array} \right\} \quad \text{Equation 30}$$

where R_F = Restraint factor, function of base type, joint spacing, thickness, modulus

6. After predicting the concrete temperature, CTE, shrinkage, creep-adjusted modulus of elasticity, free strains, and the resulting stresses from restraint, the total critical stresses of the concrete pavement slab at each age can be compared to the concrete's predicted strength at the same age. From this comparison, the cracking risk for the first 72 hours of the concrete pavement slab can be assessed. As shown in Figure 3, HIPERPAV III displays the results in an analysis tab which shows the critical stresses at the bottom of the slab in blue, critical stresses at the top of the slab in yellow, the maximum critical stress as a solid red line, and the tensile strength of the concrete slab as a solid blue line. If the stress exceeds the strength as shown in this sample figure, HIPERPAV III displays a warning at that respective age. However, since cracking can initiate if the tensile stresses in the concrete pavement are about 70 percent of the ultimate tensile strength of concrete [43],

steps should be taken to not only keep the induced tensile stresses below the tensile strengths, but also to ensure that these stresses are minimized as much as possible.

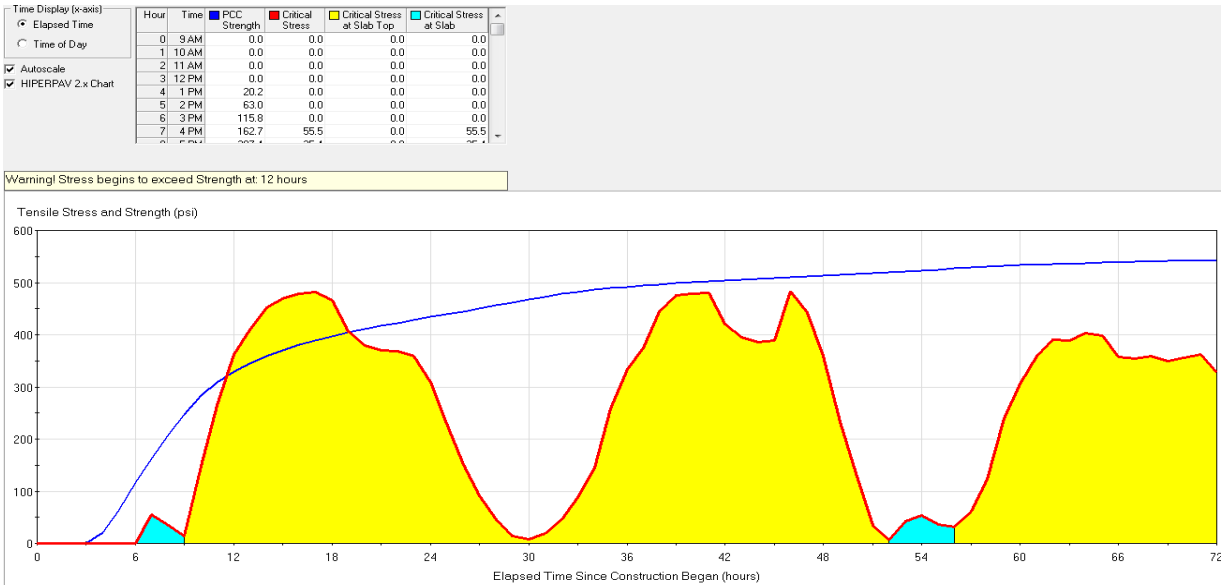


Figure 3: HIPERPAV III Sample Analysis Output

2.4.2 ConcreteWorks

ConcreteWorks was designed at the Concrete Durability Center at the University of Texas to be a user-friendly software package which allows contractors to optimize the concrete mixture proportioning, perform temperature and thermal analysis on mass concrete elements, perform concrete pavement temperature simulations, and calculate the chloride service life analysis of mass concrete and bridge deck members [21]. ConcreteWorks, with its built-in material behavior models, allows engineers and contractors to model early age temperature development while reducing the amount of laboratory testing needed [30]. Unlike HIPERPAV, ConcreteWorks shows the predicted temperature as an output. The software uses the same concepts as HIPERPAV in modeling and predicting concrete temperature.

CHAPTER 3: MATERIALS AND METHODS²

3.1 Materials

Six concrete mixtures were prepared for this study to compare the calcium chloride-based accelerator with the calcium nitrate-based accelerator at different dosages. Four of the mixtures included either a calcium chloride-based accelerator (CA) or a calcium nitrate-based accelerator (CHAD, CAD, CDAD), both in compliance with ASTM C494 – Type E [44]. To represent field mixtures, the mixtures containing either accelerator also included a water reducing/retarding admixture meeting ASTM C494 - Type D, and an air-entraining admixture which complies with ASTM C260 [45]. For this reason, two control mixtures without accelerator were used: the first control, C, did not have any admixtures, while the second, CNA, included the water reducing/retarding and air entraining admixtures without any accelerator.

3.1.1 Cement Properties

The same Type I/II cement was used for all mixtures; its oxide chemical composition, potential compound composition, mineralogical and physical properties are shown in Table 1 through Table 3. The mineralogical composition was determined using Rietveld refinement in accordance with ASTM C1365 [46] and the fineness was determined using a Blaine apparatus and Method A of ASTM C204 [47].

² Portions of this chapter were previously published in [48]. Permission is included in Appendix A.

Table 1: Oxide Chemical Composition of As-Received Cement [48]

Analyze	Type I/II cement (wt %)
SiO ₂	20.40
Al ₂ O ₃	5.20
Fe ₂ O ₃	3.20
CaO	63.10
MgO	0.80
SO ₃	3.60
Na ₂ O	0.10
K ₂ O	0.38
TiO ₂	0.28
P ₂ O ₅	0.12
Mn ₂ O ₃	0.03
SrO	0.08
Cr ₂ O ₃	0.01
ZnO	<0.01
L.O.I(950°C)	2.80
Total	100.10
Na ₂ O _{eq}	0.35
Free CaO	2.23
SO ₃ /Al ₂ O ₃	0.69

* Test conducted by a certified commercial laboratory

Table 2: Bogue-calculated Potential Compound Content for As – Received Cement [48]

Phase	Type I/II (w/o lime Correction)	Type I/II (with lime Correction)
C ₃ S	52	50

Table 2 Continued

C ₂ S	19	19
C ₃ A	8	8
C ₄ AF	10	9
C ₄ AF+2C ₃ A	26	26
C ₃ S+4.75C ₃ A	92	89

Table 3: Cement Mineralogical Composition Using Rietveld Analysis and Fineness [48]

Cement Phase	Type I/II
Tricalcium Silicate, C ₃ S (%)	52.0
Dicalcium Silicate, C ₂ S (%)	20.7
Tricalcium Aluminate, C ₃ A (%)	10.2
Tetracalcium Aluminoferrite, C ₄ AF (%)	5.7
Gypsum	4.4
Hemihydrate	1.6
Anhydrite	0.2
Calcite	2.1
Lime	0.1
Portlandite	2.0
Quartz	0.9
ASTM C204-Blaine Fineness (m ² /kg)	442

3.1.2 Chemical Admixtures

Both accelerators used in this study were commercially developed for use where accelerated set and hardening properties of concrete are required. Due to this, the accelerators were a mixture of chemicals, not just calcium chloride or calcium nitrate. Table 4 shows the composition of each accelerator based on their respective Material Safety Data Sheets (MSDS).

Table 4: Chemical Admixture Compositions

Admixture	Component	Percent (max)
Calcium-Nitrate Based Type E	Calcium nitrate	30-50%
	Calcium nitrite	2-5%
	Sodium thiocyanate	2-5%
	TEA	0.1-1%
Calcium-Chloride Based Type E	Calcium chloride	25-50%
	Potassium chloride	1-10%
	Sodium chloride	1-10%
	TEA	1-10%
Calcium-Lignosulfonate Based Type D	Sulfite liquors and cooking liquors, spent, alkali-treated	25-50%
	Molasses	10-25%
	TEA	1-10%
Air Entraining Admixture (AEA)	Fatty acids, tall oil, sodium salts	2-5%
	Fatty acids, tall oil, potassium salts	2-5%

The calcium nitrate-based accelerator also included small amounts of calcium nitrite, sodium thiocyanate, and TEA for their hardening properties. Calcium nitrite has been a very popular chloride-free accelerator since patented in 1969 [49]; it has been shown to be a very effective form of protection from corrosion [17], [49]–[51] and has shown strength development comparable to calcium chloride [14]. Sodium thiocyanate is added to concrete mixtures as a hardening accelerator. Justnes described it as possibly the “most promising single compound” as a hardening accelerator showing compressive mortar strength increase of 121% after 1 day at 20°C and 113% at two days at 5°C [8]. Calorimetry measurements by Abdelrazig et al. showed sodium thiocyanate to have a small effect on shortening the induction period with a large increase in the main hydration peak [17]. Small dosages of TEA are usually used with other accelerators and rarely by itself as it has been shown to have an accelerating effect on the hydration of tricalcium aluminate, C₃A [4].

Table 4 shows the composition of the water reducer/retarder used in the mixtures. The admixture is calcium lignosulfonate-based and also includes TEA; at high dosages, it causes retardation of C_3S hydration [14]. Since both the accelerator and the water reducer/retarder contain TEA, its dosage throughout the mixture is likely high.

The composition of the air entraining admixture used in this study is also shown in Table 4. The dosage of the air-entrainer was very low as the intended location of these mixtures was not subjected to freeze thaw conditions. It is not expected to affect hydration kinetics or the apparent activation energy as shown previously by Poole et al. [24].

3.1.3 Aggregates

Aggregates selected were typical of materials used by the Florida Department of Transportation (FDOT) for concrete repair slabs. An Oolitic limestone in accordance with ASTM C33 #57 [52] was used as a coarse aggregate. The measured specific gravity (SSD) is 2.49 and the absorption capacity is 3.04%. Siliceous sand was used as a fine aggregate with a specific gravity (SSD) of 2.64, an absorption capacity of 0.34%, and a fineness modulus of 2.35.

A stock sample of both the fine and coarse aggregate was graded. The gradation of coarse and fine aggregates as used in concrete mixtures are shown in Figure 4 and Figure 5. In preparing concrete mixes, aggregates were graded and then compiled according to the grading curves presented here in order to maintain uniformity.

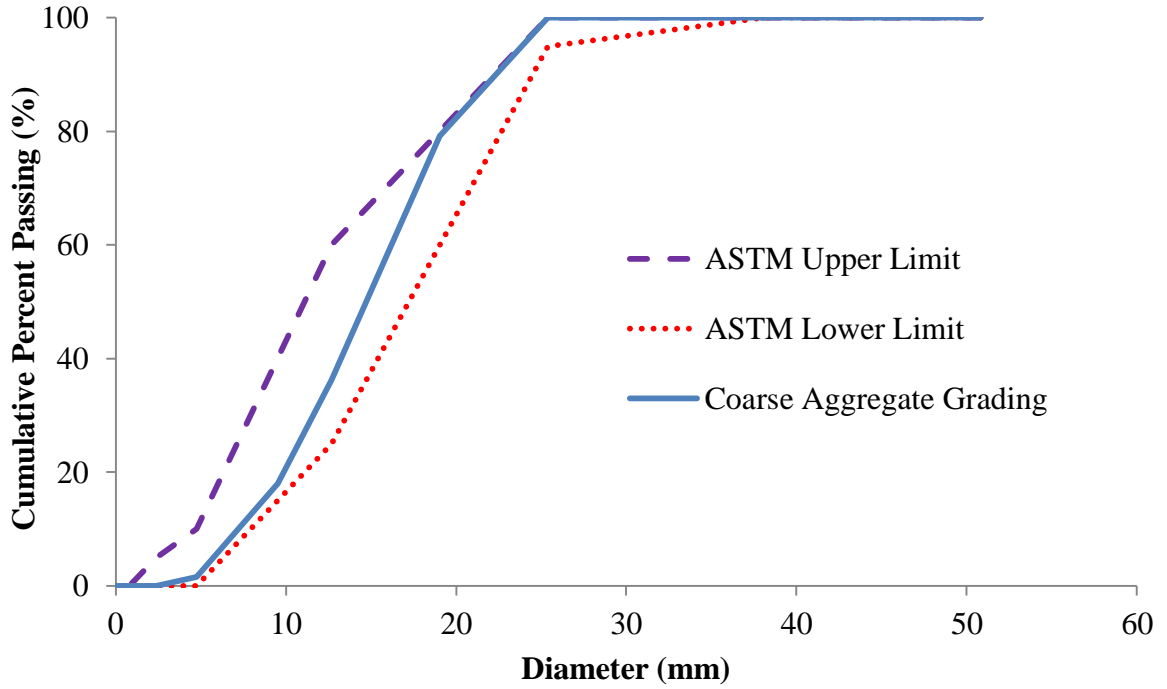


Figure 4: Coarse Aggregate Gradation

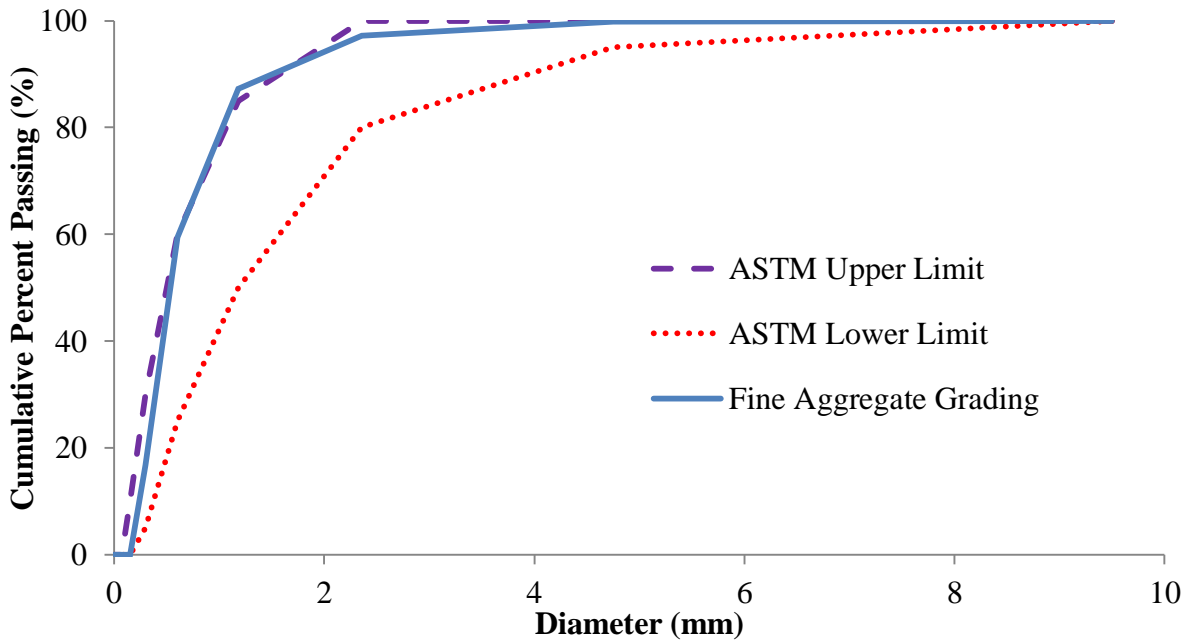


Figure 5: Fine Aggregate Gradation

3.1.4 Concrete Mixture Designs

Table 5 shows the six concrete mixture designs used throughout this study. CA is the approved FDOT mixture design containing the calcium chloride-based accelerator. The single dosage for the calcium-nitrate accelerator, CAD, was based on a similar set time at 38°C as the single dosage calcium chloride-based accelerator, CA, since many repair slabs are mixed at higher temperatures to gain high early strength. CHAD is the same mixture design as CAD except it has half of the calcium nitrate based accelerator dosage, while CDAD has double the CAD amount.

Table 5: Mixture Design per Cubic Yard

Materials	Mixture					
	C	CNA	CA	CHAD	CAD	CDAD
Cement (lb/yd ³)	900	900	900	900	900	900
Coarse Agg (SSD) ((lb/yd ³)	1680	1680	1680	1680	1680	1680
Fine Agg (SSD) ((lb/yd ³)	831	831	831	831	831	831
Mixture Water ((lb/yd ³)	348	348	325	333	321	296
AEA (oz/100 lbs cement)	-	0.33	0.33	0.33	0.33	0.33
Type D (oz/100 lbs cement)	-	5	5	5	5	5
Type E (chloride-based) (oz/100 lbs cement)	-	-	42.7	-	-	-
Type E (nitrate-based) (oz/100 lbs cement)	-	-	-	32	64	128
w/c ratio	0.38	0.38	0.38	0.38	0.38	0.38

In order to maintain a constant water-cement ratio (w/c), of 0.38, the amount of mixing water added was adjusted for each mixture to account for the water present in the accelerating admixtures. The calcium chloride-based accelerator had a water content of 61%, while the calcium

nitrate-based accelerator had a water content of 46%. The water from the AEA and Type D admixtures was low and therefore was not taken into account.

3.2 Experimental Testing

3.2.1 Mixing Procedure

The coarse aggregate was brought to a saturated surface dry condition (SSD) at least 24 hours before mixing. This was accomplished by assessing the water required to bring the aggregates to the SSD condition from an oven dry (OD) moisture state using the absorption capacity of the coarse aggregates. This protocol is necessary in order to ensure that the aggregates pore structure, accessible to the aggregate surface, is completely filled with water prior to mixing. Due to a very low absorption capacity, the fine aggregate was left in the OD state, and the low amount of water needed to attain the SSD condition was added back to the mixing water. The admixtures were batched in the order recommended by the admixtures manufacturer. The air entraining admixture was first added in with the coarse and fine aggregates, while the Type D admixture was added to the mixing water. Once the cement and then water were added, the concrete was mixed for three minutes followed by a three minute rest period. The concrete was mixed for two more minutes before the Type E admixture was added. Mixing was resumed for another 30 seconds to one minute to ensure the accelerator was mixed properly.

3.2.2 Fresh Concrete Properties

The fresh concrete properties of each mixture were measured and used in the semi-adiabatic calorimetry data analysis. Air content, unit weight and slump measurements were conducted in accordance with ASTM C231 [53], ASTM C138 [54], and ASTM C143 [55], respectively.

3.2.3 Maturity

Following ASTM C1074, the equivalent age and strength-based apparent activation energy of each mixture was determined. Mortar cubes, 2x2x2 inch³, were prepared and tested in accordance with ASTM C109 [56]. The cubes were mixed and cured at three different temperatures: 23°C, 38°C, and 53°C. The activation energy was first calculated and then used with the recorded concrete temperature and strength data to calculate the equivalent age. Both the strength-based apparent activation energy and the equivalent age of each mixture were used as inputs in HIPERPAV modeling.

3.2.4 Isothermal Calorimetry

In order to assess the effects of accelerators, type and dosage, on temperature rise due to cement hydration, heat of hydration measurements [57] were conducted using a TAM Air isothermal calorimeter manufactured by TA Instruments. The isothermal calorimetry testing was also used to calculate the heat of hydration-based apparent activation energy. Paste samples were mixed following the internal mixing procedures in accordance with ASTM 1702 method A [58] at three temperatures: 23°C, 38°C, and 48°C. The same 0.38 w/c ratio was used for these paste samples. The effects of the admixtures on the rate of heat release were observed in the shifts in time and peak height of the hydration peaks of the mixtures. The first hydration peak occurs immediately upon mixing and is associated with ionic dissolution. The second hydration peak is due to the tricalcium silicate (C₃S) phase, while the third is attributed to the exhaustion of sulfates [2]. The effects of the admixtures on the second and third hydration peaks were studied.

3.2.5 Semi-adiabatic Calorimetry

A total of 6 different concrete mixtures were prepared for this portion of the study with the primary goal of assessing the effects of variable dose of a nitrate-based accelerator versus a chloride-based accelerator on the cracking potential of concrete pavement slabs. From semi-adiabatic calorimetry tests, the hydration parameters, α_u , β , and τ that describe the concrete adiabatic heat of hydration (amount and rate) behavior were determined. The hydration parameters are necessary inputs to operate HIPERPAV modeling of concrete cracking potential.

Semi-adiabatic calorimetry measurements were conducted using the equipment constructed at the University of South Florida [48]. Three semi-adiabatic calorimeters were made and used for testing to verify the consistency of the testing method and accuracy of the reported values. 6x12inch concrete cylinders were prepared and placed in the individual calorimeters which recorded the temperature at three locations – MID, EXT 1 and EXT 2– every five minutes for 150 hours. A schematic diagram showing the details of the calorimeters is presented in Figure 6.

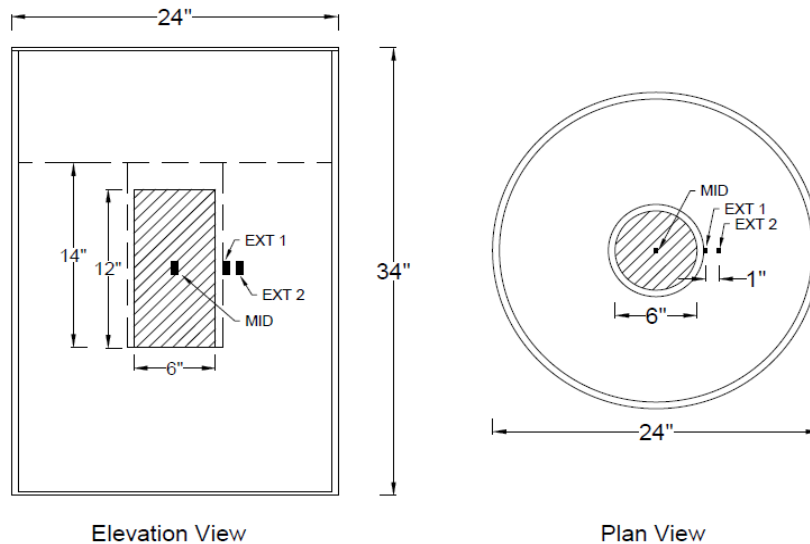


Figure 6: Semi-Adiabatic Calorimeter Detail

Type T thermocouples were used to measure the temperature at the center of the concrete specimen and at two specific locations within the insulation. The center thermocouple (MID) was placed 6 inches into the center of the fresh concrete. A plug-in for this thermocouple is available at the edge of the opening as seen in Figure 7. A second thermocouple (EXT 1) was attached at the inner edge of the insulation, just outside of the cylindrical void. A third thermocouple (EXT 2) was embedded in the insulation, 1 inch away from second thermocouple. Since the thickness of material and temperature of each thermocouple can be measured at specific locations, the insulating properties of the calorimeter can be determined through a calibration process described later in this section. After initial testing, it was assessed that the heat loss between the second and third thermocouple produce more consistent test results. For this reason, the heat flux between these thermocouples was used for the calculations.



Figure 7: Middle Thermocouple Placed and Plugged In

Pico Technology hardware and software was used to record and collect the temperatures. PicoLog Recorder software recorded data using a USB TC-08 thermocouple data logger to collect the temperatures at each calorimeter and the room temperature with an accuracy of $\pm 0.5^{\circ}\text{C}$.

Temperature measurements from the thermocouples were recorded for a minimum of 160 hours after the concrete was initially placed.

Obtaining the adiabatic temperature rise for a concrete mixture involved calibration of the semi-adiabatic calorimeter, determining mixture temperature sensitivity through isothermal calorimetry, preparing each concrete mixture for testing, and analyzing the data collected during the test. Since no standard of testing is currently available, the steps outlined in the “Hydration Study of Cementitious Materials using Semi-Adiabatic Calorimetry” by Poole et al. were followed closely to determine the adiabatic temperature rise. The following 14 steps were taken to determine the adiabatic temperature rise of each mixture [25]:

1. A calibration test was performed on the semi-adiabatic calorimeters to determine the specific calibration factors. Calibration of the semi-adiabatic calorimeter was an important step in obtaining the adiabatic temperature rise of the concrete mixture as it provided a means to establish a baseline of potential heat loss by the instrument. The calibration protocol described in [25] was used for the calorimeters, and the rate of heat loss, or correction factors (C_{f1} , C_{f2}), was computed. De-ionized water was used in calibrating the calorimeters since it has a known density of $1,000 \text{ kg/m}^3$ and a known specific heat of $4,186 \text{ J/(kg}\cdot\text{°C)}$. It is preferable to heat the water sample to the potential temperature of the concrete structure; therefore, the water sample in this study was heated to 80°C and put into a 6x12 inch cylindrical mold. The cylinder was weighed before and after filling it with the heated water, and then placed into the calorimeter. The following steps (A-D) were then used to calculate the calibration factors (C_{f1} C_{f2}):

- A. Record the time (t in hrs), water temperature (T_w in $^{\circ}\text{C}$), and heat loss between the two external thermocouples (T_d in $^{\circ}\text{C}$) at 5 minute intervals for 160 hours. The first 5 hours of data was not used since the interior of the calorimeter had to first stabilize with the higher temperature of the test specimen.
- B. Calculate the change in temperature of the water (ΔT_w) at each time, t, and record the sum of the changes in temperature ($\Sigma \Delta T_w$).
- C. Model the change in temperature of the water using its known density, ρ_w , and specific heat of water, $C_{p,w}$, with the calibration factors (C_{f1} and C_{f2}) using Equation 31 and Equation 32:

$$\Delta q_h = T_d \cdot (-C_{f1} \cdot \ln(t) + C_{f2}) \quad \text{Equation 31}$$

where Δq_h = heat transfer ($\text{J/h} \cdot \text{m}^3$); T_d = change in temperature between thermocouples Ext 1 and Ext 2; C_{f1} = Calibration factor ($\text{W}/^{\circ}\text{C}$); C_{f2} = Calibration factor ($\text{W}/^{\circ}\text{C}$); t = time elapsed from start of test (hrs)

$$\sum \Delta T_w^* = \sum \frac{\Delta q_h \cdot \Delta t}{\rho_w \cdot C_{p,w} \cdot V_w} \quad \text{Equation 32}$$

where $\Sigma \Delta T_w^*$ = the sum of the modeled change in water temperature ($^{\circ}\text{C}$); ρ_w = density of water ($1000 \text{ kg}/\text{m}^3$); $C_{p,w}$ = specific heat of water ($4,186 \text{ J}/\text{kg} \cdot ^{\circ}\text{C}$); V_w = volume of water sample (m^3); Δt = time step (s)

- D. Perform a regression analysis using the R-squared method with the Solver function in MS Excel to match the modeled change in water temperature to the measured change in water temperature. The Solver function generates the best fit calibration factors (C_{f1} and C_{f2}) which are used to model the change in water temperature.

- Place the concrete mixture in the mold and weigh the mold. Place the concrete in the calorimeter and record the concrete temperature and time every 5 minutes for the first 160 hours as shown in Figure 8.

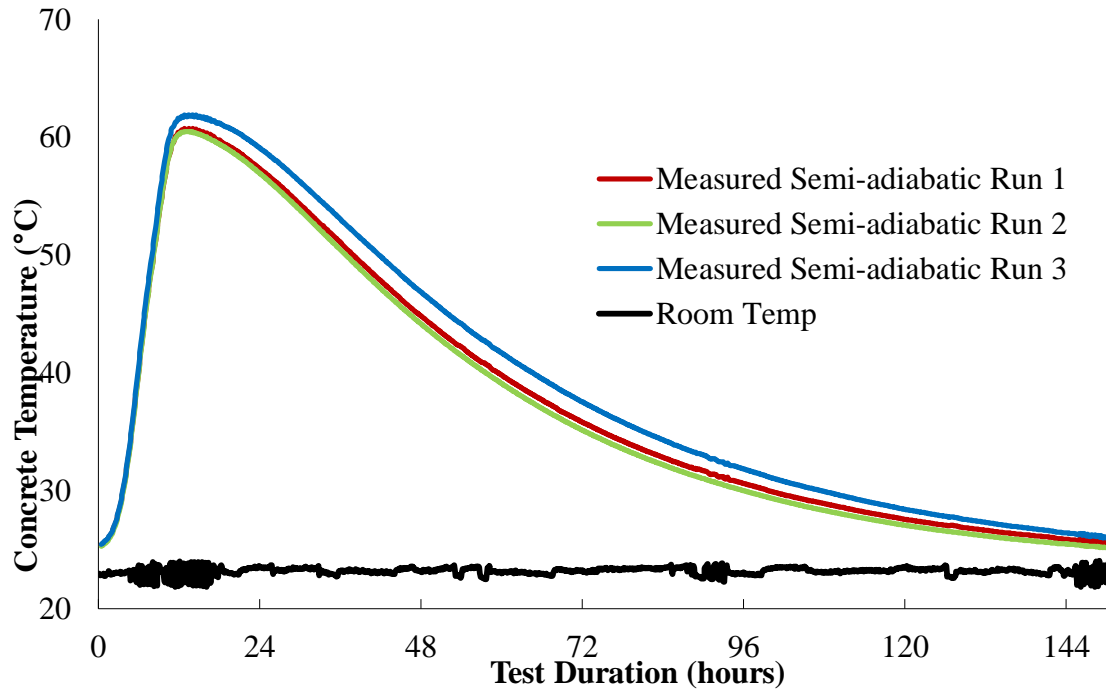


Figure 8: Measured Semi-Adiabatic Temperature C

- Determine the heat-based activation energy (E_a) through isothermal calorimetry using the internal mixing protocol [25].
- As part of the iterative method to estimate the true adiabatic temperature of the mixtures, the equivalent age (t_e) needs to be calculated. The equivalent age is computed according to Equation 33 using the mixture activation energy (E_a) and Equation 2 in ASTM C1074 [39]:

$$t_e(T_r) = \exp \left[\left(\frac{-E_a}{R} \right) \cdot \left(\frac{1}{273 + T_c} - \frac{1}{273 + T_r} \right) \Delta t \right] \quad \text{Equation 33}$$

where t_e (T_r)= equivalent age at the reference temperature (hours); T_r = reference temperature, 23°C; E_a = activation energy from isothermal calorimetry (J/mol); R = universal gas constant, 8.314 J/ (mol·K); T_c =Concrete temperature at time interval (°C); Δt = time interval (hours)

5. Calculate the degree of hydration using the equivalent age of the mixture and the hydration parameters – α_u , β , and τ .

The three parameter exponential function was first introduced by Freiesleben Hansen and Pedersen in 1977 [59] to represent the heat development of concrete. Pane and W. Hansen later showed in 2002 the relation between degree of hydration and time can be modelled as Equation 34 [25]:

$$\alpha(t_e) = \alpha_u \cdot \exp\left(-\left(\frac{\tau}{t_e}\right)^\beta\right) \quad \text{Equation 34}$$

where $\alpha(t_e)$ = degree of hydration at respective equivalent age; α_u = ultimate degree of hydration; τ = time parameter (hrs); β = shape parameter, dimensionless; t_e = equivalent age (hrs)

A visual presentation on the effect of the hydration parameters on the degree of hydration is presented in Figure 9 through Figure 11. The range of parameters selected was similar to the resulting values from the mixtures. A higher α_u , simply shifts the curve up, while a higher β value indicates a higher slope in the hydration curve, and a higher τ value shifts the hydration curve to longer times.

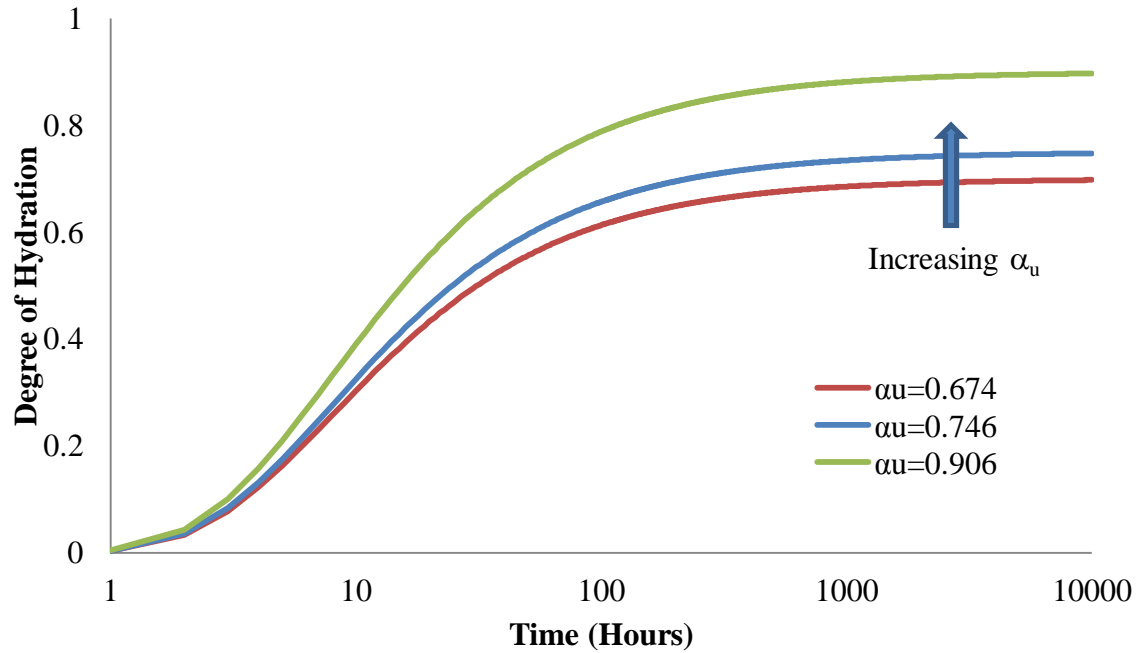


Figure 9: Influence of α_u on Hydration

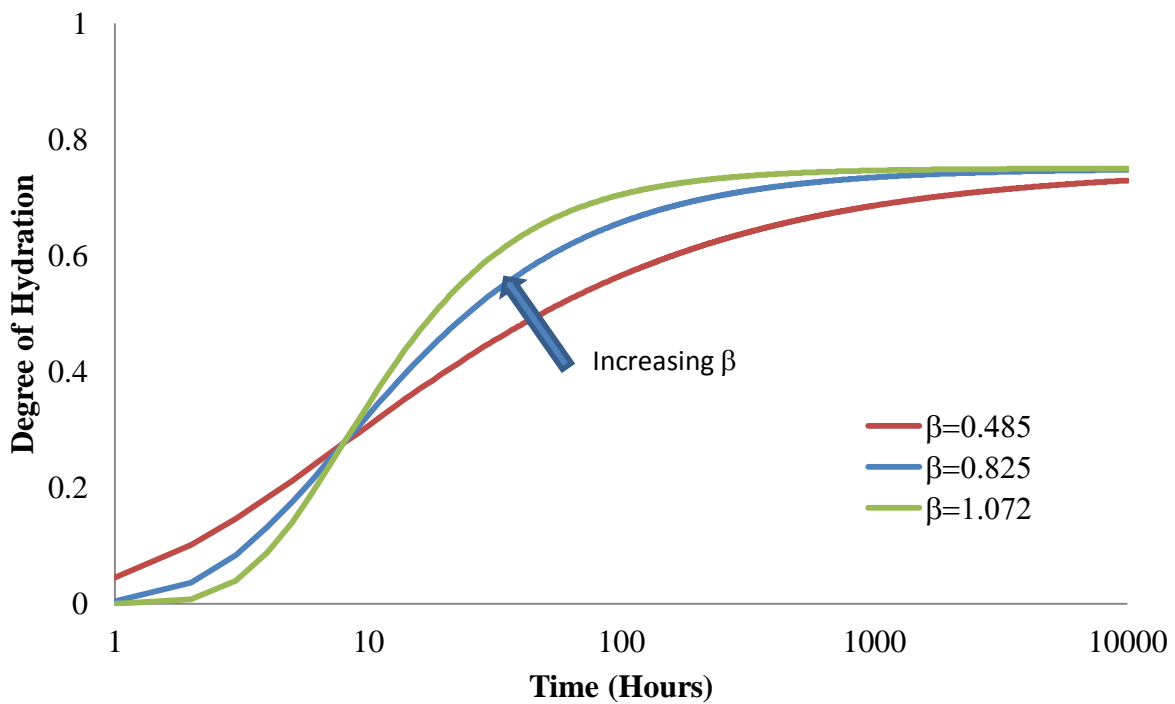


Figure 10: Influence of β on Hydration

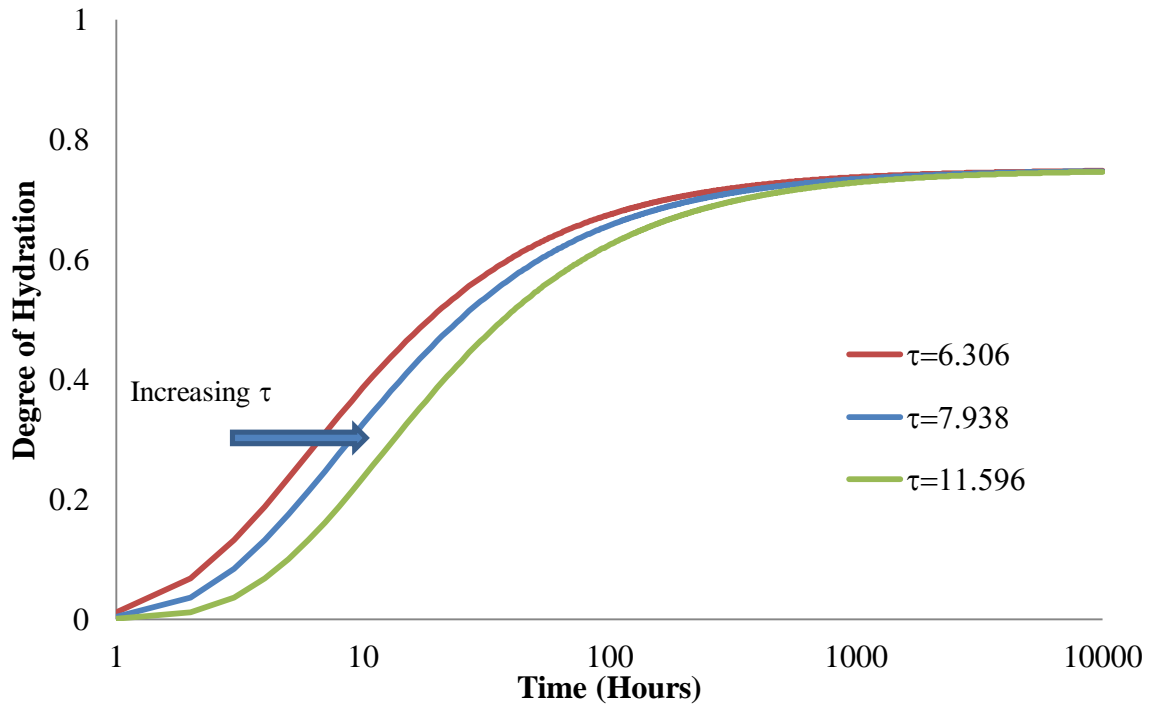


Figure 11: Influence of τ on Hydration

6. Calculate the heat evolved at each time step using the hydration parameters α_u , β , and τ and the ultimate heat of hydration, H_u . H_u is the sum of the total heat of hydration from cement, H_{cem} , along with the total heat of hydration from supplementary cementitious materials (SCMs). Since no SCMs were used in this testing, $H_u=H_{cem}$. The cement used in this study had an H_u of 481.8 kJ/kg calculated using Equation 35:

$$H_{cem} = 500 \cdot p_{C_3S} + 260 \cdot p_{C_2S} + 866 \cdot p_{C_3A} + 420 \cdot p_{C_4AF} + 624 \cdot p_{SO_3} + 1186p_{FreeCa} + 850 \cdot p_{MgO} \quad \text{Equation 35}$$

where p_x =mass fraction of phase content

7. Quantify the heat evolved using Equation 36 [60]:

$$Q_h(t) = H_u \cdot W_c \cdot \left(\frac{\tau}{\sum t_e}\right)^\beta \cdot \left(\frac{\beta}{\sum t_e}\right) \cdot \alpha(t_e) \cdot \left(\frac{t_e}{\Delta t}\right) \quad \text{Equation 36}$$

where $Q_h(t)$ = rate of heat generation ($J/h \cdot m^3$); H_u = total heat of hydration (J/g); W_c = weight of cement in mixture (kg/m^3)

8. Calculate the specific heat of concrete, which is used to determine the change in temperature, using Equation 37 and Equation 38 [26]:

$$C_p(\alpha) = \frac{1}{\rho} \cdot [W_c \cdot \alpha(t_e) \cdot C_{cef} + W_c \cdot (1 - \alpha(t_e)) \cdot C_c + W_a \cdot C_a + W_w \cdot C_w] \quad \text{Equation 37}$$

$$C_{cef} \approx 8.4 \cdot T_c + 339 \quad \text{Equation 38}$$

where $C_p(\alpha)$ = current specific heat of concrete ($J/(kg \cdot ^\circ C)$); ρ = unit weight of concrete mixture (kg/m^3); C_{cef} = fictitious specific heat of cement ($J/(kg \cdot ^\circ C)$); C_c = specific heat of cement ($J/(kg \cdot ^\circ C)$); W_a = weight of aggregate (kg/m^3); C_a = specific heat of aggregate ($J/(kg \cdot ^\circ C)$); W_w = weight of water (kg/m^3); C_w = specific heat of water ($J/(kg \cdot ^\circ C)$)

9. Calculate the concrete temperature rise using the heat generation and specific heat from Equation 36 and Equation 37 as shown in Equation 39:

$$\Delta T = Q_h \frac{\Delta t}{\rho \cdot C_p} \quad \text{Equation 39}$$

where ΔT = change in temperature from placement over time interval, Δt in hrs ($^\circ C$); Q_h = heat flow ($J/h \cdot m^3$); ρ =density of concrete specimen (kg/m^3); C_p = specific heat ($J/kg \cdot ^\circ C$)

10. Start from the original concrete temperature and sum up the change in temperature at each time step as shown in Equation 40. The resulting temperature is the “false” adiabatic temperature (T_{adia}^*) since it does not take into account the heating/hydrating process of the concrete and therefore is lower than the “true” adiabatic temperature. However, it is

important as it is used to model the temperature for the concrete cylinder in the semi-adiabatic calorimeter.

$$T_{adia}^* = T_c + \Delta T \quad \text{Equation 40}$$

11. Account for the change in concrete temperature due to the heat losses. Use Equation 41 to calculate the heat transfer (Δq_h) using the calibration factors determined in Step 1. Next, calculate the ΔT_L for the concrete specimen using Equation 42.

$$\Delta q_h = T_d \cdot (-C_{f1} \cdot \ln(t) + C_{f2}) \quad \text{Equation 41}$$

$$\Delta T_L = \frac{\Delta q_h \cdot \Delta t}{\rho_c \cdot C_{p,c} \cdot V_c} \quad \text{Equation 42}$$

where Δq_h = heat transfer ($J/h \cdot m^3$); T_d = change in temperature between thermocouples Ext 1 and Ext 2; C_{f1} and C_{f2} = Calibration factors ($W/^\circ C$); t = time elapsed from start of test (hrs); ΔT_L = change in concrete temperature from losses ($^\circ C$); ρ_c = density of concrete mixture (kg/m^3); $C_{p,c}$ = specific heat of concrete mixture ($J/kg \cdot ^\circ C$); V_c = volume of concrete sample (m^3); Δt = time step (s)

12. Sum the change in temperature from losses at each time step from Equation 42. Then subtract the sum of the changes in temperature from losses at each time step from the false adiabatic temperature from Equation 40 to determine the modelled semi-adiabatic concrete temperature (T_c^*) shown in Equation 43.

$$T_c^* = T_{adia}^* - \sum \Delta T_L \quad \text{Equation 43}$$

13. Repeat steps 4-12 for each time step. This modelled semi-adiabatic concrete temperature (T_c^*) can now be compared to the actual concrete temperature (T_c) over the entire test

period. Use the coefficient of determination (R^2) calculated by comparing the measured concrete cylinder temperature (T_c) to the modelled concrete cylinder temperature (T_c^*) for the assumed α_u , β , and τ value to best fit these two temperature developments. This is an iterative process and is best performed using an automated solver algorithm. The Solver function in MS Excel was therefore used to determine the best fit hydration parameters for this comparison. The measured semi-adiabatic concrete temperature can then be plotted versus the modelled semi-adiabatic concrete temperature for each mixture.

14. The “true” adiabatic temperature (T_{adia}) can now be modelled using the best fit hydration parameters found in Step 13. A time step of 0.1 hrs for the first 25 hrs, then a step of 2.5 hrs afterwards was used. The initial concrete temperature was used for the first step, then steps 4-9 were repeated for each time step, using the concrete adiabatic temperature from the previous time step as the concrete temperature in step 4, instead of the measured semi-adiabatic concrete sample temperature (T_c). The concrete temperature from the previous time step was used to produce the “true” adiabatic temperature rise as seen in Equation 44:

$$T_{adia} = T_c + \Delta T \quad \text{Equation 44}$$

where T_{adia} = True adiabatic temperature ($^{\circ}\text{C}$); T_c = Concrete temperature from previous time step ($^{\circ}\text{C}$); ΔT = Change in concrete temperature due to heat from hydration ($^{\circ}\text{C}$)

The resulting temperature is the “true” adiabatic temperature. It is important to note that the “true” adiabatic temperature should be higher than the “false” adiabatic temperature as shown in Figure 12 since the higher hydration rate from the higher adiabatic temperature during curing is accounted for.

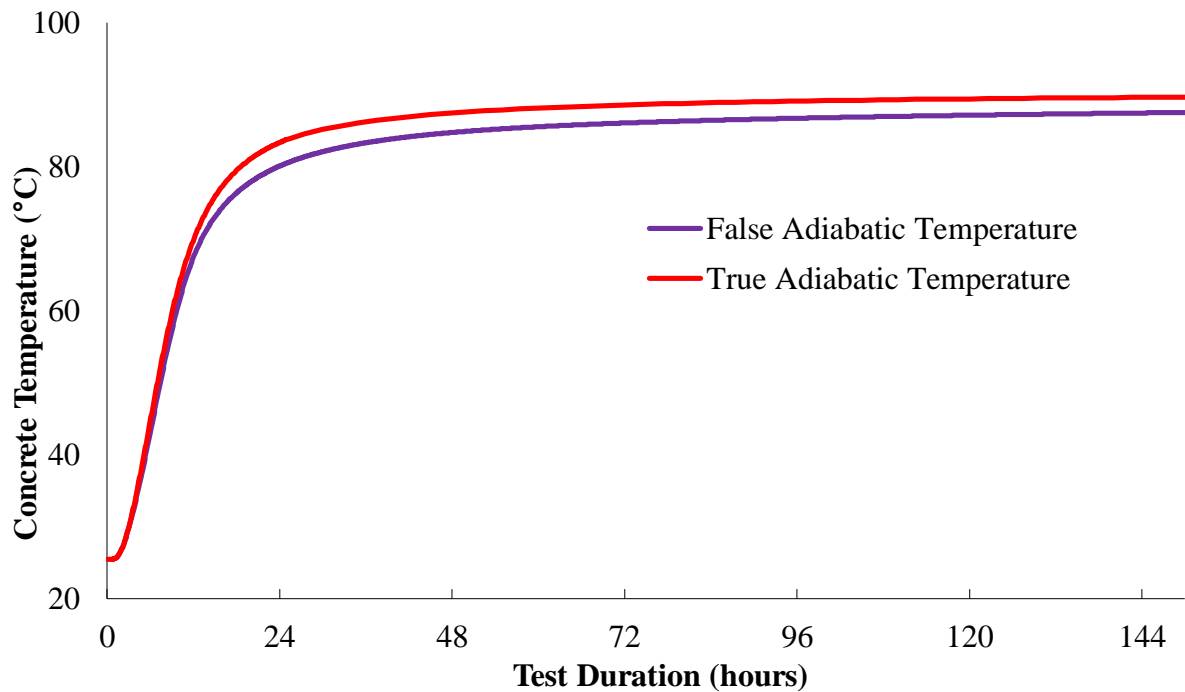


Figure 12: True vs False Adiabatic Temperature of C

3.2.6 Time of Set

Accelerating and water reducing/retarding admixtures have a significant effect on setting time. To determine the effects of the admixtures on initial and final set, concrete was wet sieved and the mortar portion was tested in accordance with ASTM C403 [61]. The time of set for the mortar was measured at three different temperatures, 23°C, 38°C, and 53°C. Three temperatures were chosen so that mortar cubes could be demolded after final set and tested to determine the strength-based activation energy following ASTM C1074.

3.2.7 Concrete Mechanical Properties

To determine the effect of admixtures on the hardened properties of each concrete mixture and develop the mechanical property-maturity relationship for each concrete mixture, 4x8inch cylinders were prepared at 23°C. The compressive strength, tensile strength, and modulus of elasticity of each mixture were tested at 4 hours, 6 hours, 12 hours, 1 day, 3 days, 7 days, and 28

days as seen in Figure A-1 through Figure A-3. The compressive strength, splitting tensile strength and elastic modulus were determined in accordance ASTM C39 [62], ASTM C496 [63], ASTM C469 [64], respectively.

3.2.8 Free Shrinkage

A free shrinkage frame shown in Figure 13 was constructed at the University of South Florida [65] following steps outlined in Meadows thesis [66] to measure autogenous shrinkage rates of different concrete mixtures. All six mixtures had the same w/c ratio of 0.38, which is below the 0.45 at which Holt and Leivo [22] showed autogenous shrinkage to occur. Testing in the free shrinkage frame was performed to determine the effect of different admixtures and their combination on concrete autogenous shrinkage behavior. The frame, which is completely sealed in plastic, to prevent any moisture transfer to or from the concrete specimen, allows for the unrestrained concrete movement on two symmetrical sides. 6x6x23.5 inch concrete specimens were prepared and tested to determine the amount of shrinkage. Linear measurements and temperature recordings were taken every minute during testing to record any shrinkage, creep, or thermal effects occurring after final set.

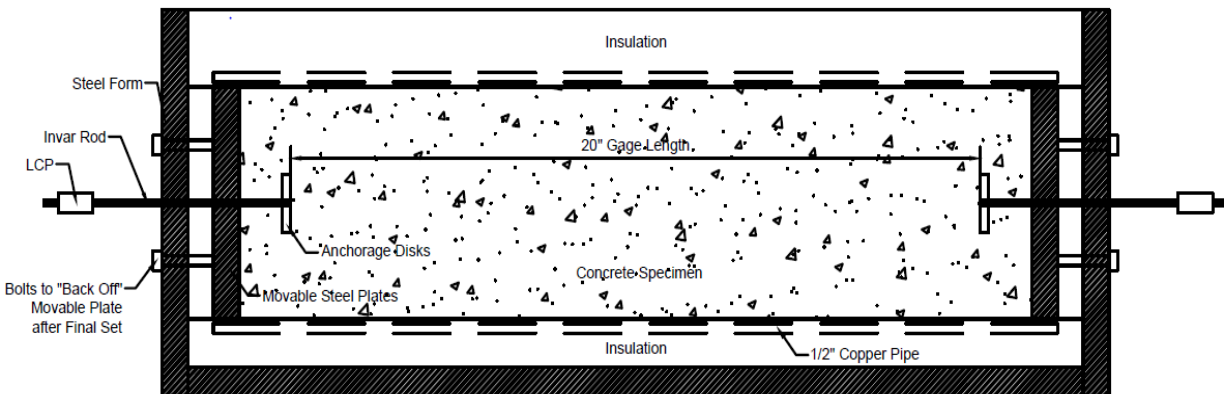


Figure 13: Free Shrinkage Frame

To control the temperature of the specimen in the free shrinkage frame and rigid cracking frame, a VWR circulating bath with a 50/50 mixture of ethylene glycol and water was used to follow the temperature profiles output from ConcreteWorks. Hoses were quick connected from the bath to the respective frame, and the bath fluid temperature regulated the concrete specimen temperature to match the temperature profile output from ConcreteWorks.

3.2.9 Rigid Cracking Frame

A rigid cracking frame (RCF) shown in Figure 14 was also constructed at the University of South Florida [65] following work performed at Auburn University [33] to determine the cracking potential of concrete mixtures under restraint. The accelerator mixtures were tested in the RCF under two realistic temperature profiles. The realistic temperature profiles were generated using ConcreteWorks and mimicked the concrete temperature at the center of an actual slab if the concrete were placed at 23°C or 38°C. The mixtures were also tested without any temperature control in the insulated formwork. The insulated concrete forms retained some of the hydration heat, allowing the concrete temperature to increase with the hydration and slowly cool. In this test, the environment in which the frame was kept was maintained at 23°C.

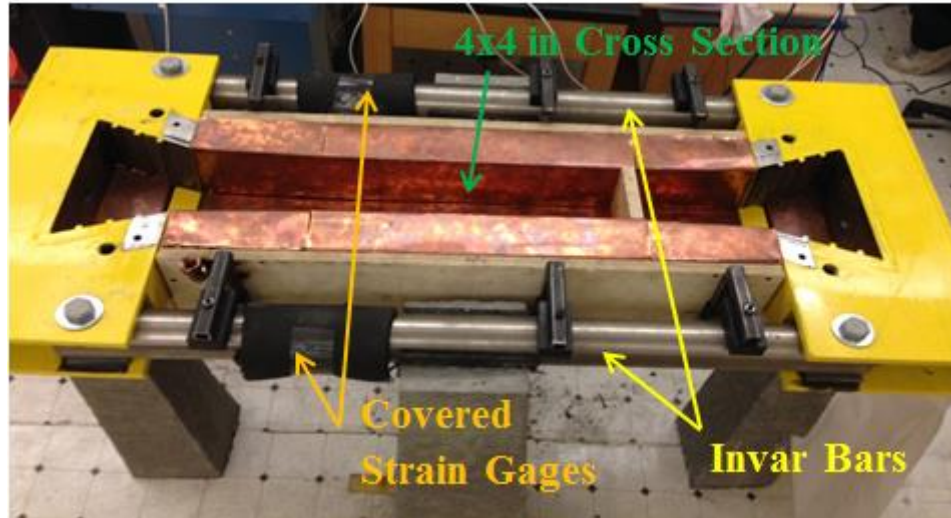


Figure 14: Rigid Cracking Frame

To calculate the stress of the concrete specimen at the smallest cross section (4x4 in), the forces of the concrete are determined from the strain gage data collected from the two invar bars. To calculate these forces, a calibration procedure must be performed which records the strain on the invar bars while the frame is loaded at multiple points (from 1 to 10 kips) using a load cell and DWIDAG bar through the center. The calibration factors needed to determine the load from the strain gages on each invar bar can then be determined as depicted in Appendix- Figure A-4.

To prepare the RCF for testing, plastic sheeting was placed on the bottom and sides, and caulking was used to seal any edges. After placing the concrete, a layer of plastic was placed over the specimen and taped down in order to completely seal the specimen and prevent any moisture loss. The top formwork was then placed and three OMEGA TJ36-CPSS-316U-6 thermocouples were positioned to measure the temperature at the middle height of the concrete specimen: one at the center of the frame and one at the middle of each crosshead of the frame. Insulated hoses were then attached to the VWR water bath and to the connections on the RCF as seen in Figure A-5 which lead to a maze of copper piping throughout the formwork, Figure A-6. The respective

temperature profile was selected and set to control the center thermocouple, and the tests were run for 48 hours, at which time cooling was induced at 1°C/hr. The invar strain values and temperature from each thermocouple were measured every minute to be used during the analysis. The resulting tensile stresses were compared to determine the cracking risk of each mixture.

3.3 Modeling

3.3.1 ConcreteWorks Inputs

ConcreteWorks [21] used the geometric properties, material properties, construction methods, environmental conditions, and hydration parameters of each mixture to predict the temperature profile throughout the depth of a concrete pavement slab. Heat of hydration parameters were obtained through semi-adiabatic testing, ultimate heat of hydration was based on cement mineralogical composition as determined from Rietveld analysis, and heat of hydration-based apparent activation energy was calculated from isothermal calorimetry measurements. These parameters defined the heat generation from the concrete and were the main factors used to predict the temperature profile experienced by a field slab.

3.3.2 HIPERPAV Inputs

HIPERPAV software was used to model and predict the cracking potential of different concrete pavement mixtures. In order to be able to use the software, several mixture properties had to be determined prior to its implementation. These properties were determined by performing laboratory testing on each mixture that included the following:

1. Cement properties were determined by a series of tests: Blaine fineness, elemental oxide, chemical composition using X-ray fluorescence and mineralogical analysis using X-ray diffraction and Rietveld analysis.

2. Heat of hydration-based activation energy was determined using isothermal calorimetry on cement pastes.
3. Semi-adiabatic calorimetry measurements were performed on concrete mixtures to determine the hydration parameters, α_u , β and τ . These values were used to determine the degree of hydration of each mixture at each age. There is currently no standard of testing for semi-adiabatic calorimetry measurements; therefore, the steps provided by Poole et al. in “Hydration Study of Cementitious Materials using Semi-Adiabatic Calorimetry” [25] were followed closely.
4. Strength-based activation energy and the equivalent age of each mixture were measured by preparing and testing mortar cubes at 3 hr, 6 hr, 12 hr, 1 day, 2 days, 3 days, 7 days, and 28 days at three isothermal temperatures of 23°C, 38°C, and 53°C [39].
5. Concrete mechanical properties were measured to determine the compressive and tensile splitting strengths and moduli of the concrete at each age. Concrete cylinder testing was performed following the specifications in ASTM C39 to determine the compressive strength, ASTM C496 to determine the tensile splitting strength, and ASTM C469 to determine the modulus of elasticity.
6. Coefficient of thermal expansion [48] for the concrete mixture was measured following ASTM C531. The concrete CTE for the mixtures made with the same cement should not be significantly different from each other. This is because the small difference in water content or admixtures should have a negligible effect on the CTE. The CTE values used for this study were estimated by HIPERPAV.

HIPERPAV was also used to simulate the effects of changes in construction parameters such as time of placement on each mixture. Placement time of a mixture, especially under high

temperature conditions, is significant since the maximum in concrete heat of hydration could coincide with the peak ambient temperature. Upon cooling, this would lead to high thermal stresses which would increase the cracking potential. Riding et al. [67] and the Transtec Group [68] observed optimal concrete placement times throughout the night from 7 PM to 5 AM.

CHAPTER 4: RESULTS AND DISCUSSION³

The following sections show the results from both experimental testing and modeling, and provide a discussion of the findings.

4.1 Concrete Mechanical Properties

Table 6 shows the compressive strength results for all mixtures. All accelerator-containing mixtures showed higher early compressive strengths up to one day. This early increase in strength was expected since both accelerators are classified as hardening accelerators for use in applications where early strength gain is desirable. However, at three days, the control mixture, C, surpassed the strength of the chloride-based accelerator mixture, CA, while the nitrate-based accelerator mixtures – CHAD, CAD, and CDAD – were still higher. Aggoun et al. [7] and Tokar [69] have shown similar results when using calcium nitrate. Aggoun specifically showed that for cements of similar tricalcium silicate content, the cement of higher C_3A had the highest strength at one day. Rietveld analysis showed the cement used for this study had a high C_3A content of 10.2% [48] which is similar to the high C_3A cement (8.33%) in Aggoun et al. study. The 28 day compressive strength was highest for the nitrate-based accelerator mixtures with C slightly below and CA having the lowest ultimate strength. This could be explained by Justnes [9] who showed calcium nitrate with the addition of sodium thiocyanate to offset the effects of a lignosulfonate plasticizer better than calcium chloride alone for both 1 day and 28 day strengths. Justnes et al. [70] also studied porosity and diffusivity of concrete with calcium nitrate and indicated the higher strength

³ Portions of this chapter were previously published in [48]. Permission is included in Appendix A.

could be due to a denser coarse aggregate/paste interface or morphology changes leading to smaller calcium hydroxide crystals.

Table 6: Compressive Strength of Cylinders at 23°C

Time (days)	Compressive Strength (psi)					
	C	CNA	CA	CHAD	CAD	CDAD
0.2	60	-	70	370	260	640
0.3	280	100	980	990	1030	1710
0.5	1470	910	2110	3030	2510	3140
1	3670	2810	3390	4710	4230	4910
3	5670	5250	5900	6970	6530	7300
7	7150	6430	6910	-	-	-
28	8730	8010	7860	9300	8870	9250

The tensile splitting strength of the mixtures is shown in Table 7. The accelerator containing mixtures increase the early tensile strength gain; however, after 1 day, the tensile strength of C surpasses that of CA. The results show that although the CAD mixture had little to no effect on the ultimate compressive strength, the addition of any of these admixtures decreases the ultimate tensile strength compared to the control C at 28 days.

Table 7: Tensile Splitting Strength of Cylinders at 23°C

Time (days)	Tensile Splitting Strength (psi)					
	C	CNA	CA	CHAD	CAD	CDAD
0.2	10	-	20	55	-	90
0.3	50	20	160	145	130	230
0.5	225	165	270	360	325	365
1	370	325	335	440	480	500
3	585	490	470	625	580	645
7	640	625	570	-	-	-
28	765	685	640	705	725	750

The ultimate modulus of elasticity follows the same trends as the splitting tensile strengths as seen in Table 8. The accelerator-containing mixtures show a higher modulus at early ages, while C surpasses all mixtures at 3 days. The effect of accelerators on modulus development is important as the higher early modulus means the concrete is stiffer and possibly more susceptible to cracking at early ages.

Table 8: Modulus of Elasticity

Time (days)	Modulus of Elasticity (ksi)					
	C	CNA	CA	CHAD	CAD	CDAD
0.25	750	450	1550	1600	1550	2100
0.5	1950	1850	2450	3150	2700	3000
1	3450	3050	3400	3850	3500	3850
3	4500	4000	4200	4450	4250	4400
28	5350	4950	4700	5350	5050	5125

4.2 Maturity Studies

4.2.1 Mortar Cube Compressive Strengths

The results from the compressive strength mortar cube testing at 23°C, 38°C, and 53°C are shown in Figure 15, Figure 16, and Figure 17, respectively. At 23°C, the same early trends shown in the concrete cylinder compressive testing are observed with an increase in strength for the accelerator mixtures. At 28 days, the C mixture shows the highest strength, with the CA mixture showing the lowest. At 38°C, all of the mixtures sustained their ultimate strength except for CDAD which is considerably lower. Increasing the temperature to 53°C increased the early strength for all mixtures.

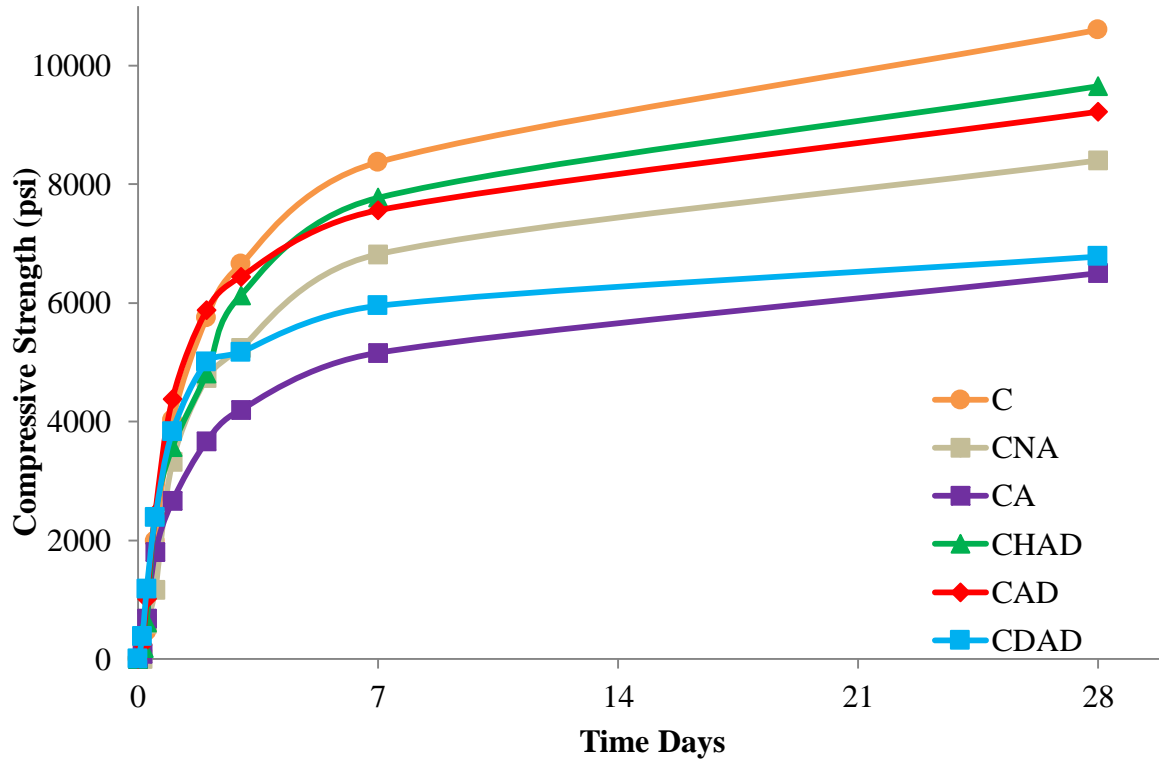


Figure 15: Mortar Cube Strengths at 23°C

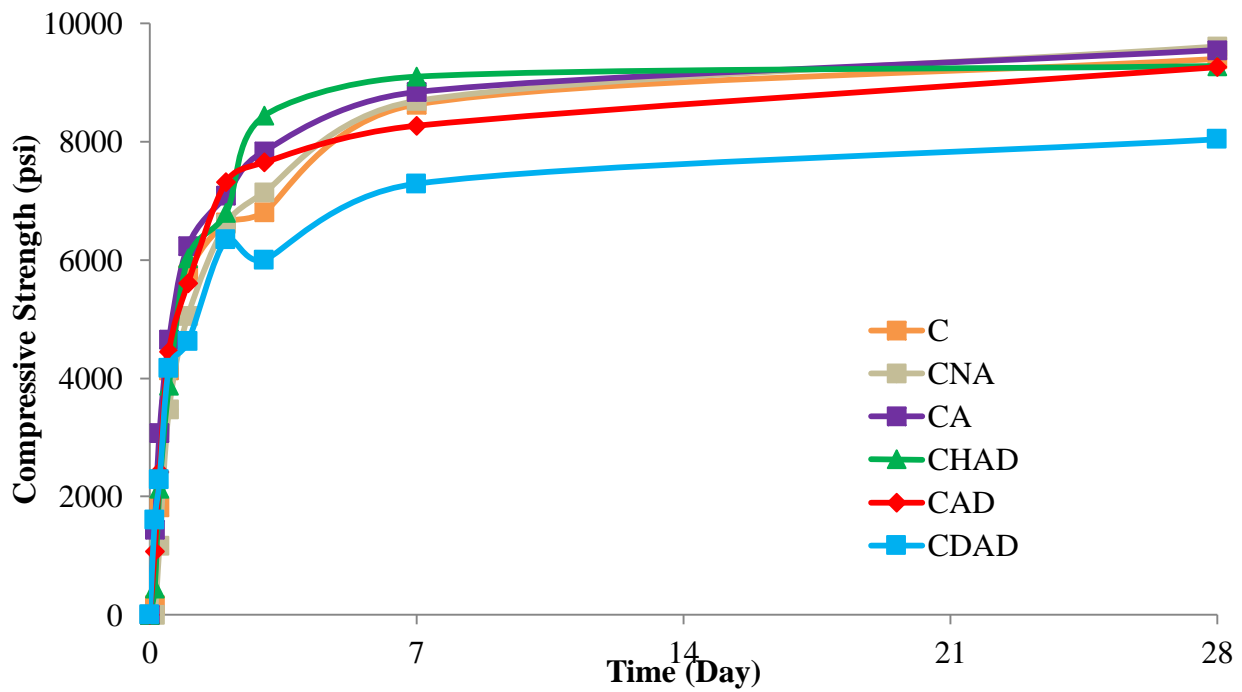


Figure 16: Mortar Cube Strengths at 38°C

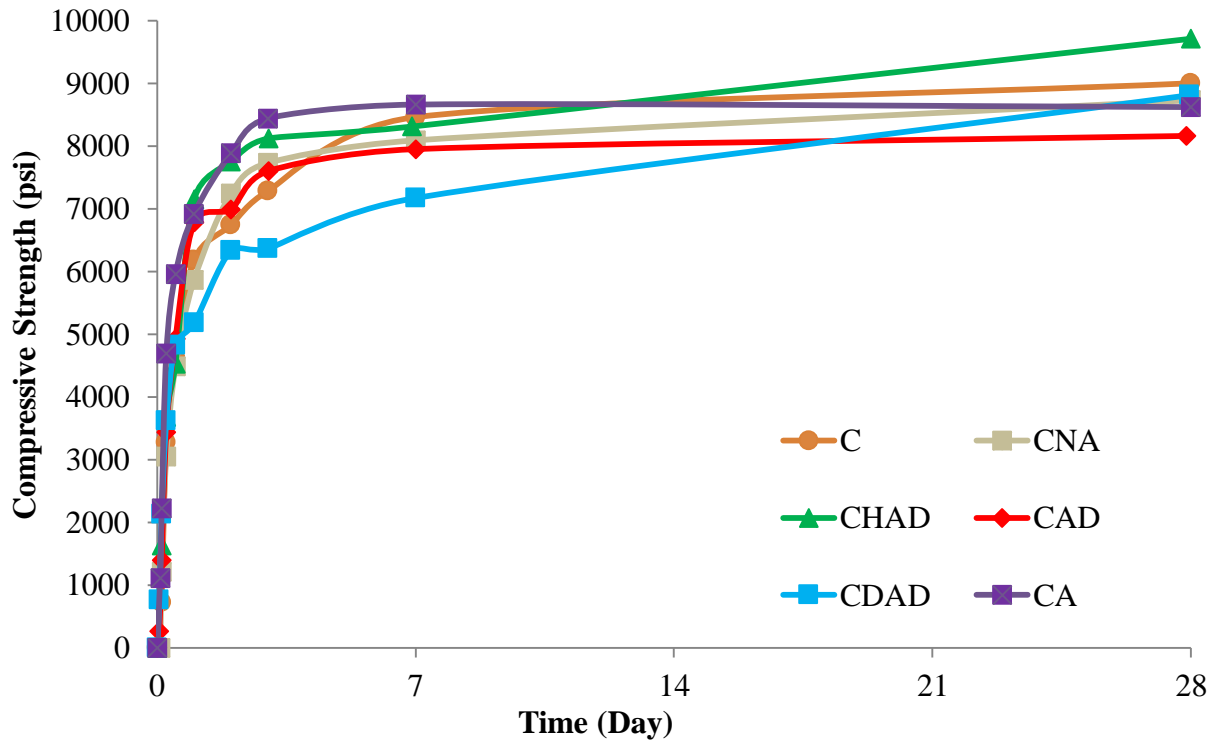


Figure 17: Mortar Cube Strengths at 53°C

4.2.2 Strength-Based Apparent Activation Energy

The strength based apparent activation energy was calculated using the mortar cube compressive strength results. Figure 18 shows the resulting activation energy (kJ/mol) calculated using the hyperbolic and the exponential functions. There was slightly less calculated error using the exponential function, with an R-squared value of 0.991 versus 0.988 for the hyperbolic function. The exponential function shows a clear trend of a decrease in the activation energy as the calcium nitrate-based accelerator dosage is increased. The activation energy for calcium nitrate-based mixtures are also lower than the CA mixture. This indicates that increasing temperature has less of an effect on the strength gain for the higher dosages of calcium-nitrate based accelerator mixtures.

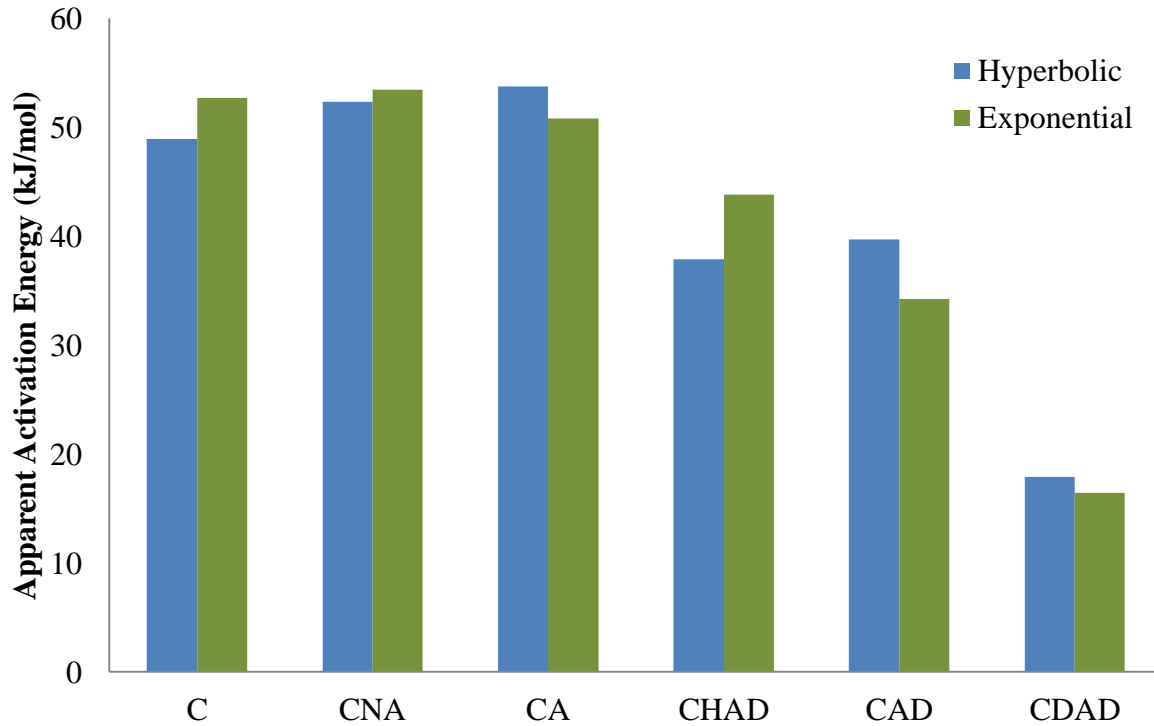


Figure 18: Strength-Based Activation Energy

4.3 Calorimetry

4.3.1 Isothermal

Isothermal calorimetry results for all mixtures showed an increased amount of heat flow as the temperature was increased from 23°C to 38°C to 48°C as observed in Figure 19 through Figure 21. This agrees with the findings of Xu et al. [71] where the maximum rate of heat generation and area under the main peak increased with increasing temperature. At 23°C, the accelerator mixtures accelerated the occurrence of the main hydration peak, while the CNA mixture retarded the hydration as expected. CA showed a higher peak than the calcium nitrate-based mixtures which agrees with the findings of both Cheung et al. [6] and Abdelrazig et al. [17] where it was observed that calcium chloride increases the rate of hydration more than calcium nitrate at the same dosage. At higher dosage, CDAD shifted the main peak further left than CA; however, it was lower in

intensity. The accelerator mixtures continue to offset the retarder and further accelerate the main hydration peak at 38°C while also increasing the intensity of the peak. CNA continues to retard the mixture while decreasing the intensity of the main peak. A clear peak after the main hydration peak can be seen at 38°C for the control mixtures and the CA mixture, but not for the nitrate-based mixtures. At 48°C, the control shows the highest intensity for the main peak. This shows that higher temperature may have an adverse effect on the accelerator containing mixtures.

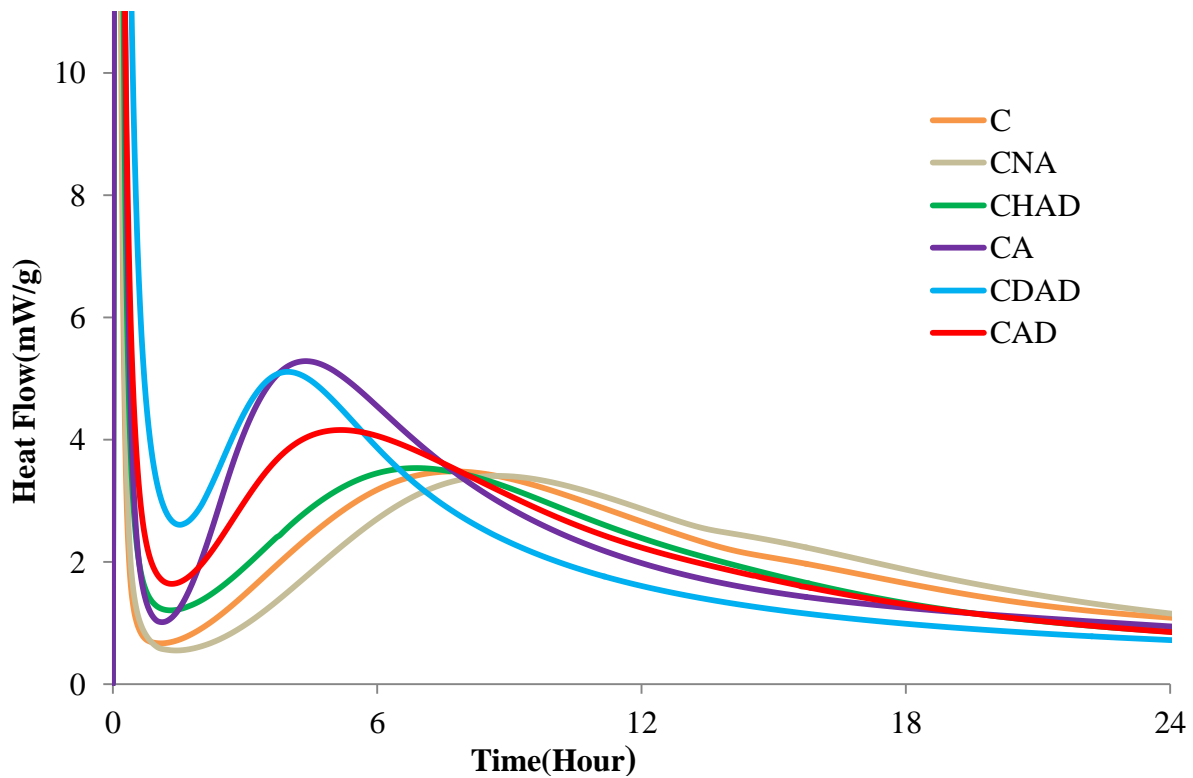


Figure 19: Heat Flow Rate by Isothermal Calorimetry 23°C

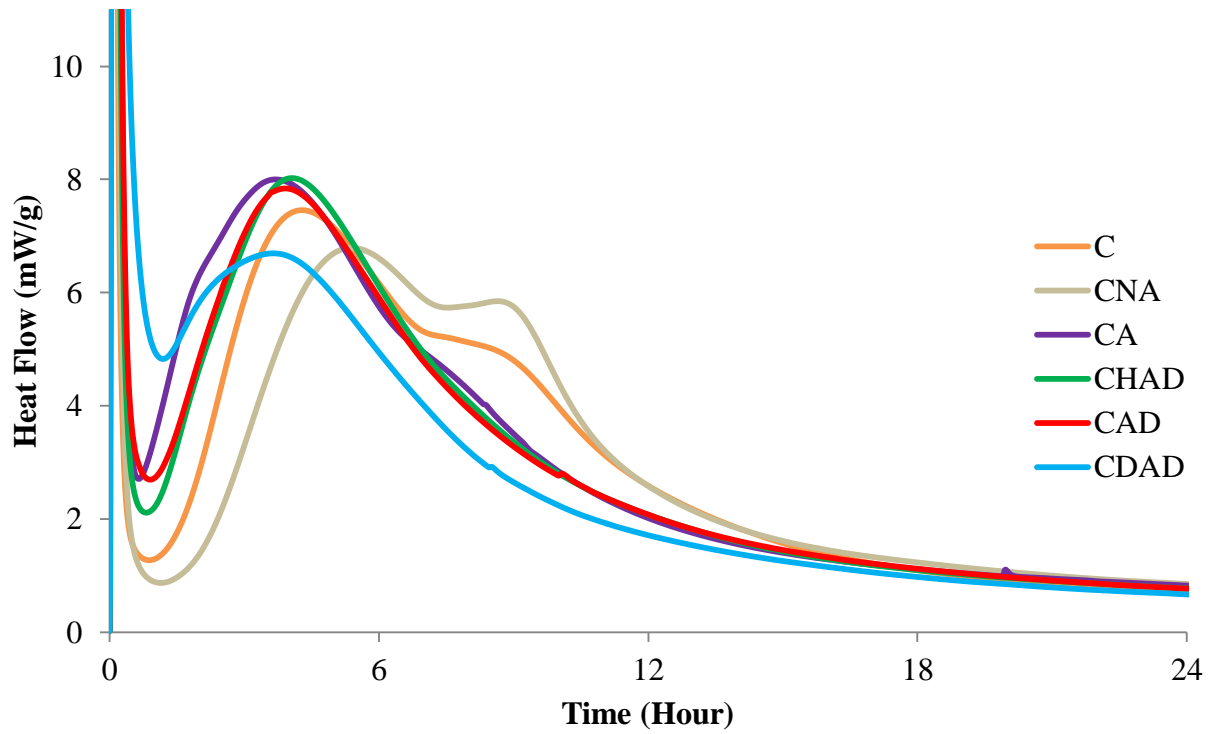


Figure 20: Heat Flow Rate by Isothermal Calorimetry 38°C

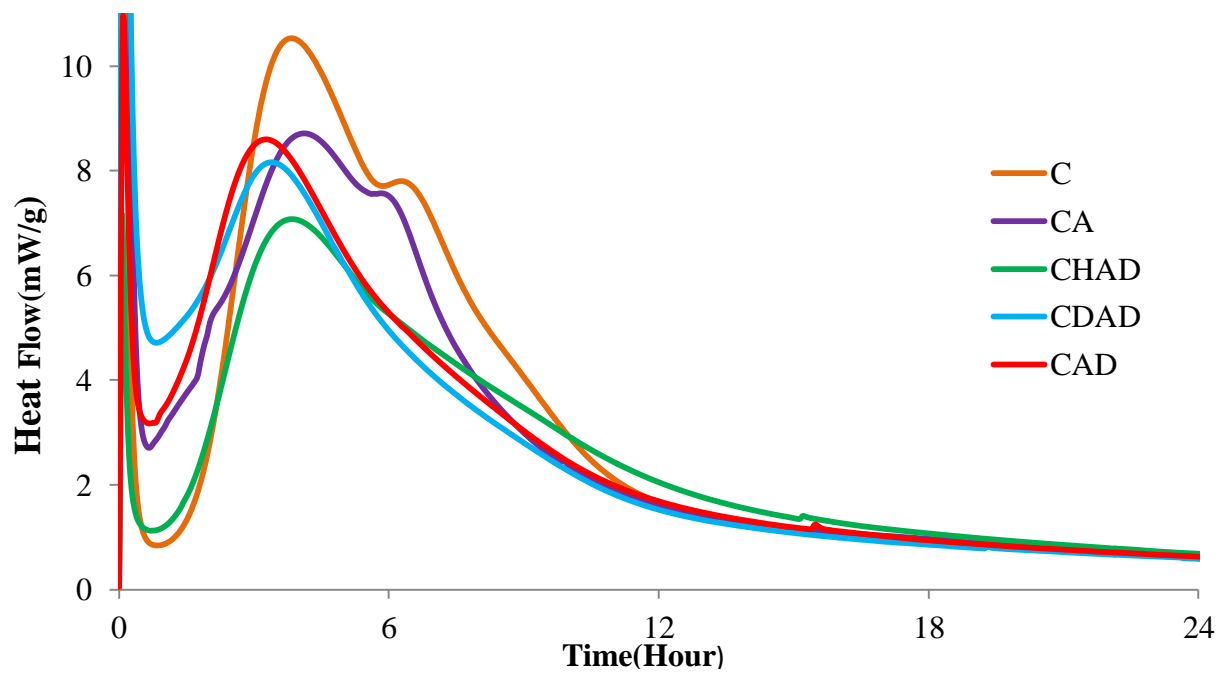


Figure 21: Heat Flow Rate by Isothermal Calorimetry 48°C

The heat of hydration-based activation energy was calculated and the results are shown in Table 9.

Table 9: Heat of Hydration-Based Activation Energy

	C	CNA	CA	CHAD	CAD	CDAD
$E_A(\text{kJ/mol})$	33.0	30.8	25.4	26.5	21.3	32.4

4.3.2 Semi-Adiabatic

As indicated previously in section 3.2.5, following the construction of each calorimeter, the system had to be calibrated to determine the coefficients which would make it possible to establish the baseline of the instrument's heat loss potential and subsequent determination of the adiabatic temperature rise of concrete mixtures. The best fit calibration factors are presented in Table 10. Figure 22 shows the plot of the measured versus modeled temperature losses as determined from the calibration protocol implemented for Calorimeter 1 used in this study. The resulting temperature curves show the measured and modeled temperature losses to be in good agreement.

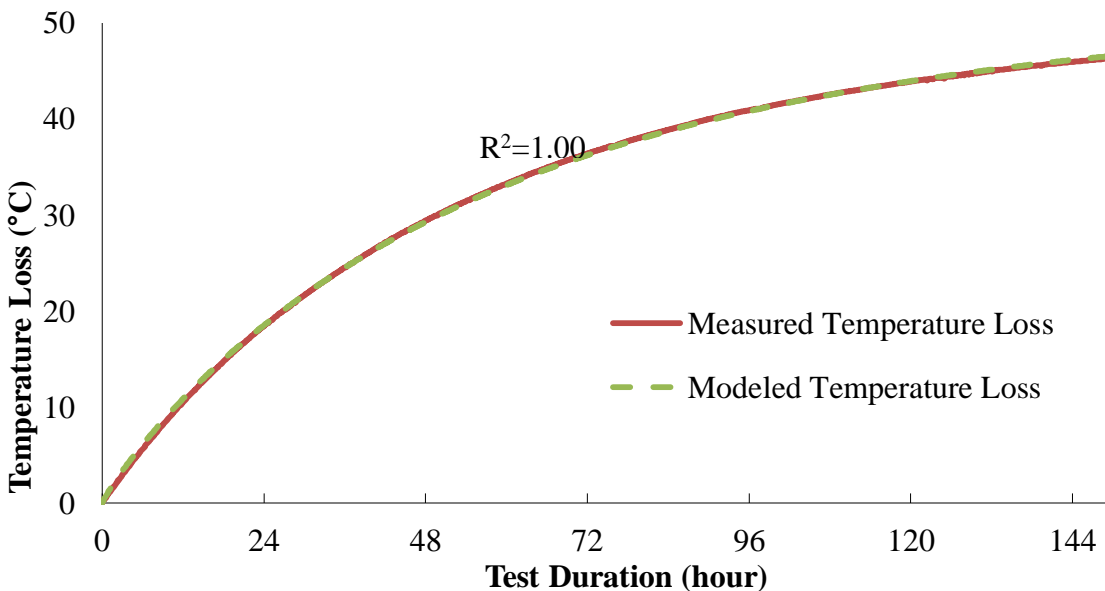


Figure 22: Semi-Adiabatic Calorimeter Water Calibration

Table 10: Calibration Factors

Calorimeter	C _{f1}	C _{f2}
1	0.1104	1.5188
2	0.0356	1.3261
3	0.0395	0.5808

The average hydration parameters – α_u , β , and τ – calculated from semi-adiabatic calorimetry and used to model the adiabatic temperature rise of each mixture are shown in Table 11. For CNA, the results from semi-adiabatic calorimetry showed the same trends observed by Xu et al. [71]. Using isothermal calorimetry, it was concluded that the use of water reducer generally decreases α_u , but increases β and τ . The results also show the accelerator containing mixtures to offset the effect of the water reducer/retarder on the slope parameter, β . The time parameter, τ , shows a decrease in time of occurrence of the main hydration peak for all accelerator mixtures which agrees with the findings of Riding et al. [27]. The nitrate based mixtures all have a lower τ value than the CA mixture, even at the half dosage, CHAD. For adiabatic temperature rise, it should be noted that although the CNA mixture shows a longer induction period, it acts as a delayed accelerator causing increased rate of hydration once the main hydration peak begins [6].

Table 11: Hydration Parameters and Adiabatic Temperature Rise

Average Semi-Adiabatic Parameters	Mixtures					
	C	CNA	CA	CHAD	CAD	CDAD
$\beta =$	0.836	1.072	0.825	0.867	0.757	0.485
τ (hrs)=	11.596	11.931	7.938	7.594	6.944	6.306
$\alpha_u =$	0.741	0.687	0.746	.674	0.744	.906

The results displayed in Figure 23 indicate an increase in dosage of calcium nitrate accelerator has an increasing effect on the α_u . There appears to be a decreasing trend in the shape parameter, β , with an increase in the nitrate based accelerator. This signifies the slope of the hydration curve is not as steep with increasing the dosage. The time parameter, τ , also has a downward trend with increasing the accelerator dosage as seen in Figure 24. A decrease in τ shifts the hydration curve to the left. This indicates that hydration occurs at an earlier time as the accelerator dosage is increased. This trend is expected since one application of accelerators is to shorten the time to setting [72].

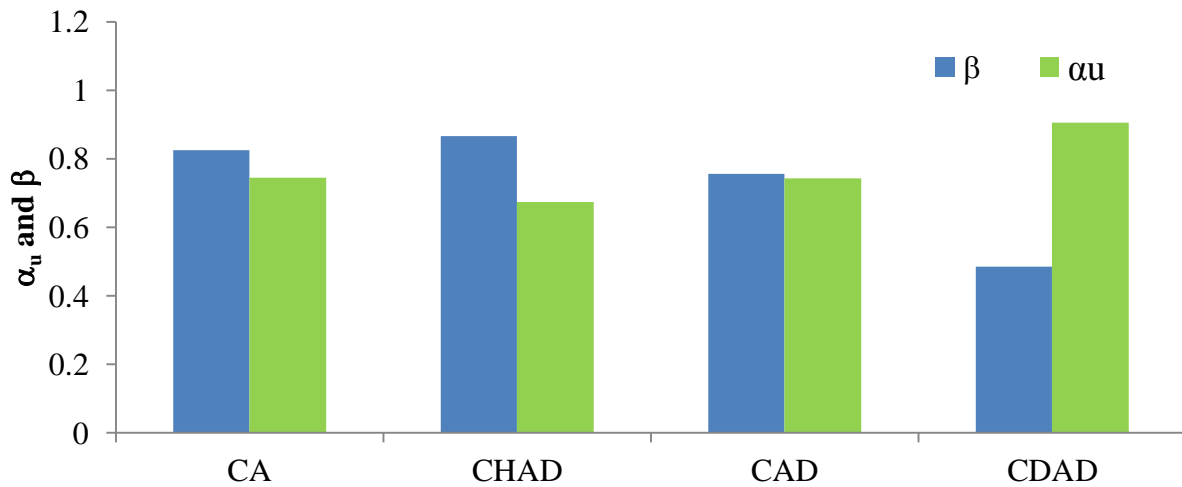


Figure 23: Effect of Accelerators on α_u and β

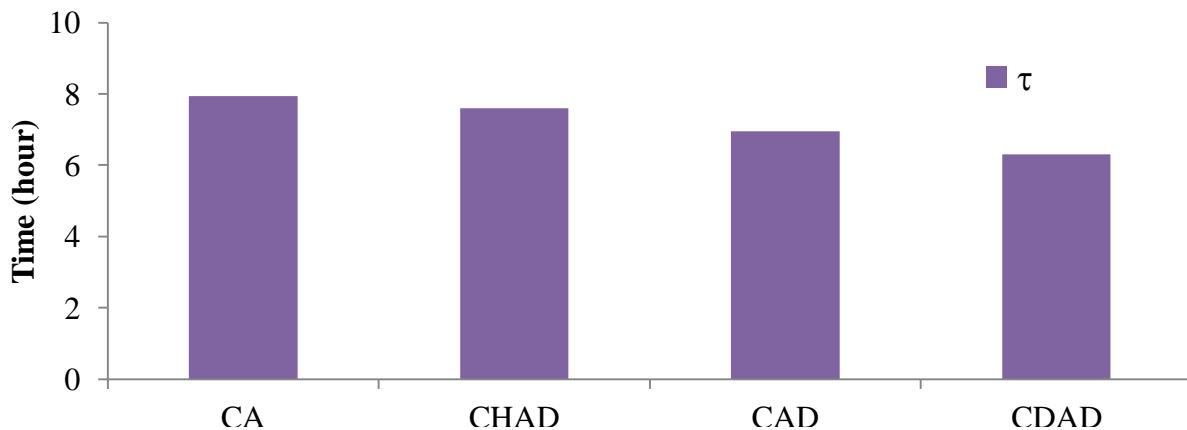


Figure 24: Effect of Accelerator Dose on the τ

The hydration parameters were used to determine the best fit curve to model the experimentally measured semi-adiabatic temperature. The measured semi-adiabatic concrete temperature and the modeled semi-adiabatic temperature for each mixture are shown in Figure 25 through 30 where it can be seen that the measured and modeled curves show excellent agreement.

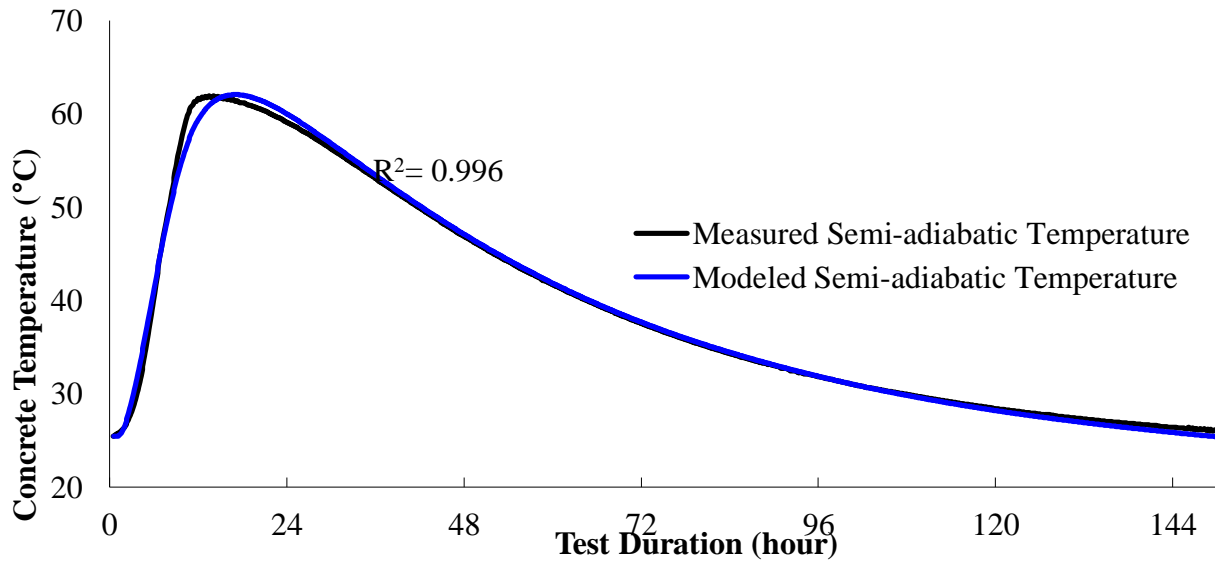


Figure 25: Measured vs. Modeled Semi-adiabatic Temperature C

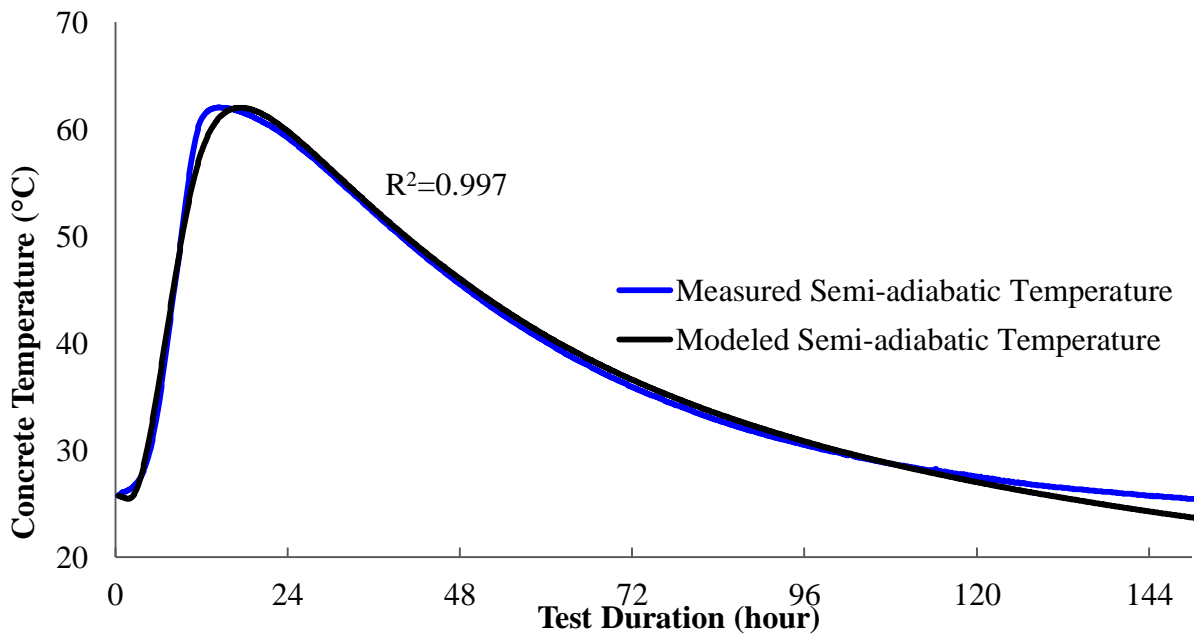


Figure 26: Measured vs. Modeled Semi-adiabatic Temperature CNA

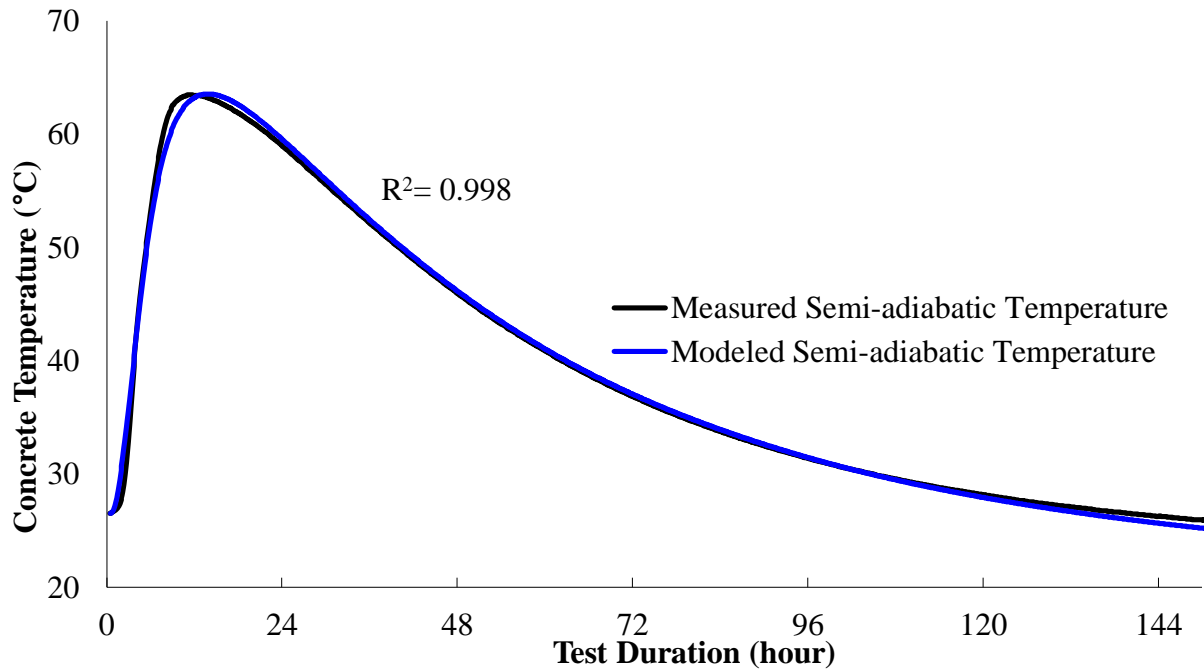


Figure 27: Measured vs. Modeled Semi-adiabatic Temperature CA

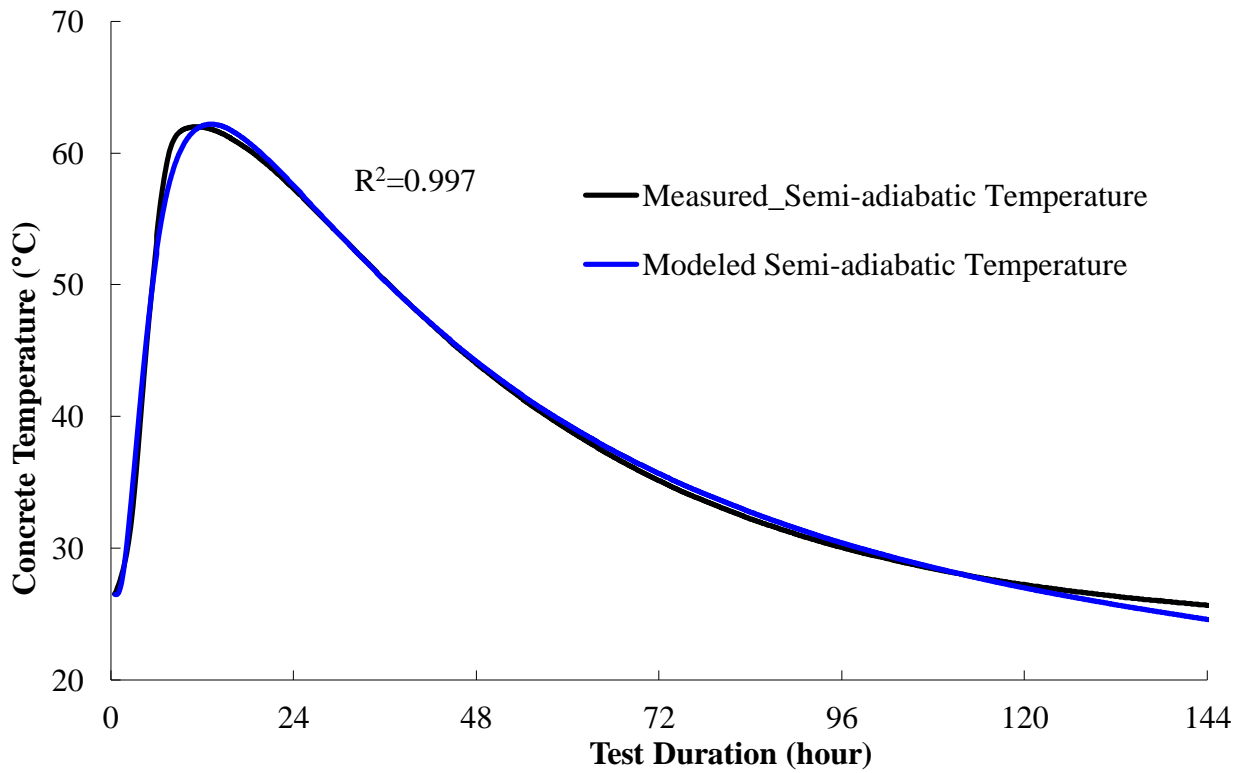


Figure 28: Measured vs. Modeled Semi-adiabatic Temperature CHAD

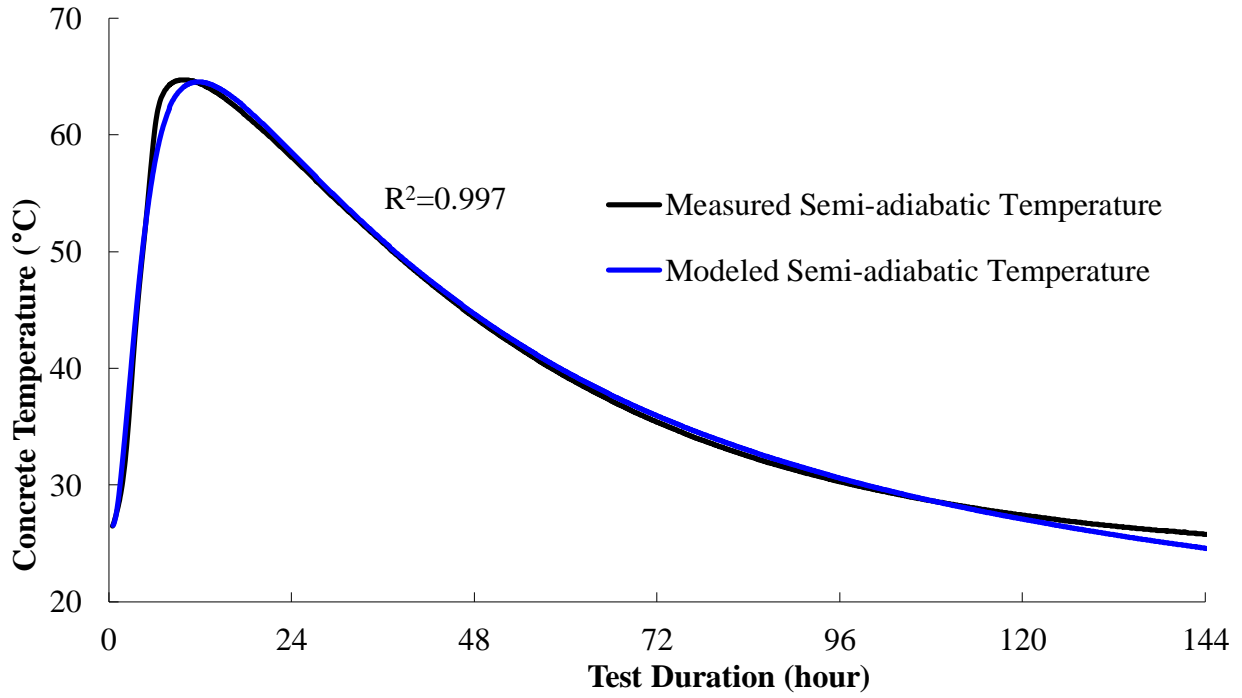


Figure 29: Measured vs. Modeled Semi-adiabatic Temperature CAD

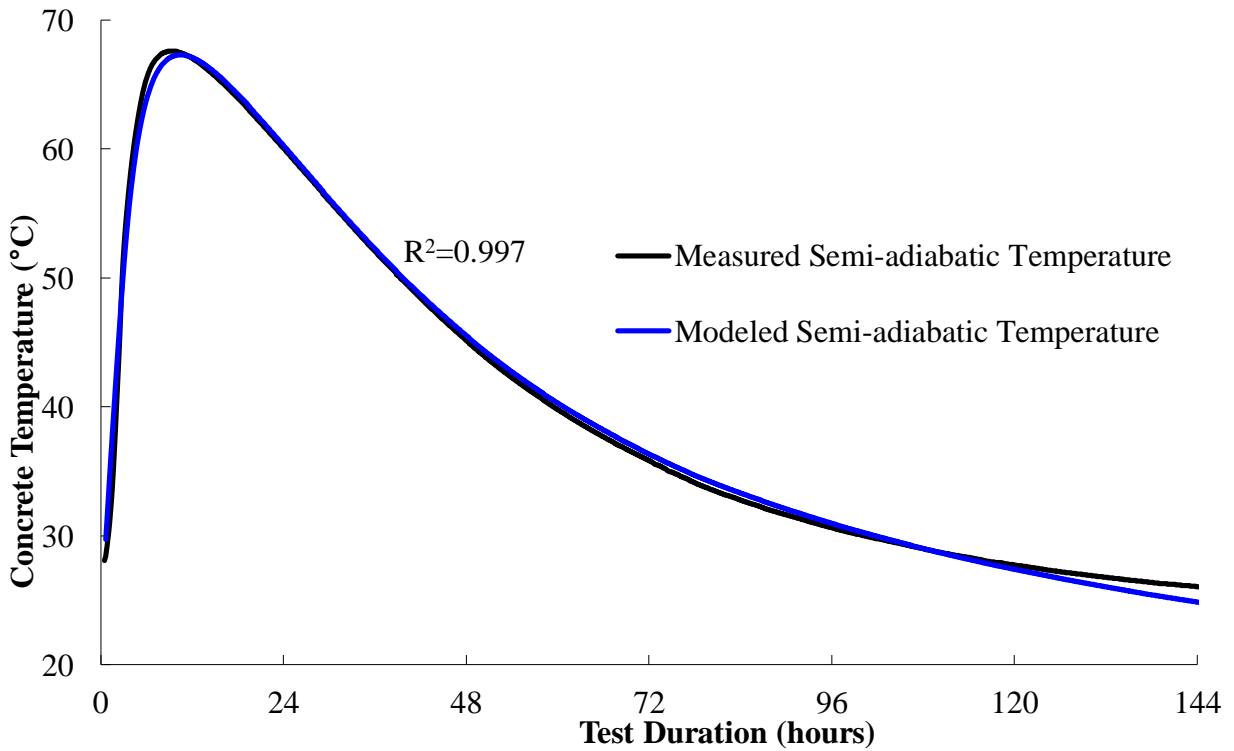


Figure 30: Measured vs. Modeled Semi-adiabatic Temperature CDAD

4.4 Setting Time

The setting time results at three different curing temperatures are shown in Figure 31 and Figure 32 for initial and final set. At 23°C it can be seen that the addition of either accelerator decreases the time of initial and final set even offsetting the effect of the water reducer/retarder. At 23°C, CAD sets before CA, while the setting times at 38°C and 53°C are similar. At each temperature for final and initial set, there is a clear trend showing that increasing the dosage of the calcium nitrate-based accelerator decreases the setting time. The setting time also decreases as the initial temperature of each mixture increases from 23°C to 38°C and 53°C. The final setting time trends agree with the τ values observed from semi-adiabatic calorimetry.

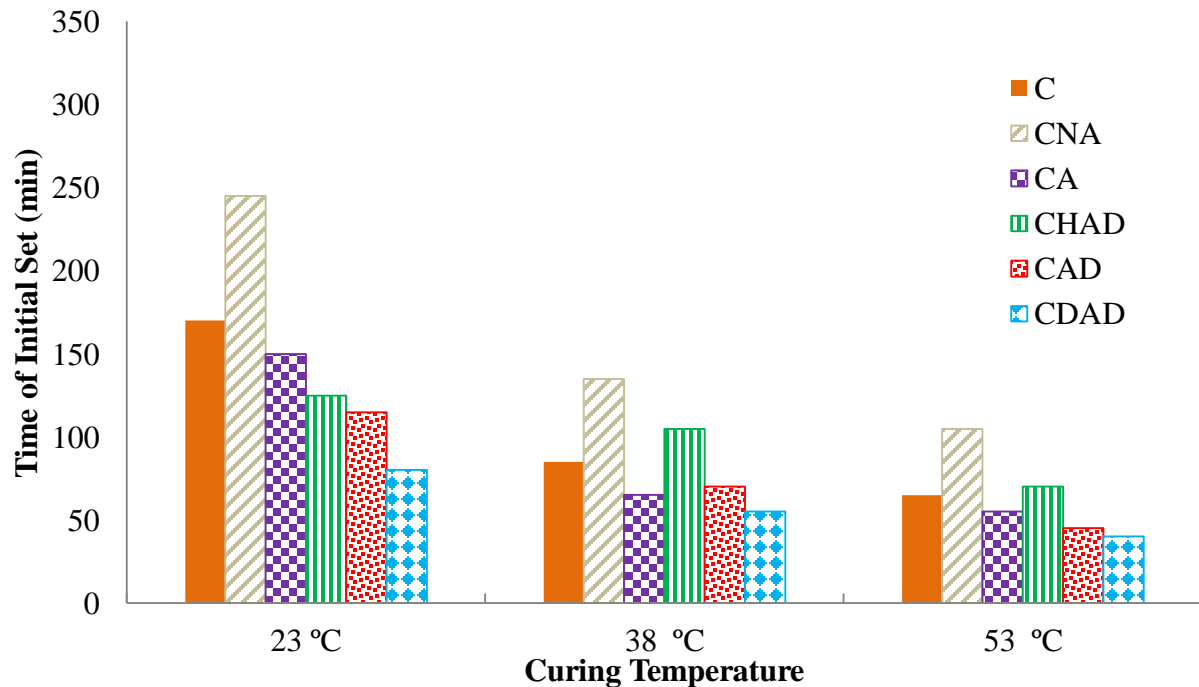


Figure 31: Time of Initial Set

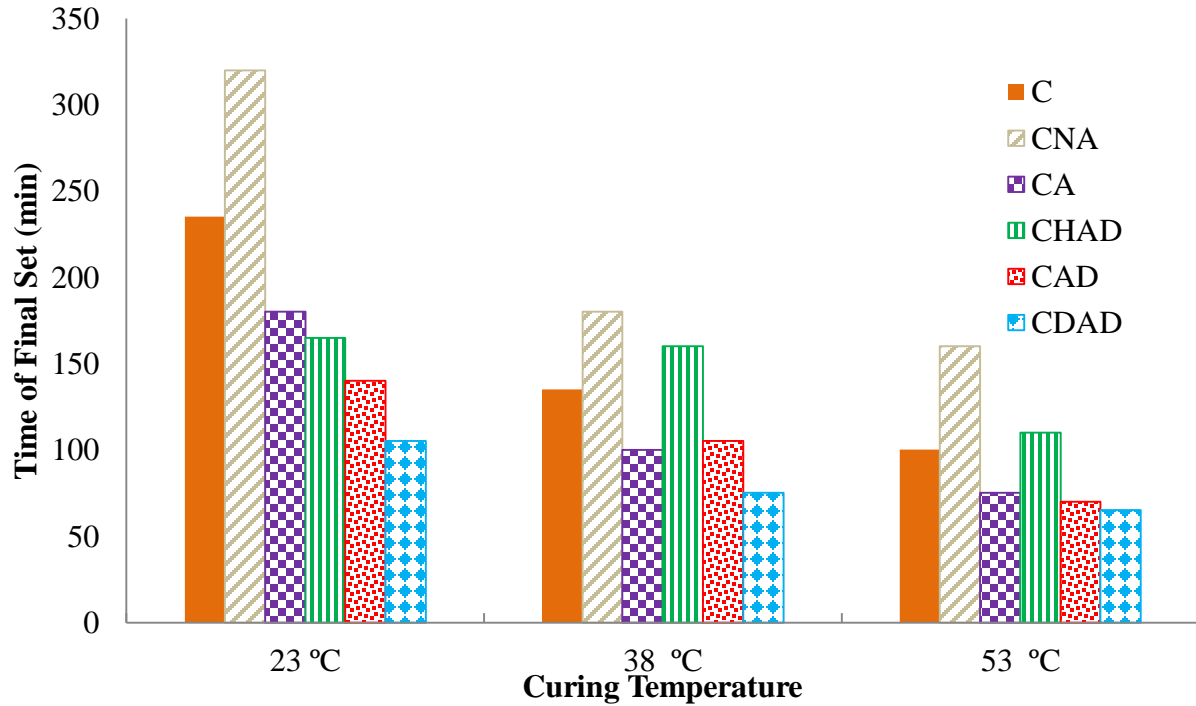


Figure 32: Time of Final Set

4.5 Free Shrinkage

The free shrinkage and rigid cracking frame tests were conducted at 23°C and 38°C following realistic temperature profiles generated through ConcreteWorks. These realistic temperature profiles use the starting temperature of either 23°C or 38°C, and follow a temperature profile similar to what would be found in the center of an actual pavement slab. The general inputs used in ConcreteWorks to generate the temperature profiles for the free shrinkage and rigid cracking frame tests are shown in Table 12.

Table 12: ConcreteWorks General Inputs

<i>Geometric Inputs</i>	
Pavement Thickness	11 in
Subbase Thickness	3 in
Subbase Type	Asphalt Concrete
<i>Batch Proportions</i>	
Cement (lb/yd ³)	900
Water (lb/yd ³)	325

Table 12 Continued

Coarse Aggregate (lb/yd ³)	1680
Fine Aggregate (lb/yd ³)	831
<i>Material Properties</i>	
Cement Type	Type I/II
Blaine Fineness	442 m ² /kg
Coarse Aggregate Type	Limestone
Fine Aggregate Type	Siliceous River Sand
<i>Construction Inputs</i>	
Placement Temperature	23 °C
Pavement Curing	Single Coat Compound
Cure Method Color	Light Grey
Curing Application	1 hr

The environmental inputs used for the ConcreteWorks analysis include a range of actual weather data over a four day period obtained from www.weatherspark.com for the FDOT State Materials Office location in Gainesville on 10/24/2013 as shown in Table 13.

Table 13: ConcreteWorks Environmental Inputs

Day	Max Temp(°F)	Min Temp(°F)	Max Wind (mph)	Avg. Cloud Cover(%)	Max Hum.(%)	Min Hum.(%)
1	73	52	9.2	0	90	36
2	78	47	12.8	0	90	33
3	76	45	5.8	0	96	30
4	78	43	8.1	100	96	30

The concrete temperature of each mixture following the ConcreteWorks profile generated at 23°C and 38°C is presented in Figure 33. The free shrinkage measurements shown in Figure 34 and Figure 35 are for data collected after final set at each respective temperature. The results show similar initial expansion for all of the 23°C mixtures except for CDAD which is much higher than the other mixtures. The expansion for the control and nitrate based mixtures at 38°C was lower than the 23°C mixtures, while the CA mixture showed an opposite trend.

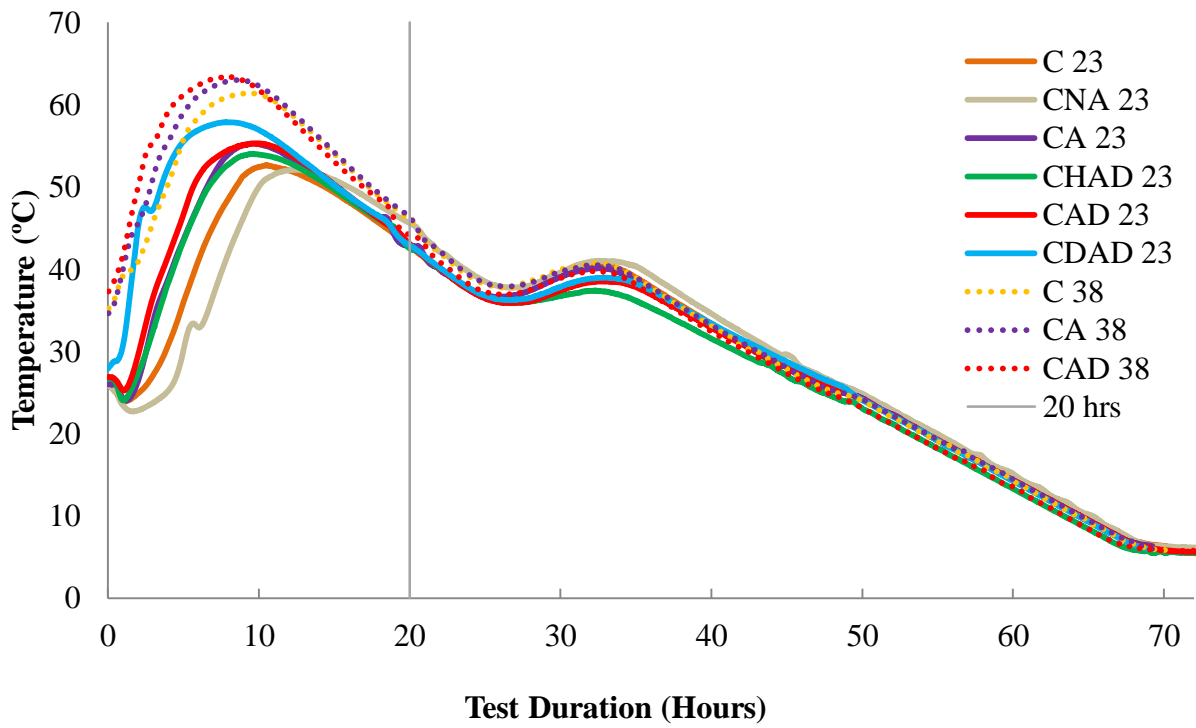


Figure 33: Free Shrinkage Realistic Temperature Profiles

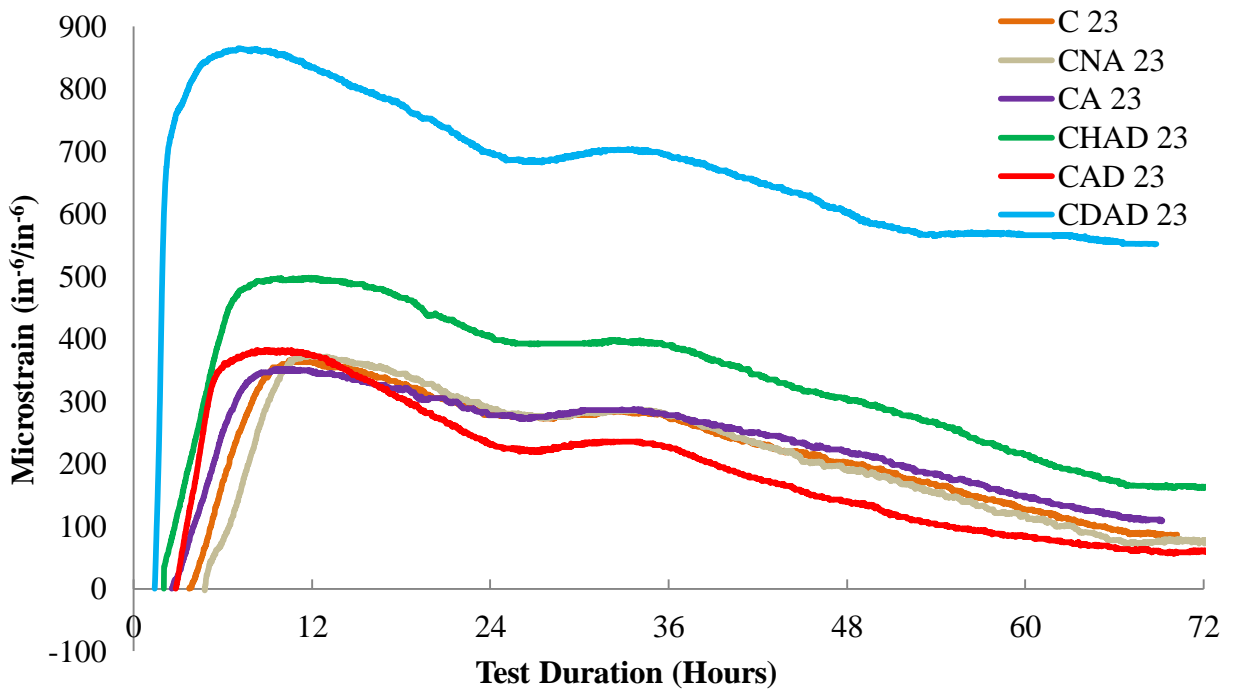


Figure 34: Realistic Free Shrinkage Analysis at 23°C

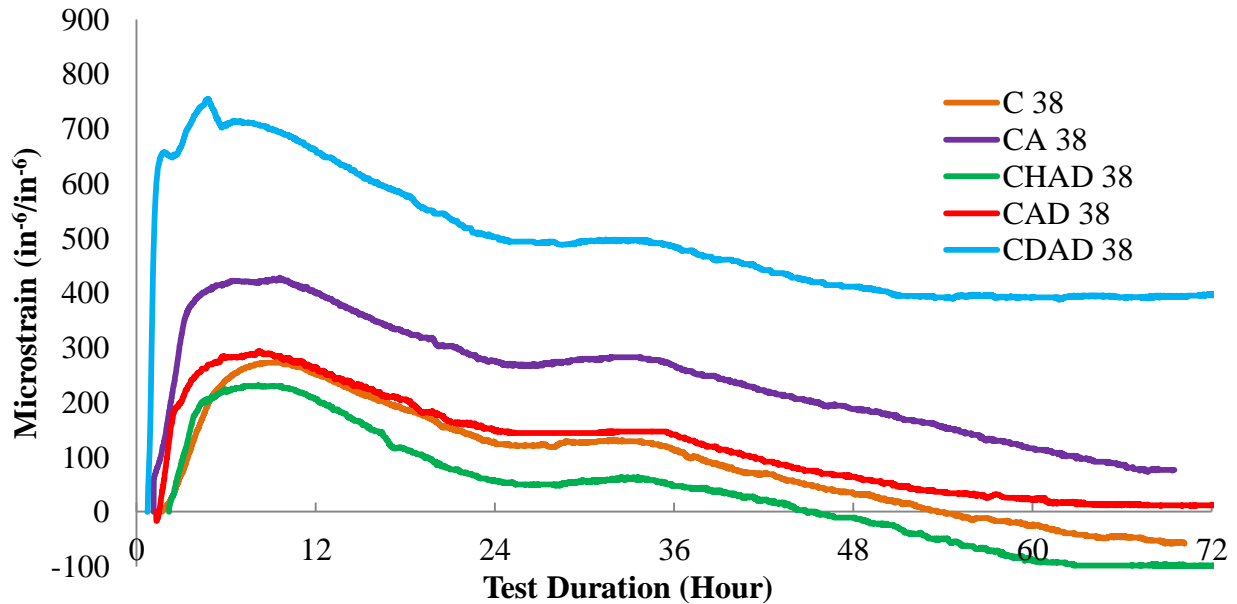


Figure 35: Realistic Free Shrinkage Analysis at 38°C

Although it is not possible to separate the thermal and autogenous volume change occurring simultaneously in these mixtures, it is possible to compare the relative amount of volume change between mixtures, especially after 20 hours since the temperature change after 20 hours was very similar between mixtures as can be seen in Figure 33. This analysis starting at 20 hours is presented in Figure 36 and Figure 37 for the 23°C and 38°C mixtures, respectively. At 23°C, Figure 36 shows all of the nitrate-based accelerator mixtures to increase the autogenous shrinkage compared to C, while CA decreases it. This agrees with the findings of Clemmens et al. [18] where higher chemical shrinkage values were reported at early ages for mixtures containing calcium nitrate than calcium chloride. It was proposed that higher shrinkage for calcium nitrate mixes was due to restricted diffusion due to the morphology of calcium hydroxide gathering into larger clusters rather than being evenly distributed [73].

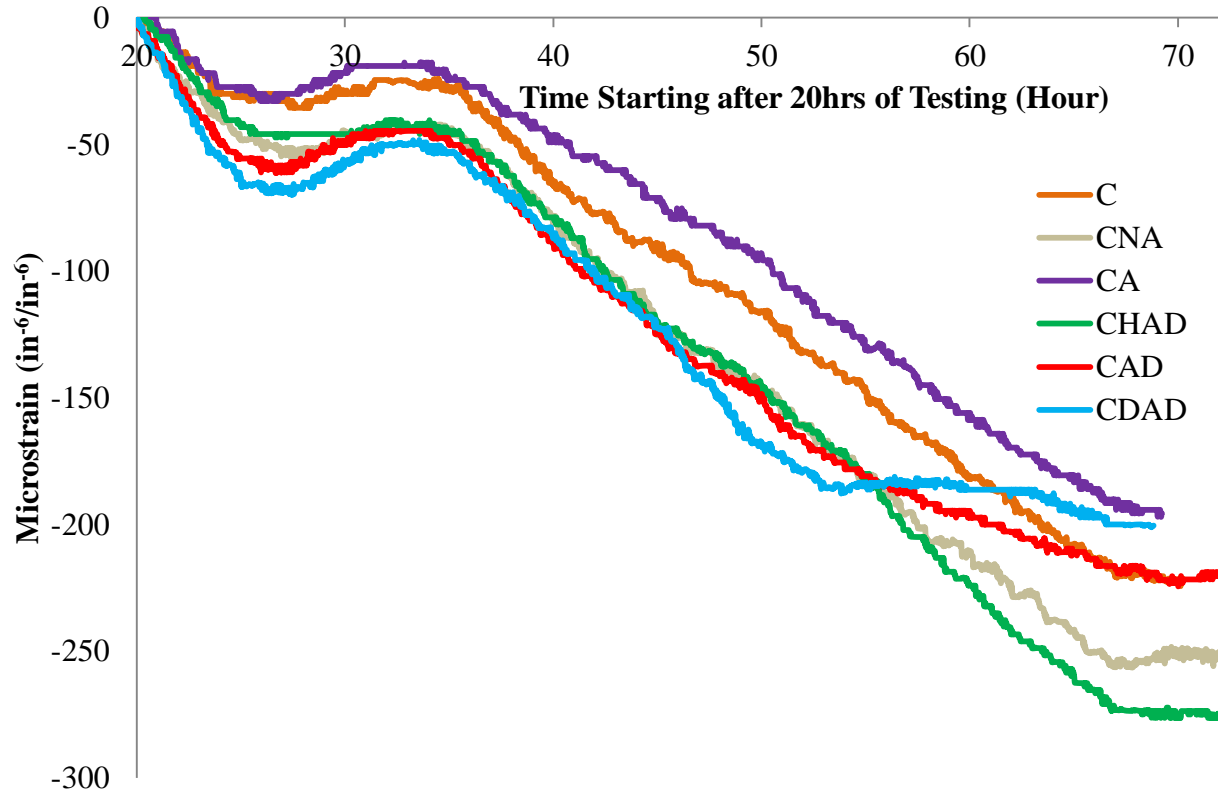


Figure 36: Realistic 23°C Mixtures Compared after 20 Hours

The opposite effect was observed at 38°C as shown in Figure 37, where the nitrate based accelerator mixtures decreased autogenous shrinkage. The increase in initial temperature had a larger effect on shrinkage for the CA and C mixture, while the shrinkage for the calcium nitrate based accelerator mixtures stayed about the same.

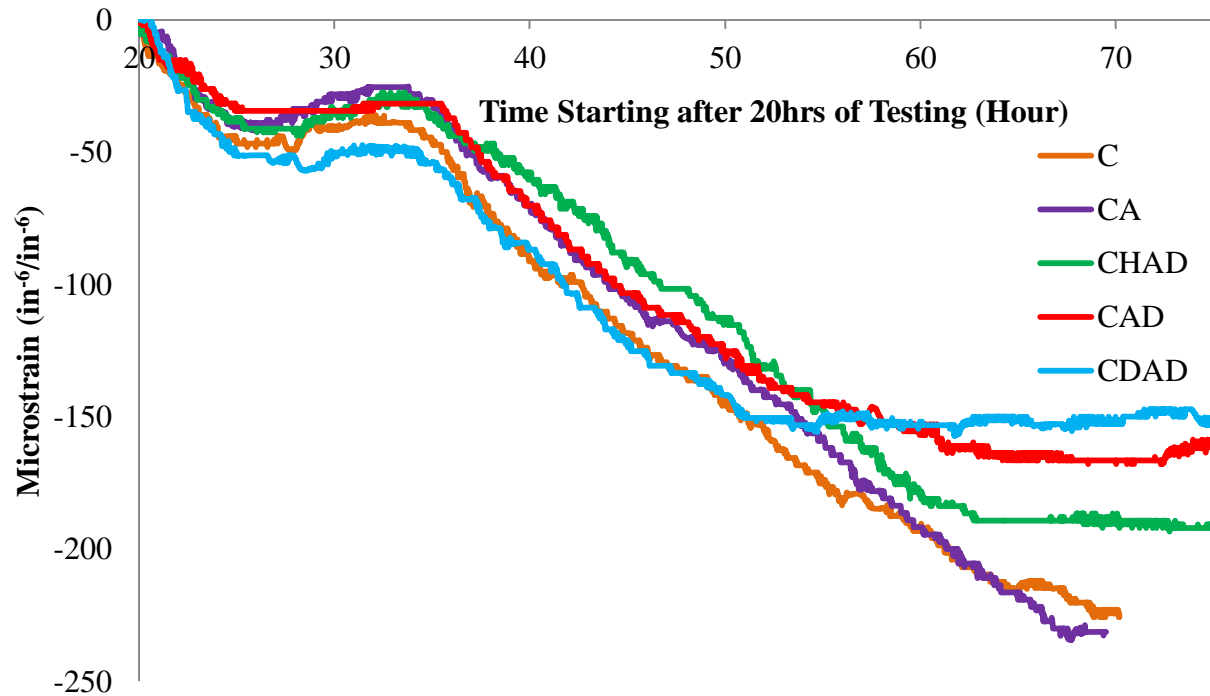


Figure 37: Realistic 38°C Mixtures Compared after 20 Hours

After about 50 hours, CAD and CDAD start to show a decrease in the rate of autogenous shrinkage at both 23°C and 38°C, while the same effect can be seen for CHAD at 38°C. This trend was also visible in the rigid cracking frame results. The cause of this decrease in autogenous shrinkage after 50 hours in the calcium nitrate based accelerator mixtures is still unknown and perhaps indicates the need for further morphological studies of the microstructure.

4.6 Rigid Cracking Frame

The temperature and stress analysis of the insulated rigid cracking frame tests without any imposed temperature control is shown in Figure 38 and Figure 39. The CAD mixture showed a much higher rate of tensile stress development in the insulated rigid cracking frame tests, most likely because of its higher peak temperature and a higher autogenous shrinkage rate as observed from the 23°C free shrinkage testing. Although the CA tensile stresses are similar to the C mixture,

the rate of tensile stress development was accelerated in the former. This is most likely due to a larger thermal change over the same amount of time since the CA insulated temperature had a higher peak temperature than the C mixture as can be observed from Figure 38.

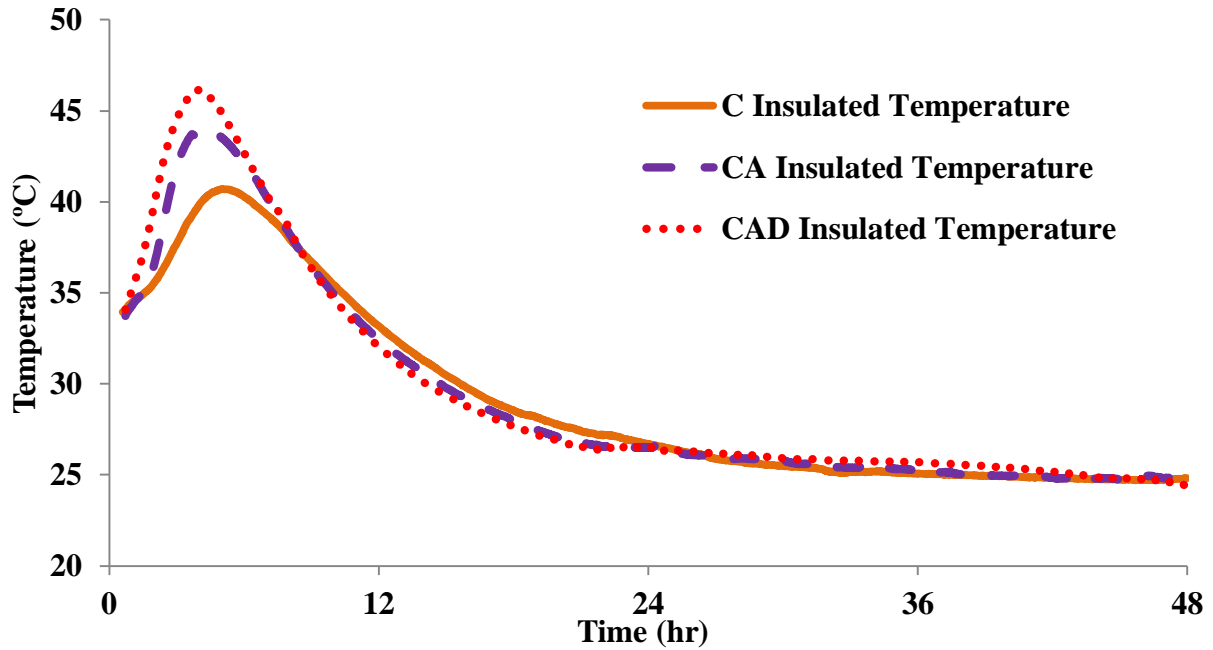


Figure 38: Insulated RCF Temperature

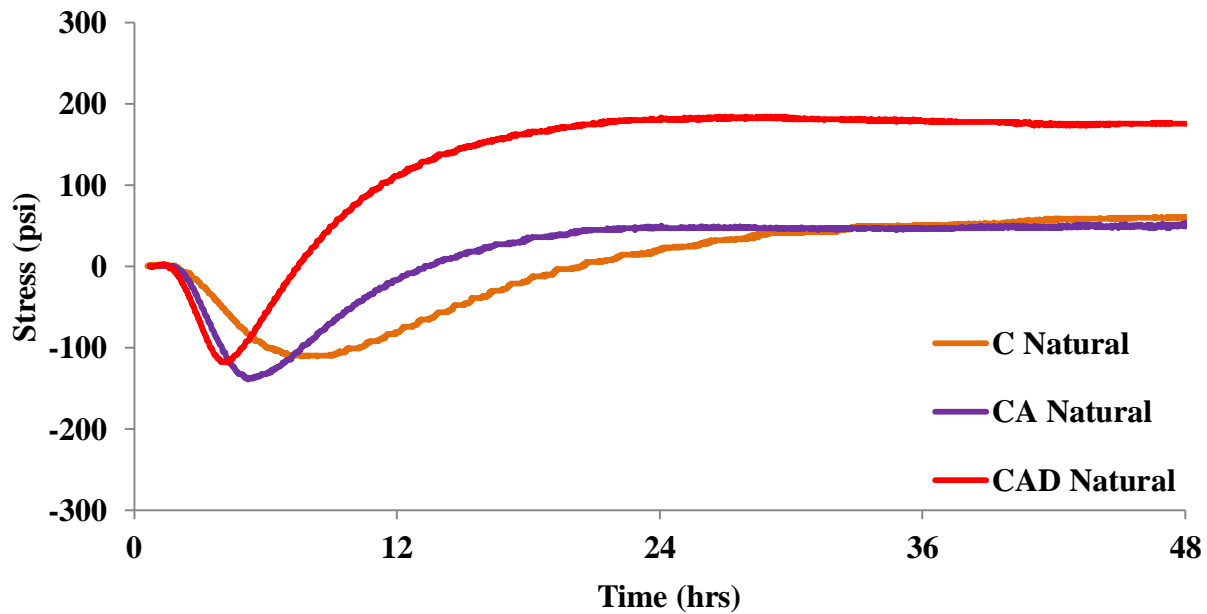


Figure 39: Insulated RCF Stress

The concrete temperature and rigid cracking frame analysis using the 23°C realistic temperature profile is shown in Figure 40 and Figure 41, while the 38°C results are shown in Figure 42 and Figure 43. The 23°C results show the nitrate based accelerator mixtures developed higher tensile stresses than C and CA. An increase in dosage of nitrate based accelerator also increased the tensile stresses at 23°C. At about 50 hours of testing, CAD and CDAD showed a reduction in the induced tensile stresses at 23°C. This trend was also observed in the free shrinkage frame around this time for the same mixtures at the same temperature as can be seen in Figure 34. This stress relaxation could help reduce the concrete cracking potential, if cracking has not yet occurred due to volume changes from cooling after the large thermal rise and autogenous shrinkage.

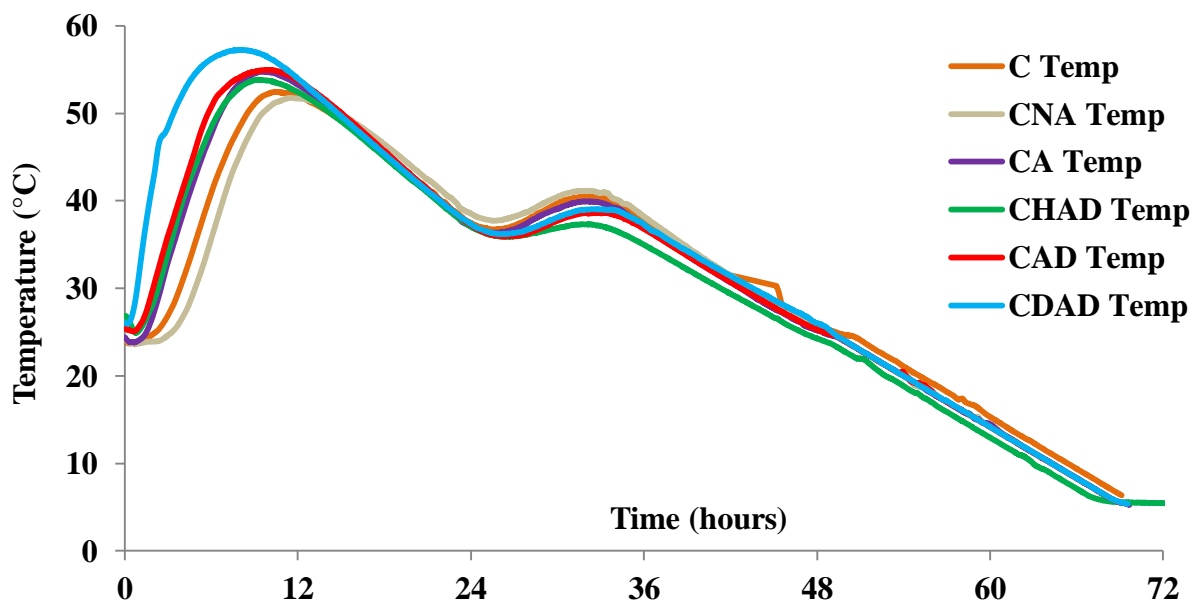


Figure 40: RCF 23°C Realistic Temperature Profiles

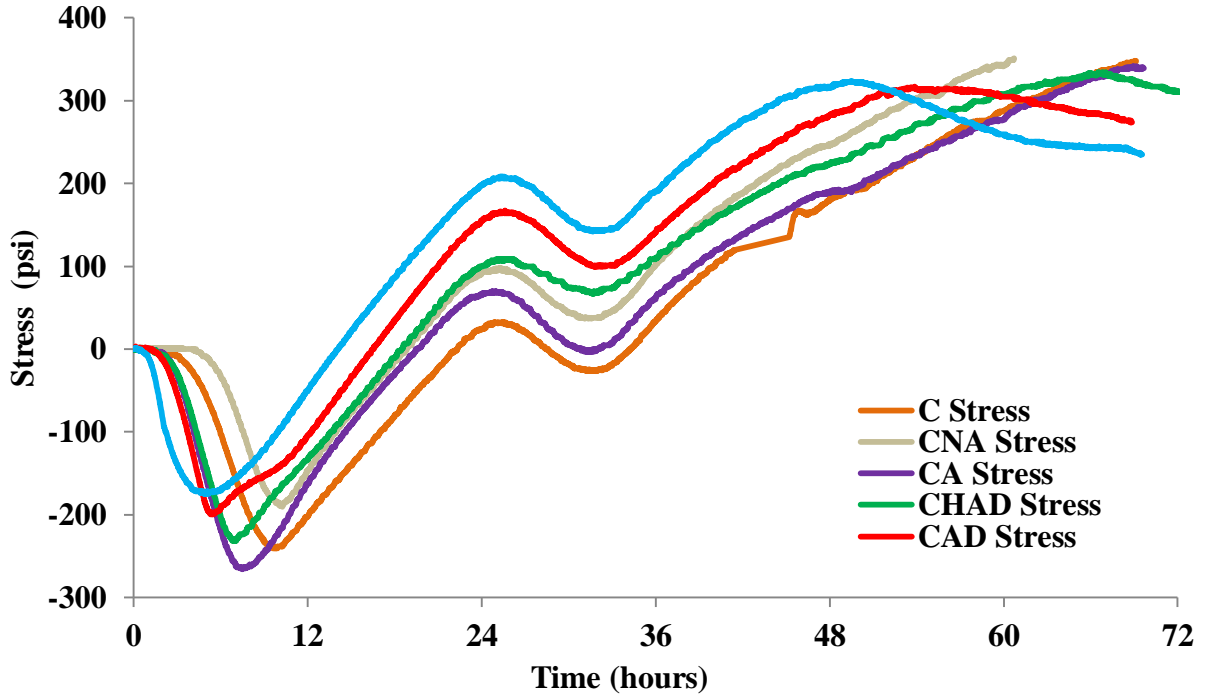


Figure 41: RCF 23°C Realistic Stress Profiles

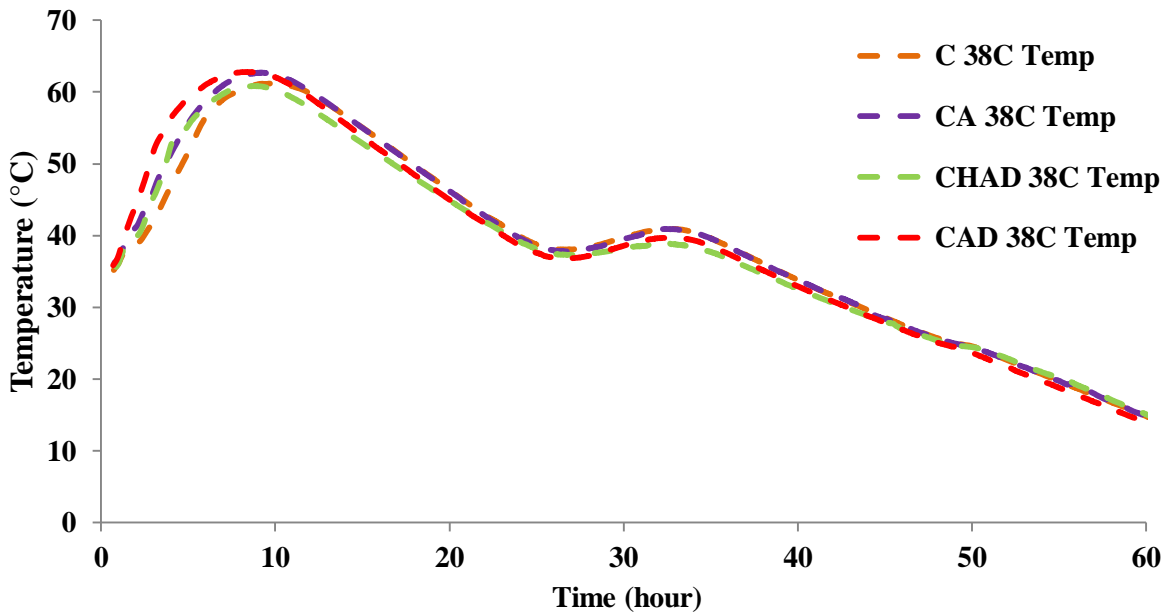


Figure 42: RCF 38°C Realistic Temperature Profiles

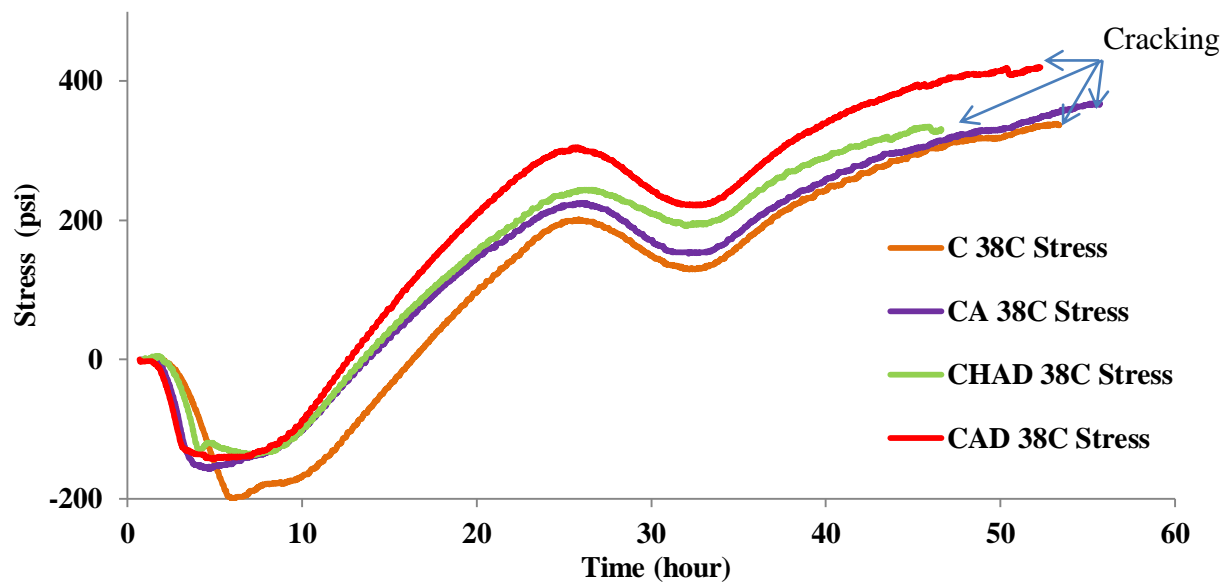


Figure 43: RCF 38°C Realistic Stress Profiles

For all of the mixtures, increasing the placement temperature to 38°C resulted in much higher tensile stresses, 150% for C at 50 hours. This is due to the higher peak temperature from the heat of hydration and larger subsequent drop in temperature. Based on stress development, it appears that CHAD and CAD experienced the lowest stress relaxation, whereas the CA mixture has slightly higher stress relaxation than any of the other mixtures as can be seen in Figure 43. The higher stress relaxation for CA could be due to the chloride effect on pore size refinement [18]. Although CAD experienced the highest stresses, it still cracked around the same time at 52 hours as the C and CA mixtures. This indicates that the differences in stress relaxation between mixtures were small enough to preclude choosing between these two accelerators on that basis alone.

The rigid cracking frame is a strong comparative tool to study different admixtures. However, it is limited in that it does not account for drying shrinkage, temperature or moisture gradients which could cause curling/warping, or environmental conditions such as solar radiation

or humidity. HIPERPAV was used to model the effects of these parameters on the mixture's potential to induce tensile stresses.

4.7 HIPERPAV Analysis

The geometric and construction parameters used in HIPERPAV analysis are shown in Table 14.

Table 14: HIPERPAV Mixture Inputs

<i>General</i>	
Reliability Level (%)	90
Slab Thickness (in)	11
Slab width (ft)	12
Transverse Joint Spacing (ft)	13
<i>Slab Support</i>	
Base Material	Unbound Agg Subbase
Use Subgrade Modulus (psi)	40,000
Subbase Thickness (in)	8
Axial Restraint	Est. from Material Type
<i>Cement</i>	
ASTM Cement Type	Type I
Blaine Fineness (m ² /kg)	442
<i>PCC Properties</i>	
CTE (/°F)	Estimated from Mat.
<i>Construction Operations</i>	
Construction Day and Time	10/24/13 9:00 AM
Fresh Concrete Temperature (F)	77
Initial Subbase Temperature (F)	77
Curing Method	Plastic Sheeting
Age Curing Applied (hr)	2
Age Curing Removed (hr)	5
Saw cutting Time(hr)	Saw at Optimum Time*

*Although saw cutting was not reported for the field study, HIPERPAV strongly recommends not skipping this input as the software calculates stresses based on the assumption that the joint spacing is infinite until saw cutting is considered [36]. For this reason, the option of “optimal time” was chosen for all mixtures. It should be noted that the optimal time is not the same for each mixture.

HIPERPAV used the same geometric, heat of hydration, and construction inputs as ConcreteWorks, while also including strength values as shown in Table 15. Figure 44 shows the concrete splitting tensile strength-maturity relationships used in the analysis.

Table 15: HIPERPAV Inputs - PCC Properties

HIPERPAV	C	CNA	CA	CHAD	CAD	CDAD
Strength Type	Tensile	Tensile	Tensile	Tensile	Tensile	Tensile
28 Day Strength(psi)	765	685	640	725	705	750
28 Day Modulus(psi)	5325000	4925000	4675000	5050000	5350000	5125000
Heat of Hydration(J/kg)	481800	481800	481800	481800	481800	481800
HoH-based E_A (J/mol)	33004	30784	25420	26484	21300	32400
b =	0.836	1.072	0.825	0.757	0.867	0.485
t (hrs)=	11.596	11.931	7.938	6.944	7.594	6.306
a_u =	0.741	0.687	0.746	0.744	0.674	0.906
Maturity Data	Tensile	Tensile	Tensile	Tensile	Tensile	Tensile
Strength- based E_A (J/mol)	40467	34052	44244	34242	43836	16428

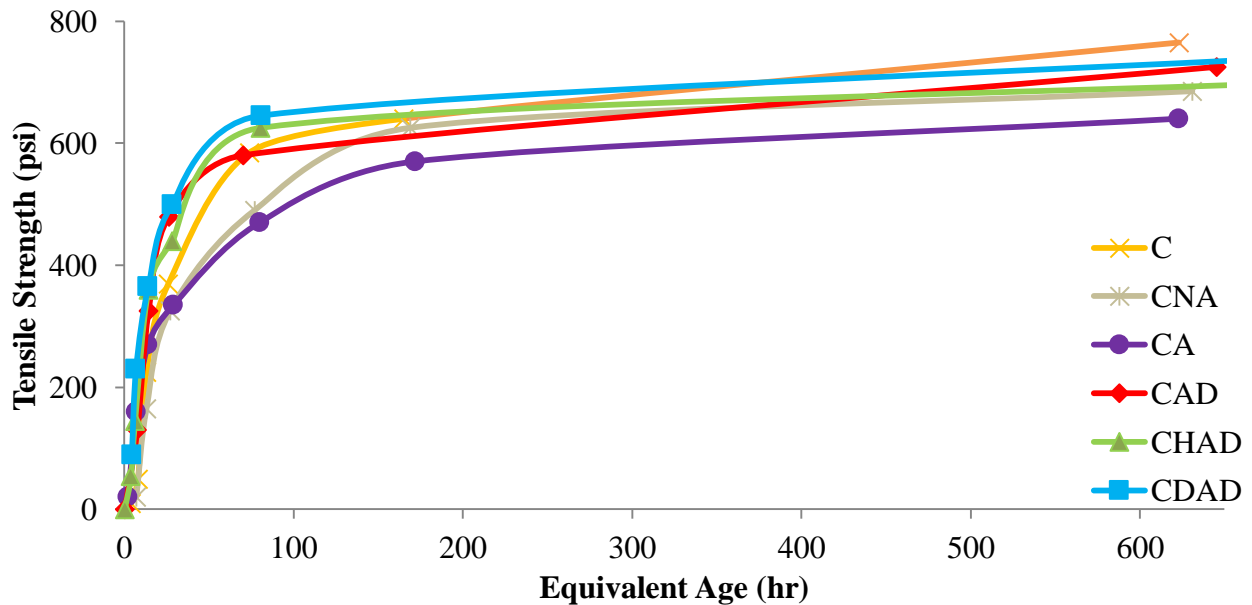


Figure 44: Tensile Strength – Maturity Relationship Input in HIPERPAV III

The environmental factors from an FDOT field study were used as inputs for all of the mixtures for the analysis in HIPERPAV. The environmental profiles were obtained from www.weatherspark.com for the respective location and date and time of the field study (FDOT State Materials Office in Gainesville, Florida on 10/24/13). While ConcreteWorks, only uses the minimum and maximum environmental factor of each day, HIPERPAV uses hourly weather data as shown in Figure 45.

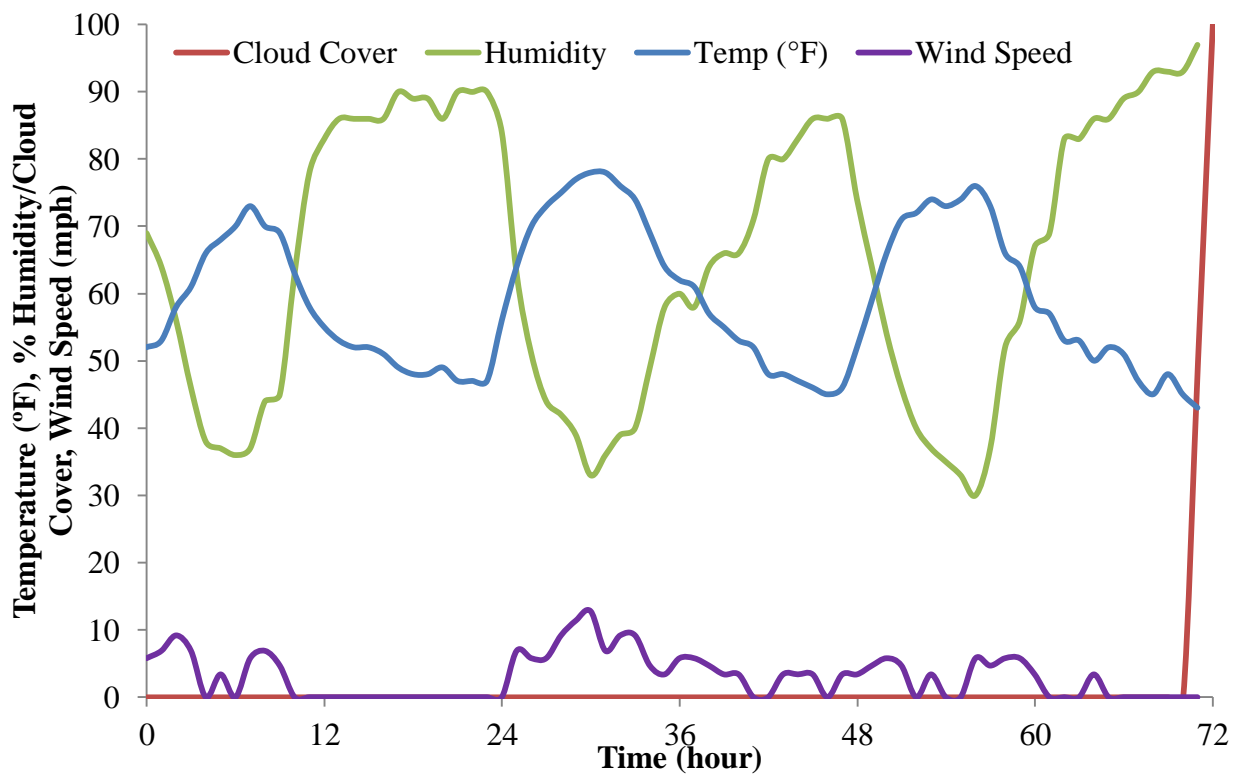


Figure 45: Environmental Inputs

4.7.1 Effect of Dosage of Nitrate-Based Accelerator

The stress to strength ratios of the mixtures are shown in Figure 46 and Figure 47 for a 9 am placement and 11 pm placement. The results show an increase in early strength for the accelerator mixtures; however, there is also an increase in the stresses as the dosage of accelerator

is increased, mainly a result of the more rapid increase in elastic modulus and higher temperature change. Since the stresses are exceeding the strengths, the results show that as there is an increase in dosage of nitrate based accelerator, there is an increase in the cracking potential at early ages. These results agree with the findings of Hope and Manning where it was observed that there is a significant increase in creep strain when a calcium chloride accelerator was added to a plain concrete mixture [74]. As the creep strains increase, the induced tensile stresses would also increase which would consequently increase the cracking potential for that mixture.

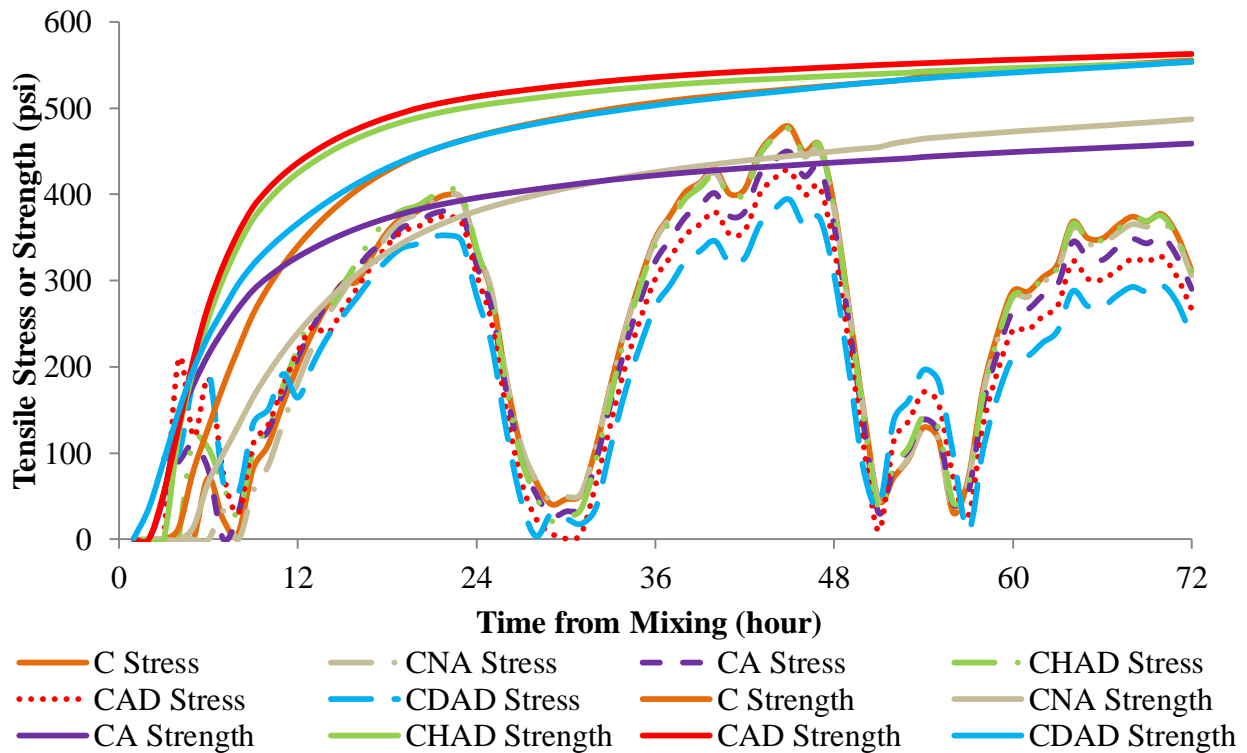


Figure 46: Tensile Stress and Strength of Each Mixture Placed at 9am

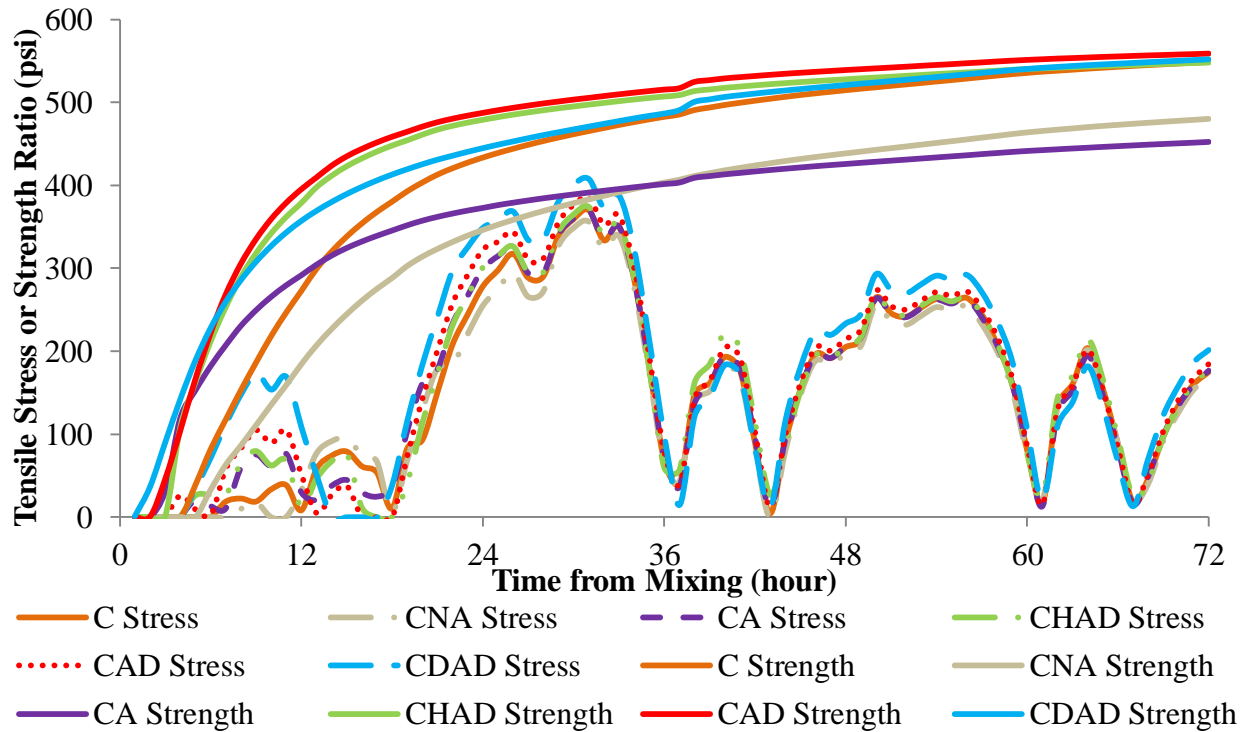


Figure 47: Tensile Stress and Strength of Each Mixture Placed at 11pm

4.7.2 Effect of Placement Time

The construction time of a slab will have a direct effect on the ambient temperature, humidity, and solar radiation profile that the concrete is subject to at early ages. These environmental factors can increase the thermal stresses in concrete and cause early-age cracking which can reduce the service life of the concrete mixture [30]. To reduce the cracking potential in a concrete mixture the construction time should be chosen carefully.

It can be seen in Figure 46 and Figure 47 that the 11 pm placement, although it has slightly lower strength values, has lower tensile stresses especially within the first 12 hours where the tensile strengths are very low. Figure 48 shows the maximum stress to strength ratio for the mixtures as the initial mix time is changed in two hour increments. The results show a lower maximum three-day cracking potential for construction times between 5 PM and 1 AM. These

results agree with the findings of Riding et al, where it was observed that tensile stresses at two days for a morning mixture (10:00 AM) were 46% higher than for the same concrete mixture cast during the night (10:00 PM) [67]. In another study, a heightened risk of cracking potential was found in concrete mixtures that were cast between 7AM and 5PM [68]. The findings in this investigation indicate that although the CA and CDAD mixtures have a consistently higher cracking risk than the other mixtures at each initial start time, the effect of a morning placement time on the cracking potential of the higher nitrate based accelerator mixtures, is greatly increased due to high early stresses.

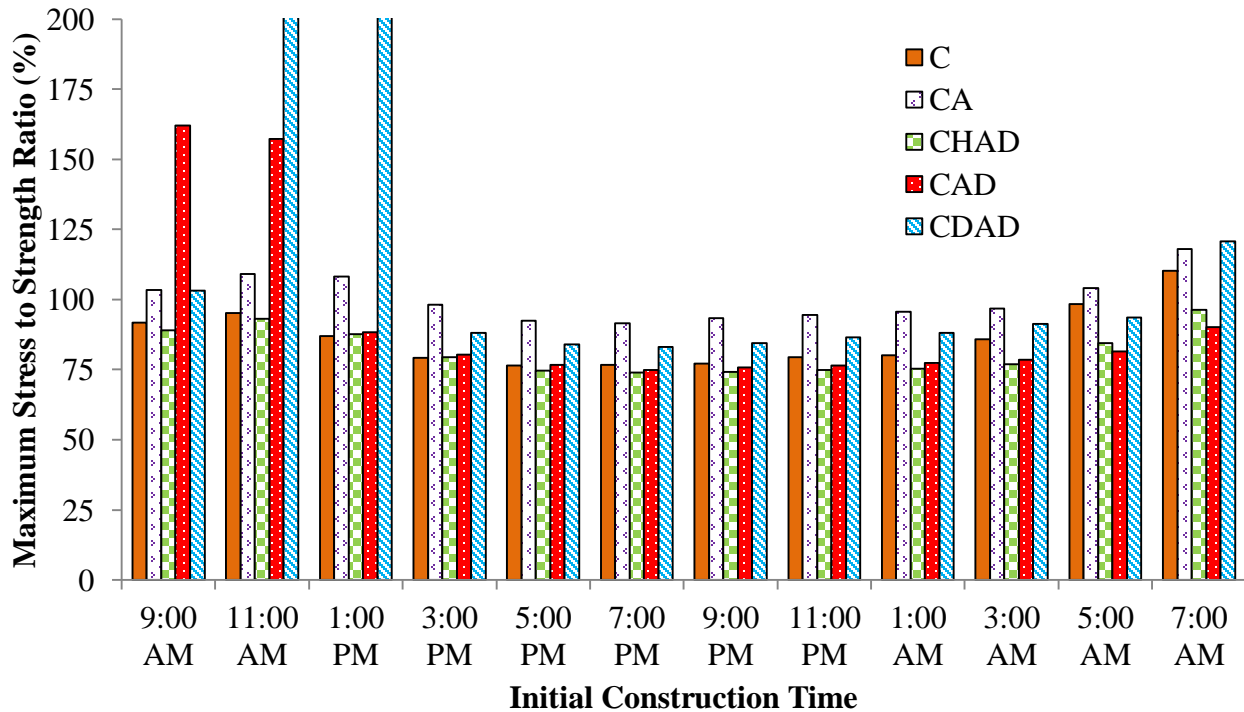


Figure 48: HIPERPAV- Max Tensile Stress at Different Construction Times

HIPERPAV outputs the stresses at the bottom and top of the slab along with the tensile strength from the maturity curves. Figure 49 through Figure 54 show the ambient temperature versus the top stress to strength ratio and bottom stress to strength ratio for both a 9 am and 11 pm placement time. It can be seen from Figure 53 that the early bottom stresses are of concern at a 9

am placement time for CAD and CDAD. This is due to the maximum heat flow from cement hydration occurring about the same time of the maximum in daily ambient temperature which increases the temperature of the surface of the slab and causes a downward curling effect. The restraint by the subbase restricts volume changes and causes tensile stresses near the bottom of the slab.

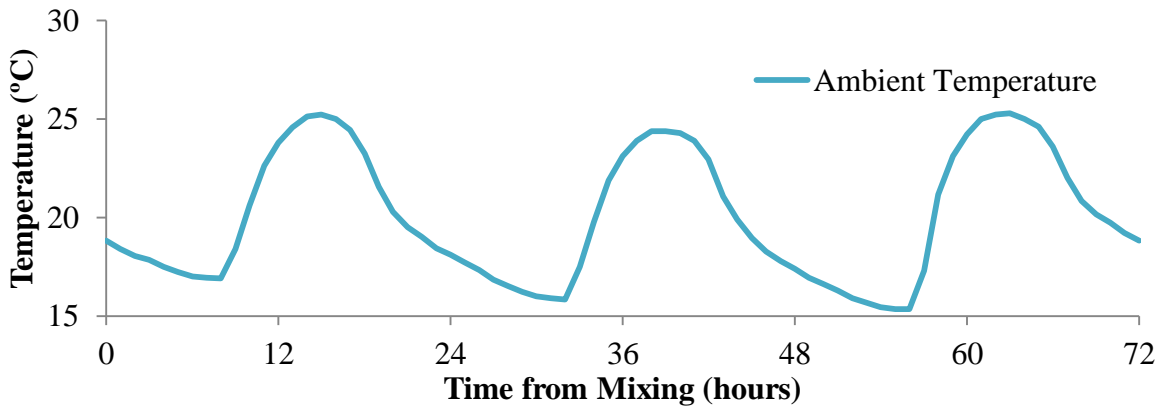


Figure 49: HIPERPAV Ambient Temperature for 11PM Construction Time

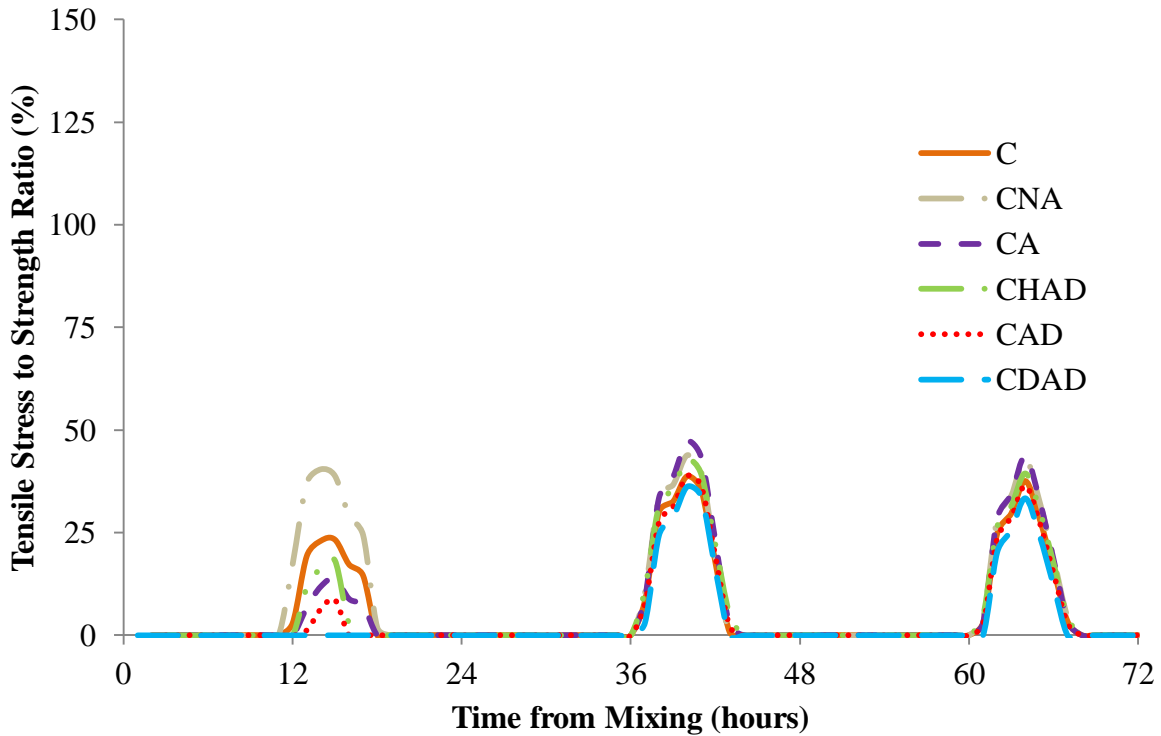


Figure 50: HIPERPAV Analysis at Bottom of Slab Using 11PM Construction Time

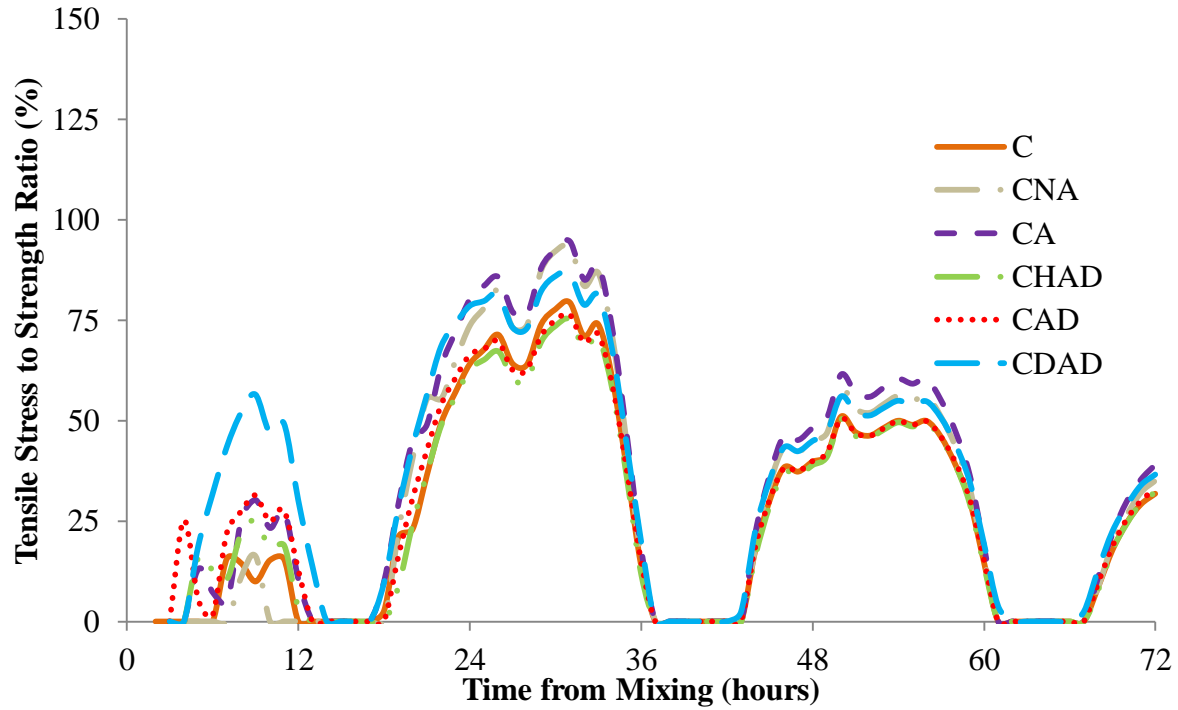


Figure 51: HIPERPAV Analysis at Top of Slab Using 11PM Construction Time

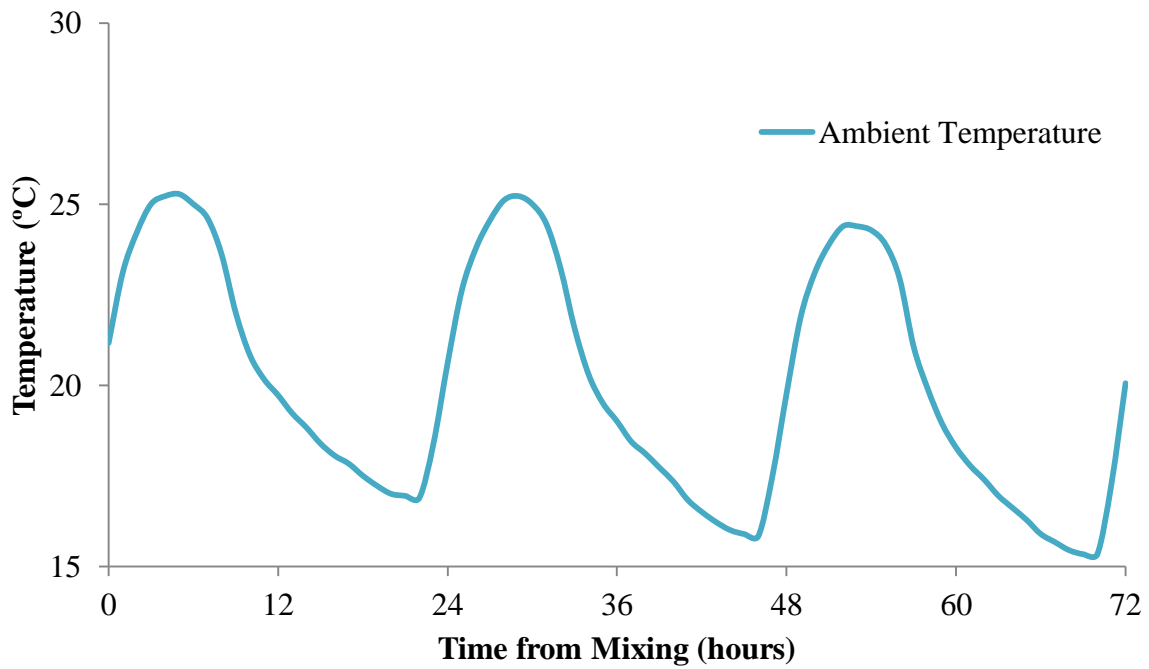


Figure 52: HIPERPAV Ambient Temperature for 9AM Construction Time

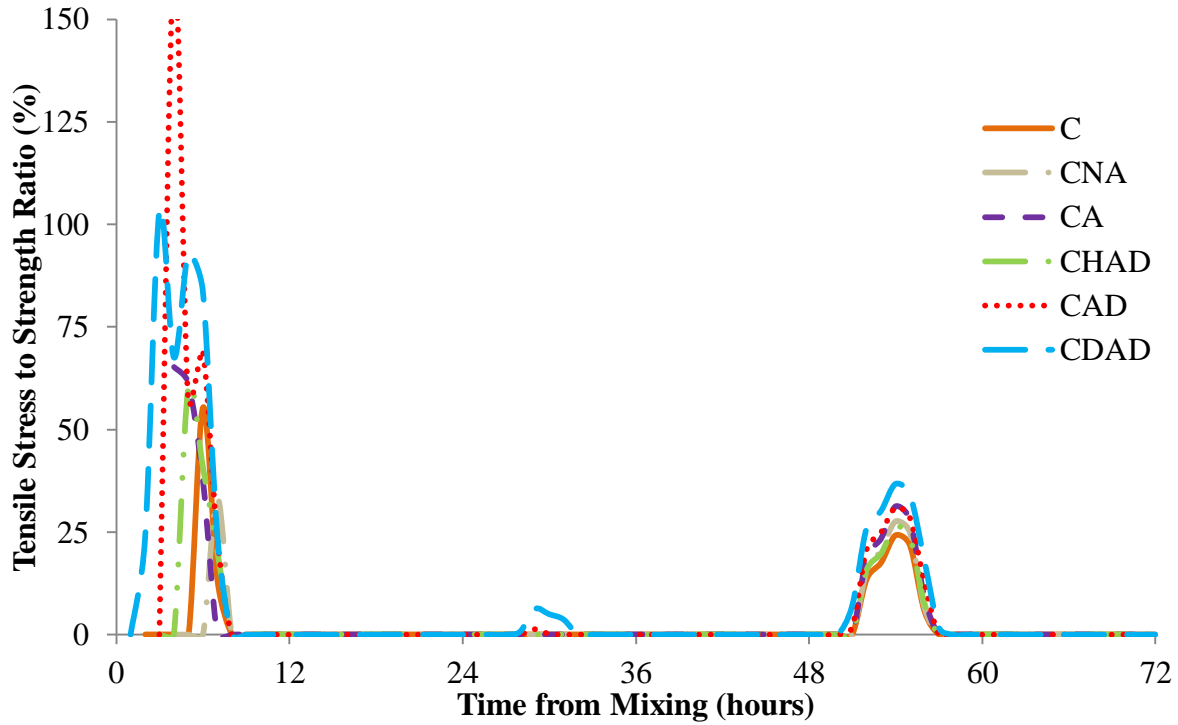


Figure 53: HIPERPAV Analysis at Bottom of Slab Using 9AM Construction Time

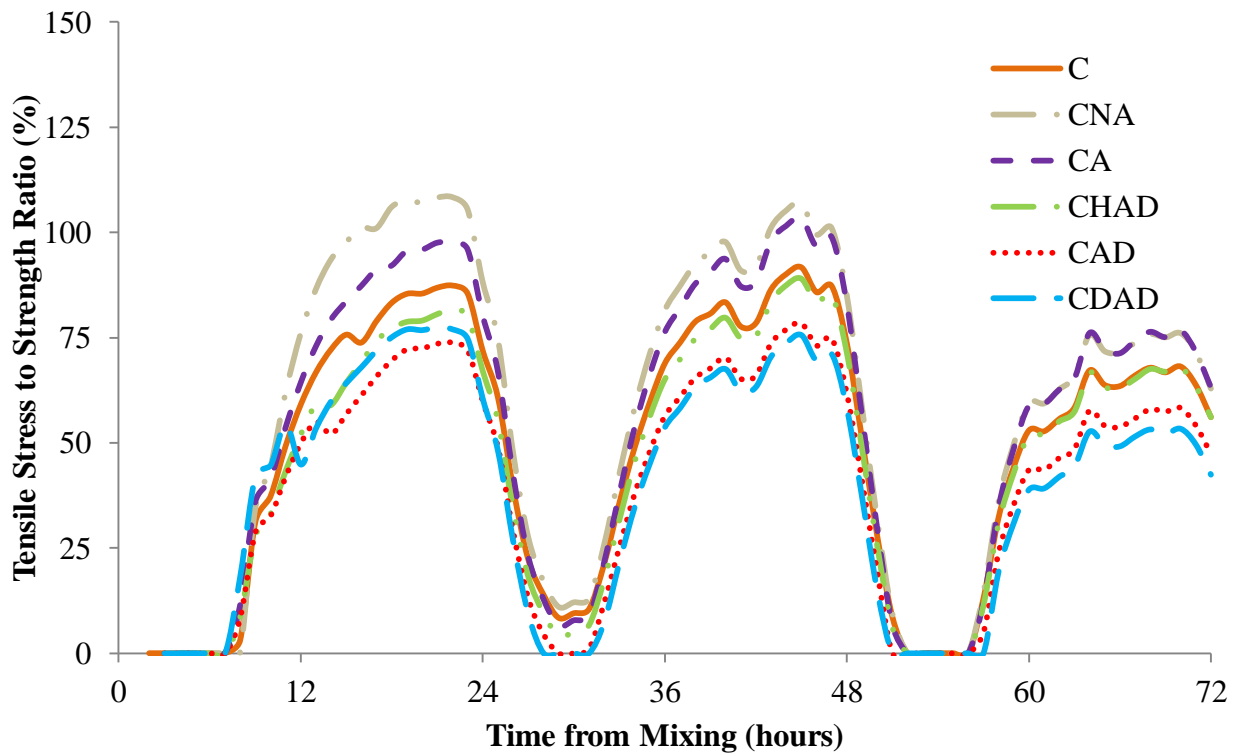


Figure 54: HIPERPAV Analysis at Top of Slab Using 9AM Construction Time

4.7.3 Effect of Initial Concrete Placement Temperature

Rapid repair concrete mixtures are typically placed hot; that is, they have a maximum placement temperature of 100.4°F (38°C) [75] to increase the strength gain rate. The field slab used in the current study had an initial placement temperature of around 78°F (25°C). HIPERPAV was used to make a comparison between mixing at different initial temperatures to show the effect that a lower initial temperature would have on the cracking potential of concrete. Figure 55 shows the results of a comparison of initial temperature of the CAD mixture if it was placed at the previously determined optimal time of 11 PM. An increase in stress-to-strength ratio can be seen as the initial temperature is changed from 60°F to 100°F. The analysis also shows an early spike in stress to strength ratio for this mixture at the lower temperatures for the first 6 hours. These higher stresses are most likely a result of early age curling causing high bottom tensile stresses. Although a lower placement temperature may show a higher stress to strength ratio over the first 6 hours, it still shows an overall lower cracking risk over the duration of the analysis where the higher temperature almost reaches 90% stress to strength ratio.

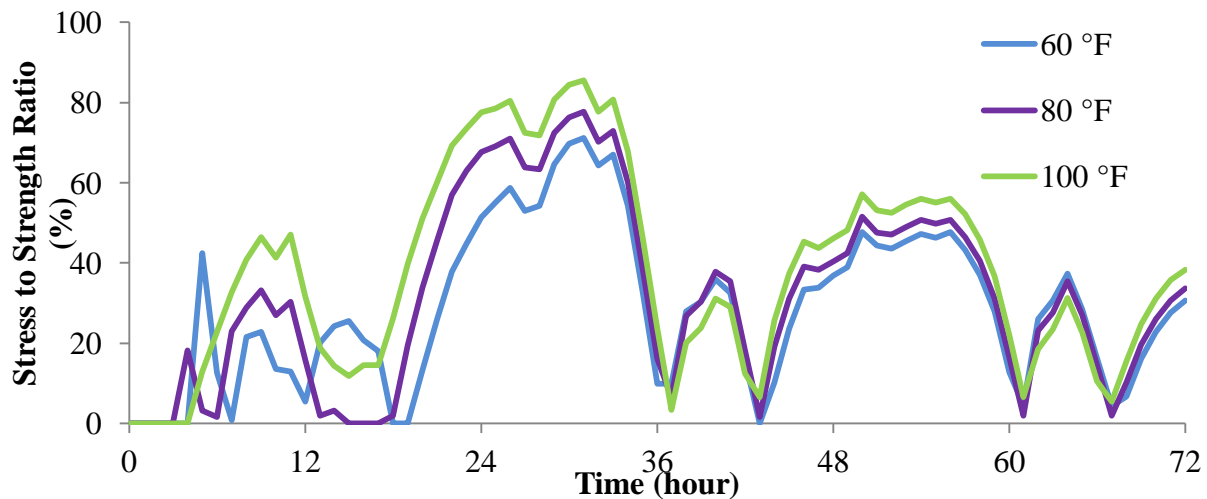


Figure 55: Effect of Initial Temperature on CAD at 11PM

CHAPTER 5: CONCLUSIONS

Both isothermal and semi-adiabatic calorimetry indicate that chloride-based and nitrate-based accelerators increase the rate of hydration and the ultimate degree of hydration throughout the length of the test. For the accelerator mixtures, isothermal calorimetry showed similar main hydration peaks at 38°C, while semi-adiabatic calorimetry showed a similar ultimate degree of hydration, both of which were higher than the control mixture.

Measurements of elastic modulus, compressive strength, and tensile splitting strength indicate that incorporation of either accelerator increased the measured mechanical properties over the first 12 hours where the nitrate-based accelerator mixtures were shown to have higher strengths than the chloride-based accelerator mixture. The ultimate tensile splitting strength of all accelerator-containing mixtures was lower than the control mixture C, while the modulus of the nitrate-based mixtures was similar to that of C.

At a placement temperature of 38°C, results from testing in the rigid cracking frame indicate that the higher tensile strength of CAD and CHAD offset the higher stresses generated when compared to the C and CA mixtures. This could explain the similarity in the cracking age observed for all mixtures when tested in the rigid cracking frame at 38°C. CA showed similar tensile stresses to the C mixture, which is possibly due to stress relaxation. Though CA and CAD have similar moduli, CA experienced more stress relaxation than CAD thus leading to a lower tensile stress generation in the former.

HIPERPAV results showed that for concrete slabs incorporating chloride-based or nitrate-based accelerator, concrete placement between 5 AM and 1 PM increases the cracking potential greatly especially for calcium nitrate-based mixtures. This is believed to be due to higher stresses generated at the bottom of the slab due to the subbase restraining the slab while it is trying to warp/curl. Between 5 PM and 1 AM, the calcium nitrate-based accelerators showed a lower cracking potential than CA, most likely due to their higher tensile strengths.

Calcium nitrate-based accelerator is a good alternative to calcium chloride accelerator when trying to avoid chloride-based accelerators in concrete repair slabs. Although testing showed higher early age shrinkage and consequently higher stresses, CHAD and CAD mixtures had a higher tensile strength and therefore a slightly lower cracking risk when placed during the night.

Future research should include phase analysis of the hydration products using x-ray diffraction in addition to pore size distribution and morphological studies of the microstructure to determine the cause(s) of the decrease in the shrinkage rate around 50 hours for the nitrate-based mixtures. Field slabs should also be placed using the calcium nitrate-based mixture to observe the effects of drying shrinkage and environmental conditions on cracking potential.

REFERENCES

- [1] S. Mindess, J. F. Young, and D. Darwin, *Concrete*, 2nd ed. Pearson Education, 2003.
- [2] G. C. Edwards and R. L. Angstadt, "The Effect of Some Soluble Inorganic Admixtures on the Early Hydration of Portland Cement," *J. Appl. Chem.*, vol. 16, no. May, pp. 166–168, 1966.
- [3] O. M. Jensen and P. F. Hansen, "Influence of temperature on autogenous deformation and relative humidity change in hardening cement paste," *Cem. Concr. Res.*, vol. 29, no. 4, pp. 567–575, Apr. 1999.
- [4] M. Rixom and N. P. Mailvaganam, *Chemical admixtures for Concrete*, 3rd ed. 1999.
- [5] Cement Admixtures Association, "Admixture Technical Sheet – ATS 4 Accelerating admixtures," 2012. [Online]. Available: [http://www.admixtures.org.uk/downloads/ATS 4 Accelerating admixtures.pdf](http://www.admixtures.org.uk/downloads/ATS_4_Accelerating_admixtures.pdf).
- [6] J. Cheung, A. Jeknavorian, L. Roberts, and D. Silva, "Impact of admixtures on the hydration kinetics of Portland cement," *Cem. Concr. Res.*, vol. 41, no. 12, pp. 1289–1309, Dec. 2011.
- [7] S. Aggoun, M. Cheikh-Zouaoui, N. Chikh, and R. Duval, "Effect of some admixtures on the setting time and strength evolution of cement pastes at early ages," *Constr. Build. Mater.*, vol. 22, no. 2, pp. 106–110, Feb. 2008.
- [8] H. Justnes, "Chloride-Free Accelerators for Concrete Setting and Hardening," *ACI*, vol. SP229, pp. 1–18, 2005.
- [9] H. Justnes, "Calcium Nitrate as a Multifunctional Concrete Admixture," in *SINTEF Technology and Society, Concrete*, 2001.
- [10] P. A. Roskopf, F. J. Linton, and R. B. Peppler, "Effect of Various Accelerating Chemical Admixtures on Setting and Strength Development of Concrete," *ASTM Int.*, pp. 322–330, 1975.
- [11] J. J. Shideler, "Calcium Chloride in Concrete," *ACI Mater. J.*, vol. 48, no. 3, pp. 537–559, 1952.
- [12] H. Justnes and E. Nygaard, "Technical Calcium Nitrate as Set Accelerator for Cement at Low Temperatures," *Cem. Concr. Res.*, vol. 25, no. 8, pp. 1766–1774, 1995.

- [13] V. S. Ramachandran and J. Beaudoin, *Handbook of Analytical Techniques in Concrete Science and Technology*. William Andrew Publishing, 2001.
- [14] R. Myrdal, "Accelerating Admixtures for Concrete," Trondheim, Norway, 2007.
- [15] L. H. Grierson, J. C. Knight, and R. Maharaj, "The role of calcium ions and lignosulphonate plasticiser in the hydration of cement," *Cem. Concr. Res.*, vol. 35, no. 4, pp. 631–636, Apr. 2005.
- [16] J. I. Bhatti, "A review of the application of thermal analysis to cement-admixture systems," vol. 189, pp. 313–350, 1991.
- [17] B. E. Abdelrazig, D. G. Bonner, D. V. Nowell, J. M. Dransfield, and P. J. Egan, "Effects of Accelerating Admixtures on Cement Hydration," in *Admixtures for Concrete Improvement of Properties*, E. Vazquez, Ed. Barcelona, Spain: Chapman and Hall, 1990, pp. 120–136.
- [18] F. Clemmens, P. Depuydt, H. Justnes, D. Van Gernert, and E. J. Sellevold, "Influence of Setting Accelerators on Chemical Shrinkage of Portland Cement," pp. 235–249.
- [19] V. M. Sounthararajan and A. Sivakumar, "Effect of Calcium Nitrate on the Pozzolanic Properties of High Early Strength Concrete," *Research J. Appl. Sci. Eng. Technol.*, vol. 6, no. 13, pp. 2502–2508, 2013.
- [20] S. Slatnick, K. A. Riding, K. J. Folliard, M. C. G. Juenger, and A. K. Schindler, "Evaluation of Autogenous Deformation of Concrete at Early Ages," *ACI Mater. J.*, vol. 108–M03, pp. 21–28, 2011.
- [21] K. A. Riding, "Early Age Concrete Thermal Stress Measurement and Modeling," The University of Texas at Austin, 2007.
- [22] E. Holt and M. Leivo, "Cracking risks associated with early age shrinkage," *Cem. Concr. Compos.*, vol. 26, no. 5, pp. 521–530, Jul. 2004.
- [23] J. M. Ruiz, A. K. Schindler, R. O. Rasmussen, P. K. Nelson, and G. K. Chang, "Concrete Temperature Modeling and Strength Prediction Using Maturity Concepts in the FHWA HIPERPAV Software," in *Seventh International Conference on Concrete Pavements: "The use of concrete in developing long-lasting pavement solutions for the 21st century,"* 2001, pp. 97–111.
- [24] J. L. Poole, K. A. Riding, M. C. G. Juenger, K. J. Folliard, and A. K. Schindler, "Effect of Chemical Admixtures on Apparent Activation Energy of Cementitious Systems," *J. Mater. Civ. Eng.*, no. December, pp. 1654–1661, 2011.

- [25] J. L. Poole, K. A. Riding, K. J. Folliard, M. c. G. Juenger, and A. K. Schindler, "Hydration Study of Cementitious Materials using Semi-Adiabatic Calorimetry," *ACI*, vol. SP 241, pp. 59–76, 2007.
- [26] J. L. Poole, "Modeling temperature sensitivity and heat evolution of concrete," University of Texas at Austin, 2007.
- [27] K. A. Riding, J. L. Poole, K. J. Folliard, M. C. G. Juenger, and A. K. Schindler, "Modeling Hydration of Cementitious Systems," *ACI*, no. 109–M23, pp. 225–234, 2012.
- [28] M. C. G. Juenger, J. Hema, and S. Solt, "The Effects of Liquid Nitrogen on Concrete Properties," *Cent. Transp. Res. Univ. Texas Austin*, 2007.
- [29] R. Springenschmid and P. Morabito, "RILEM TCE1 : Adiabatic and semi-adiabatic calorimetry to determine the temperature increase in concrete due to hydration heat of the cement," *Mater. Struct.*, vol. 30, no. October 1997, pp. 451–464, 1998.
- [30] J. L. Poole and K. A. Riding, "Early Age Cracking : A Case Study in How Materials Modeling Can Improve Concrete Quality," *ACI*, vol. SP 266–5, pp. 57–72, 2009.
- [31] K. van Breugel, "Prediction of temepature Development in Hardening Concrete," in *Prevention of Thermal Cracking in Concrete at Early Ages*, 1998, pp. 51–70.
- [32] O. Bjontegaard, "Thermal Dilation and Autogenous Deformation as Driving Forces to Self-Induced Stresses in High Performance Concrete," Norwegian University of Science and Technology, 1999.
- [33] J. A. Whigham, "Evaluation of Restraint Stresses and Cracking in Early-Age Concrete with the Rigid Cracking Frame," Auburn University, 2005.
- [34] R. O. Rasmussen, B. F. Mccullough, J. M. Ruiz, and P. J. Kim, *Fast Track Paving: Concrete Temperature Control and Traffic Opening Criteria for Bonded Concrete Overlays Volume III -HIPERPAV User's Manual*, vol. 3. .
- [35] E. B. Lee, V. Lamour, J. H. Pae, and J. Harvey, "Analysis of Sensitivity of Plain Jointed Concrete Pavement in California to Early-age Cracking using HIPERPAV," 2003.
- [36] B. F. Mccullough and R. O. Rasmussen, "Fast Track Paving: Concrete Temperature Control and Traffic Opening Criteria for Bonded Concrete Overlays Volume I -Final Report," 1999.
- [37] J. M. Ruiz, R. O. Rasmussen, G. K. Chang, J. C. Dick, and P. K. Nelson, "Computer-Based Guidelines For Concrete Pavements Volume III-Technical Appendices," 2005.
- [38] W. C. Reynolds and H. C. Perkins, *Engineering Thermodynamics*, 2nd ed. New York: McGraw-Hill, 1977.

- [39] ASTM C1074, “Standard Practice for Estimating Concrete Strength by the Maturity Method,” *Am. Soc. Test. Mater.*, pp. 1–9, 2004.
- [40] J. L. Poole, K. A. Riding, M. C. G. Juenger, K. J. Folliard, and A. K. Schindler, “Effects of Supplementary Cementitious Materials on Apparent,” *ASTM Int.*, vol. 7, no. 9, pp. 1–16, 2010.
- [41] B. Zdenek and S. Baweja, “Creep and Shrinkage Prediction Model for Analysis and Design of Concrete Structures : Model B3,” *ACI Mater. J.*, vol. SP-194, 1995.
- [42] R. D. Bradbury, *Reinforced Concrete Pavements*. Washington, D.C.: Wire Reinforcement Institute, 1938.
- [43] T. T. C. Hsu, F. Slate, G. M. Sturman, and G. Winter, “Microcracking of Plain Concrete and the Shape of the Stress-Strain Curve,” *ACI*, vol. 60, no. 14, pp. 209–224, 1963.
- [44] ASTM C494, “Standard Specification for Chemical Admixtures for Concrete,” *Am. Soc. Test. Mater.*, pp. 1–10, 2010.
- [45] ASTM C260, “Standard Specification for Air-Entraining Admixtures for Concrete,” *Am. Soc. Test. Mater.*, pp. 1–3, 2006.
- [46] ASTM C1365, “Standard Test Method for Determination of the Proportion of Phases in Portland Cement and Portland-Cement Clinker Using X-Ray Powder Diffraction Analysis,” *Am. Soc. Test. Mater.*, pp. 1–10, 2006.
- [47] ASTM C204, “Standard Test Methods for Fineness of Hydraulic Cement by Air-Permeability Apparatus,” *Am. Soc. Test. Mater.*, pp. 1–9, 2007.
- [48] A. Zayed, K. Riding, C. Ferraro, A. J. Bien-Aime, N. Shanahan, D. Buidens, T. Meagher, V. Tran, J. Henika, J. Paris, C. Tibbetts, and B. Watts, “FDOT Report BDV25-977-01: Long-Life Slab Replacement Concrete,” 2015.
- [49] R. L. Angstadt, S. Spring, and F. R. Hurley, “Accelerator for Portland Cement,” 1969.
- [50] M. Balonis, “The Influence of Inorganic Chemical Accelerators and Corrosion Inhibitors on the Mineralogy of Hydrated Portland Cement Systems,” University of Aberdeen, 2010.
- [51] A. M. Rosenberg, J. M. Gaidis, T. G. Kossivas, and R. W. Previte, “A Corrosion Inhibitor Formulated with Calcium Nitrite for Use in Reinforced Concrete,” in *Chloride Corrosion of Steel in Concrete*, D. E. Tonini, Ed. American Society for Testing and Materials, 1977, pp. 89–99.
- [52] ASTM C33, “Standard Specification for Concrete Aggregates,” *Am. Soc. Test. Mater.*, 2008.

- [53] ASTM C231, "Standard Test Method for Air Content of Freshly Mixed Concrete by the Pressure Method," *Am. Soc. Test. Mater.*, pp. 1–10, 2009.
- [54] ASTM C138, "Standard Test Method for Density (Unit Weight), Yield , and Air Content (Gravimetric)," *Am. Soc. Test. Mater.*, pp. 1–4, 2009.
- [55] C143, "Standard Test Method for Slump of Hydraulic-Cement Concrete," *Am. Soc. Test. Mater.*, pp. 1–9, 2012.
- [56] ASTM C109, "Standard test method for compressive strength of hydraulic cement mortars (Using 2-in. cube specimens)," *Am. Soc. Test. Mater.*, pp. 1–10, 2008.
- [57] A. Sedaghat, A. Zayed, and P. Sandberg, "Measurements and Predictions of Heat of Hydration of Portland Cement Using Isothermal Conduction Calorimetry," *J. Test. Eval.*, vol. 41, no. 6, 2013.
- [58] ASTM C1702, "Standard Test Method for Measurement of Heat of Hydration of Hydraulic Cementitious Materials Using Isothermal Conduction Calorimetry," *Am. Soc. Test. Mater.*, pp. 1–7, 2009.
- [59] P. Freiesleben Hansen and E. J. Pedersen, "Maturity Computer for Controlling Curing and Hardening of Concrete," *Nord. Betong*, vol. 1, no. 19, pp. 21–25, 1977.
- [60] A. K. Schindler and K. J. Folliard, "Heat of Hydration Models for Cementitious Materials," *ACI*, vol. 102, no. M04, pp. 24–33, 2005.
- [61] ASTM C403, "Standard Test Method for," *Am. Soc. Test. Mater.*, pp. 1–7, 2008.
- [62] ASTM C39, "Standard Test Method for Compressive Strength of Cylindrical Concrete Specimens," *Am. Soc. Test. Mater.*, pp. 1–7, 2009.
- [63] ASTM C496, "Standard Test Method for Splitting Tensile Strength of Cylindrical Concrete Specimens," *Am. Soc. Test. Mater.*, pp. 1–5, 2004.
- [64] ASTM C469, "Standard Test Method for Static Modulus of Elasticity and Poisson ' s Ratio of Concrete in Compression," *Am. Soc. Test. Mater.*, pp. 1–5, 2002.
- [65] Daniel A. Buidens, "Effects of Mix Design on Cracking Potential in Rapid Pavement Replacement Projects," University of South Florida, 2014.
- [66] J. L. Meadows, "Early-Age Cracking of Mass Concrete Structures," Auburn University, 2007.
- [67] K. A. Riding, J. L. Poole, A. K. Schindler, M. C. G. Juenger, and K. J. Folliard, "Effects of Construction Time and Coarse Aggregate on Bridge Deck Cracking," *ACI Mater. J.*, vol. 106–M50, 2010.

- [68] J. M. Ruiz, R. O. Rasmussen, G. K. Chang, J. C. Dick, and P. K. Nelson, "Proactive JPCP Case Study : Time of Placement Documentation," in *Computer-Based Guidelines for Concrete Pavements, Volume II: Design and Construction Guidelines and HIPERPAV II User's Manual*, 2005, pp. 87–91.
- [69] V. Tokar, "Additive Composition for Portland Cement Materials," 4337094, 1982.
- [70] H. Justnes, A. T. F. Vanparijs, and D. Van Gemert, "Porosity And Diffusivity Of Concrete With Long-Term Compressive Strength Increase Due To Addition Of The Set Accelerator Calcium Nitrate," in *9th International Conference on Durability of Building Materials and Components*, 2002, pp. 1–10.
- [71] Q. Xu, J. Hu, J. M. Ruiz, K. Wang, and Z. Ge, "Isothermal calorimetry tests and modeling of cement hydration parameters," *Thermochim. Acta*, vol. 499, no. 1–2, pp. 91–99, Feb. 2010.
- [72] D. Whiting and Federal Highway Administration, "Accelerating," *U.S. Department of Transportation*. [Online]. Available: <http://www.fhwa.dot.gov/infrastructure/materialsgrp/acclerat.htm>. [Accessed: 07-Oct-2014].
- [73] H. Justnes and E. C. Nygaard, "Changes in the Microstructure of Cement Paste and Concrete due to Calcium Nitrate Addition," *ACI*, vol. 173, no. 33, pp. 657–672, 1997.
- [74] B. B. Hope and D. G. Manning, "Creep of Concrete Influenced by Accelerators," *ACI Mater. J.*, vol. 68–36, 1971.
- [75] FDOT, "Standard Specifications for Road and Bridge Construction," 2010.

APPENDIX A: SUPPLEMENTARY MATERIALS



Figure A-1: Cylinder Testing - Compressive Strength



Figure A-2: Cylinder Testing - Modulus of Elasticity



Figure A-3: Tensile Splitting Testing

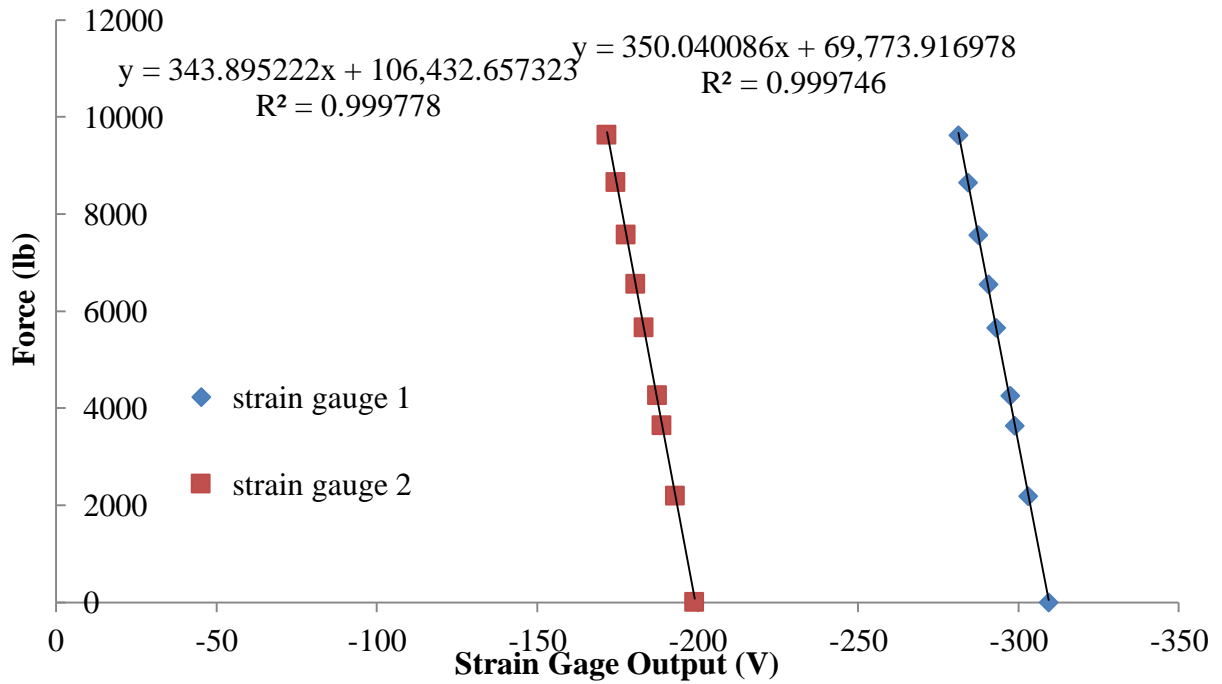


Figure A-4: Rigid Cracking Frame Calibration Data

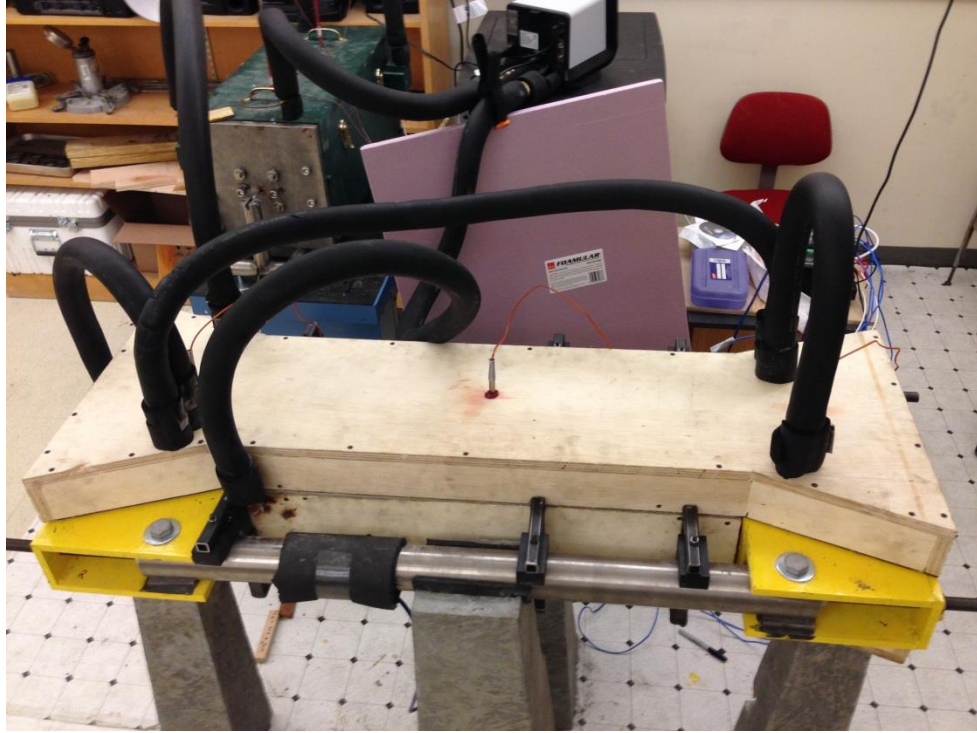


Figure A-5: RCF During Testing




Figure A-6: Copper Piping Throughout RCF Formwork

APPENDIX B: PERMISSIONS

Below is permission for use of material in Chapter 2, 3, and 4 from the FDOT Task report which included the C, CNA, and CA mixtures.

FDOT approval of use of research project material for Masters Thesis Inbox x

 DeFord, Harvey
to me

Jun 28 (8 days ago) ☆ ↶

Tom,

You have my approval, as Project Manager, to use the research from project BDV25-977-01 in your MS thesis, as long as the PI (Professor Zayed) signs off. Let me know if you have any other questions.

Thanks.

Dale

Dale DeFord, PhD
Structural Materials Research Specialist
Office: [352-955-6673](tel:352-955-6673), Fax: [850-412-8355](tel:850-412-8355)
Office Hours: M-Th 7:00 AM-5:30 PM
harvey.deford@dot.state.fl.us

Note: Most written communications to or from state officials are public records available to the public and media upon request (Florida Statute, Chapter 119).

From: Thomas Meagher [<mailto:tmeagher@mail.usf.edu>]
Sent: Sunday, June 28, 2015 8:49 PM
To: DeFord, Harvey
Cc: Abia Zayed
Subject: Masters Thesis

Dear Dr. Deford,

The majority of my research has been on the FDOT pavement project. Since I am a co-author on the pavement project final report, parts of my thesis share write-up from the final report for FDOT contract: BDV25-977-01. The university requires permission for any shared material. Does the FDOT give me permission to share the language from the final report in my thesis? My thesis can be accessed through the shared drive for the final project.

Thanks,
Tom Meagher

Below is permission for the use of material in Chapter 3 and 4 from a submitted article (not yet accepted) in this thesis. The work from the article compares CA and CAD.

Permission to use the article [150629-000117] [Reference: 150629-000117]  

 **EP Support** <support@elsevier.com>
to me 

Subject

Permission to use the article [150629-000117]

Discussion

Response Via Email (Ma. Teresa Frias)

Dear Dr Meagher,

Thank you for your e-mail and apologies for the delayed response.

About your inquiry, I wish to advise that you may use your article should you wish to include your pre print version to your thesis if this will be fine with your Institution.

Thus, I wish to advise that it is not allowed to you use your article as a reference.

You may find this Elsevier Customer Support solution useful:

Answer Title: Copyright, Rights and Permissions

Answer Link: http://help.elsevier.com/app/answers/detail/a_id/49/

Please do not hesitate to contact us again for other inquiries you have.

Should you require further assistance please visit <http://support.elsevier.com> You will find 24/7 support contact details, including live chat.

Kind regards,

Ma. Teresa Frias
Researcher Support